LONG-TERM IMPLICATIONS OF REDECKING BRIDGES WITH PRESTRESSED CONCRETE GIRDERS

By
Beeva Adhikari
Rémy D. Lequesne
William Collins

A Report on Research Sponsored by

KANSAS DEPARTMENT OF TRANSPORTATION

Structural Engineering and Engineering Materials
SM Report No. 158
March 2024

THE UNIVERSITY OF KANSAS CENTER FOR RESEARCH, INC.
2385 Irving Hill Road, Lawrence, Kansas 66045-7563

LONG-TERM IMPLICATIONS OF REDECKING BRIDGES WITH PRESTRESSED CONCRETE GIRDERS

By

Beeva Adhikari

Rémy D. Lequesne

William Collins

A Report on Research Sponsored by

Kansas Department of Transportation

Structural Engineering and Engineering Materials
SM Report No. 158
THE UNIVERSITY OF KANSAS CENTER FOR RESEARCH, INC.
LAWRENCE, KANSAS
March 2024

Abstract

Precast/prestressed concrete girders with cast-in-place decks are commonly used for bridge construction throughout the United States. There is a need to replace concrete decks on many of these bridges because girders last much longer than concrete decks. This study surveyed United States Department of Transportation (DOT) engineers to determine common deck removal practices. Survey results showed that, although most states have a need to replace bridge decks, few states have comprehensive plans for assessing the long-term effects of deck replacement on girder behavior. This study developed a Python model to estimate girder behavior over its lifespan that accounts for the effects of deck replacement, changes in loading conditions, changes in restraint conditions, and concrete deformations. Time-step analysis was used to calculate incremental changes in girder behavior throughout time, considering several lifespan stages delineated by changes in loading or boundary conditions. The B4 model (Wendner et al., 2013) was used to estimate the creep and shrinkage strain in the concrete. The model was validated against examples in the literature and applied to an example bridge to illustrate function. Modelling results suggest that deck replacement had minimal effect on long-term girder behavior for the bridge considered. A parametric study was also conducted to evaluate the influence of input parameter variations on long-term prestress loss, deflections, and stresses and strains for the example bridge. Parametric study results showed that girder behavior varies widely based on input parameters, suggesting that more research is needed to determine whether other bridge configurations would also be insensitive to deck replacement.

Acknowledgments

Financial support from the Kansas Department of Transportation (KDOT) is gratefully acknowledged. Mark Hurt (KDOT) provided important information and resources throughout the project that helped guide the efforts. Terry Fleck (Coreslab), Travis Rose (Bridges Inc.), Chris Rech (Cohron), Jesse Hinton (Emery Sapp), and DOT engineers who responded to the survey are also acknowledged for providing useful information.

Table of Contents

List of Tables

List of Figures

Notation

Symbol	Description	Units
E_c	Elastic modulus of the girder concrete	ksi
p_{4w}	Empirical creep parameters depending on cement type for B4 model (2.45 for all cement types)	
$(\Delta t)_n$	Time-step increments within $(T_e)_{n-1}$ and $(T_e)_n$	days
$(f_{b,Mr})_{deck}$	Stress at the bottom of the deck due to restraint moment	ksi
$(f_{b,sdl})_{deck}$	Stress at the bottom of the deck due to superimposed dead load	ksi
$(f_{t,Mr})_{deck}$	Stress at the top of the deck due to restraint moment	ksi
$(f_{t,sdl})_{deck}$	Stress at the top of the deck due to superimposed dead load	ksi
$(T_e)_n$	Point in time at which one time-step increment ends and another begins	days
$\Delta f_{b,dsh}(t)$	Change in stress at the bottom of the girder due to shrinkage of the deck	ksi
$\Delta f_{b,ndsh}(t)$	Change in stress at the bottom of the girder due to shrinkage of a new deck	ksi
$\Delta f_{cgp,deck}(t)$	Change in stress at the centroid of the prestressing strand due to shrinkage of the deck	ksi
Δf_{pES}	Loss due to elastic shortening of strands at release	ksi
Δf_{pR1}	Steel relaxation loss between the jacking of the strands to the time of prestress transfer	ksi
$\Delta f_{t,dsh}(t)$	Change in stress at the top of the girder due to shrinkage of the deck	ksi
$\Delta f_{t,ndsh}(t)$	Change in stress at the top of the girder due to shrinkage of a new deck	ksi
$\Delta P_{cr,ti(i-1)}$	Prestress loss due to girder creep between time t_{i-1} and t_i	kips
$\Delta P_{sh,ti(i-1)}$	Prestress loss due to girder shrinkage between time t_{i-1} and t_i	kips
$\Delta P_{ti(i-1)}$	Total prestress lost between time t_{i-1} and t_i	kips
ΔT	Temperature difference from the reference temperature at time *t*	°F
$\Delta\varepsilon_{cr,cgp}(t_n)$	Creep strain at centroid of the prestressing force at time t_n due to $\Delta P_{t(n-1)(n-2)}$ applied at time t_{n-1}	
a/c	Ratio of aggregate to cement weights in the mixture (no alternative cementitious materials, such as fly ash)	
A_c	Cross-sectional area of precast concrete girder without a bridge deck	$in.^2$
A_d	Cross-sectional area of the concrete deck	$in.^2$
aggtype	Type of aggregate used in concrete mixture	

Symbol	Description	Units
c	Cement content (no alternative cementitious materials, such as fly ash)	kg/m^3
$C_0(t,t')$	Basic creep compliance at time *t*	/Mpa
$C_d(t,t',t_0)$	Additional drying creep compliance at time *t*	/Mpa
ctype	Type of cement used in concrete mixture	
D	Effective cross-section thickness computed from V/S for the B4 model	mm
d_{gt}	Distance from the centroid of the girder to the centroid of the transformed area (considered zero)	in.
d_s	Diameter of prestressing strands	ksi
$d\varepsilon_{cr,bot}(t_i, t_{i-1})$	Total creep strain at the girder bottom fiber from time t_{i-1} to t_i	
$d\varepsilon_{cr,cgp}(t_n,t_{n-1})$	Total creep strain from time t_{n-1} to t_n	
$d\varepsilon_{cr,top}(t_i, t_{i-1})$	Total creep strain at the girder top fiber from time t_{i-1} to t_i	
$d\varepsilon_{sh,total}(t_n,t_{n-1})$	Total shrinkage strain from time t_{n-1} to t_n	
e	Eccentricity of prestressing strands relative to centroid of the precast girder at x (positive down)	in.
E_{cd}	Elastic modulus of deck concrete	ksi
e_d	Distance between the centroid of the deck and the centroid of the composite section	in.
e_{pc}	Distance between the centroid of the strands and the centroid of the composite section	in.
E_{ps}	Elastic modulus of prestressing strands	ksi
f_1	Width of the fillet at the intersection of girder top flange and web	in.
f_2	Width of the fillet at the intersection of girder bottom flange and web	in.
$f_{b,\ gdl}$	Stress at the bottom of the girder due to girder dead load	ksi
$f_{b,ddl}$	Stress at the bottom of the girder due to deck dead load	ksi
$f_{b,Mr}$	Stress at the bottom of the girder due to restraint moment	ksi
$f_{b,p}$	Stress at the bottom of the girder due to prestressing	ksi
$f_{b,sdl}$	Stress at the bottom of the girder due to superimposed dead load	ksi
f'_{cd}	Compressive strength of old deck concrete	ksi
f'_{cg}	Compressive strength of girder concrete	ksi
$f_{cgp,\Delta Pn}$	Stress at the centroid of the prestressing strands due to $\Delta P_{t(n)(n-1)}$	ksi

Symbol	Description	Units
f'_{ci}	Initial compressive strength of the girder concrete	ksi
f'_{cnd}	Compressive strength of new deck concrete	ksi
f_{Fj}	Concrete stress at the centroid of the prestressing strands due to final jacking force at the desired section	ksi
f_G	Concrete stress at the centroid of the prestressing strands due to girder dead load at the desired section	ksi
f_{PA}	Anchorage set loss (considered zero)	ksi
f_{pi}	Initial prestressing stress after accounting for anchorage set losses, strand relaxation before release, and elastic shortening at release	ksi
f_{PJ1}	Initial jacking stress applied to prestressing strands	ksi
f_{PJ2}	Final jacking stress in the prestressing strands	ksi
f_{Pu}	Ultimate tensile stress of the prestressing strands	ksi
f_{Py}	Yield stress of the prestressing strands	ksi
f_r	Modulus of rupture of girder concrete	ksi
$f_{t,ddl}$	Stress at the top of the girder due to deck dead load	ksi
$f_{t,gdl}$	Stress at the top of the girder due to girder dead load	ksi
$f_{t,Mr}$	Stress at the top of the girder due to restraint moment	ksi
$f_{t,p}$	Stress at the top of the girder due to prestressing	ksi
$f_{t,sdl}$	Stress at the top of the girder due to superimposed dead load	ksi
h	Relative humidity of the environment expressed as a decimal	
H	Overall height of the girder	in.
H_w	Depth of the girder web	in.
I_c	Transformed moment of inertia of composite section, neglecting reinforcement	$in.^4$
I_{cd}	Moment of inertia of the deck only	$in.^4$
I_{cg}	Moment of inertia of the girder only	$in.^4$
J(t,t')	Creep compliance function at time *t*	/Mpa
$J(t,T_1)$	Creep compliance function at time *t* caused by constant stress applied at age T_1	/Mpa
$J(t,T_2)$	Creep compliance function at time *t* caused by constant stress applied at age T_2	/Mpa
$J(t,T_3)$	Creep compliance function at time *t* caused by constant stress applied at age T_3	/Mpa
$J(t,T_4)$	Creep compliance function at time *t* caused by constant stress applied at age T_4	/Mpa

Symbol	Description	Units
$J(t,T_5)$	Creep compliance function at time *t* caused by constant stress applied at age T_5	/Mpa
$J(t,T_6)$	Creep compliance function at time *t* caused by constant stress applied at age T_6	/Mpa
k_h	Humidity-dependent factor for shrinkage	
K_{id}	Transformed section coefficient for the time-dependent interaction between concrete and bonded strands	
k_s	Shape parameter for the B4 model	
$k_{\epsilon a}$	Empirical aggregate-dependent parameters calculated for the B4 model (0.76 for diabase, 0.71 for quartzite; 0.95 for limestone; 1.60 for sandstone; 1.05 for granite; 2.20 for quartz diorite)	
$k_{\tau a}$	Aggregate-dependent parameter for the B4 model (0.06 for diabase, 0.59 for quartzite; 1.80 for limestone; 2.30 for sandstone; 4.00 for granite; 15.0 for quartz diorite)	
L_{cant}	Length of the cantilever deck slab over the cross-section of the bridge	ft
loc	Location of the girder in the bridge (interior or exterior)	-
loc_{harp}	Location of harping points (if any present, 0 otherwise)	ft
L_{span}	Bridge span length	ft
l_{tr}	Transfer length at the end of the girder required to transfer prestressing force from the strands to the concrete	in.
M_{cr}	Cracking moment of the girder	kip-ft
M_{ddl}	Moment due to deck dead load	kip-ft
M_{gdl}	Moment due to girder dead load	kip-ft
$M_r(t)$	Restraint moment developed at time *t*	kip-ft
$M_{r,cr}\ (t_i)$	Total restraint moment developed due to concrete creep until time t_i	kip-ft
$M_{r,cr}\ (t_i, t_{i-1})$	Restraint moment due to concrete creep from time t_{i-1} to t_i	kip-ft
$M_{r,sh}\ (t_i)$	Total restraint moment due to differential shrinkage until time t_i	kip-ft
M_{sdl}	Moment due to superimposed dead load	kip-ft
n_1	Number of time steps between T_1 and T_2	
n_2	Number of time steps between T_2 and T_3	
n_3	Number of time steps between T_3 and T_4	
n_4	Number of time steps between T_4 and T_5	
n_5	Number of time steps between T_5 and T_6	
n_6	Number of time steps between T_6 and T_7	

Symbol	Description	Units
N_{girder}	Number of girders in the bridges	
n_{pi}	Ratio of elastic modulus of the prestressing strand to the initial elastic modulus of the concrete	
$N_{sh}(t)$	Axial force due to different shrinkage at time *t*	kips
$N_{strands}$	Number of prestressing strands	
p_2	Empirical creep parameters depending on cement type for B4 model (58.6×10^{-3} for normal; 17.4×10^{-3} for rapid hardening; 40.5×10^{-3} for slow-hardening cement)	
p_{2w}	Empirical creep parameters depending on cement type for B4 model (3 for all cement types)	
p_3	Empirical creep parameters depending on cement type for B4 model (39.3×10^{-3} for all cement types)	
p_{3a}	Empirical creep parameters depending on cement type for B4 model (-1.10 for all cement types)	
p_{3w}	Empirical creep parameters depending on cement type for B4 model (0.40 for all cement types)	
p_4	Empirical creep parameters depending on cement type for B4 model (58.6×10^{-3} for all cement types)	
p_{4a}	Empirical creep parameters depending on cement type for B4 model (-0.90 for all cement types)	
p_5	Empirical creep parameters depending on cement type for B4 model (777×10^{-3} for normal; 94.6×10^{-3} for rapid hardening; 496×10^{-3} for slow-hardening cement)	
p_{5a}	Empirical creep parameters depending on cement type for B4 model (-1 for all cement types)	
p_{5H}	Empirical creep parameters depending on cement type for B4 model (8 for normal; 1 for rapid hardening; 8 for slow-hardening cement)	
$p_{5\epsilon}$	Empirical creep parameters depending on cement type for B4 model (-0.85 for all cement types)	
P_e	Effective prestressing force at the considered section	kips
$P_{e,\ t(i)(i-1)}$	Prestressing force at the end of time step t_i	kips
$P_{e,t}$	Effective prestressing force at time *t*	kips
$P_{e,t(i+1)(i)}$	Prestressing force at the end of time step t_{i+1}	kips
P_{J1}	Initial jacking force applied to prestressing strands (after deducting the anchorage set loss)	kips
P_{J2}	Final jacking force in the prestressing strands	kips
pstype	Type of prestressing strands (low-relaxation or stress-relieved)	

Symbol	Description	Units
$p_{\epsilon a}$	Empirical shrinkage parameter depending on cement type for the B4 model (-0.80 for all cement types)	
$p_{\epsilon c}$	Empirical shrinkage parameter depending on cement type for the B4 model (0.11 for all cement types)	
$p_{\epsilon w}$	Empirical shrinkage parameter depending on cement type for the B4 model (1.10 for normal; -0.27 for rapid hardening; 1.00 for slow-hardening cement)	
$p_{\tau a}$	Empirical shrinkage parameter depending on cement type for the B4 model (-0.33 for all cement types)	
$p_{\tau c}$	Empirical shrinkage parameter depending on cement type for the B4 model (-0.10 for normal; -2.70 for rapid hardening; 3.80 for slow-hardening cement)	
$p_{\tau w}$	Empirical shrinkage parameter depending on cement type for the B4 model (-0.06 for normal; -2.40 for rapid hardening; 3.55 for slow-hardening cement)	
q_2	Parameter for aging viscoelastic creep for the B4 model	
q_3	Parameter for non-aging viscoelastic creep for the B4 model	
q_4	Parameter for flow for the B4 model	
q_5	Parameter for drying creep for the B4 model	
R	Gas constant	$J.mol^{-1}.K^{-1}$
r_{nc}	Radius of gyration of the non-composite girder	in.
r_t	Autogenous shrinkage parameter depending on cement type for the B4 model (-4.50 for all cement types)	
R_T	Vertical scaling factor to account for the effect of temperature as defined in the B4 model	
r_α	Autogenous shrinkage parameter depending on cement type for the B4 model (1.00 for normal; 1.40 for rapid hardening; 1.00 for slow-hardening cement)	
$r_{\epsilon a}$	Autogenous shrinkage parameter depending on cement type for the B4 model (-0.75 for all cement types)	
$r_{\epsilon w}$	Autogenous shrinkage parameter depending on cement type for the B4 model (-3.50 for all cement types)	
$r_{\tau w}$	Autogenous shrinkage parameter depending on cement type for the B4 model (3.00 for all cement types)	
S(t)	Modification factor in the B4 shrinkage model for time since removal from curing	
S_{bc}	Section modulus at the bottom of the girder, considering composite section and neglecting reinforcement	$in.^3$
S_{bnc}	Section modulus at the bottom of a precast girder, omitting bridge deck and neglecting reinforcement	$in.^3$

Symbol	Description	Units
span	Type of span (end or mid-span)	
sprofile	Profile of prestressing strands in the girder (straight, parabolic, singly-harped, or doubly-harped)	
S_{tc}	Section modulus at the top of the precast girder, considering composite section and neglecting reinforcement	$in.^3$
S_{tnc}	Section modulus at the top of the precast girder, omitting bridge deck and neglecting reinforcement	$in.^3$
t	Age of concrete	days
T	Mean environmental temperature before and after load application	°F
t'	Age of loading of concrete	days
t_0	Age of concrete when exposed to the environment (i.e., age of concrete when removed from curing)	days
t_0'	Maximum value of age of environmental exposure (t_0) and age of loading (t')	days
t_{0d}	Age when old deck concrete is removed from curing	days
t_{0nd}	Age when new deck concrete is removed from curing	days
T_1	Time of prestress transfer (i.e., age of concrete when prestress and self-weight of the girder are applied)	days
T_2	Age of girder concrete when deck slab is placed and continuity diaphragm is cast	days
T_3	Age of girder concrete when superimposed dead loads of wearing surface/barrier/curbs are applied on the deck	days
T_4	Age of girder concrete when the deck is removed	days
T_5	Age of girder concrete when a new deck slab is added	days
T_6	Age of girder concrete when new superimposed dead loads are added to the new deck	days
T_7	Final age of the concrete	days
T_{bf1}	Thickness of the girder bottom flange at the end	in.
T_{bf2}	Thickness of the girder bottom flange at the intersection of web and flange	in.
T_{cur}	Temperature at curing (between 20°C and 30°C)	°F
t_d	Thickness of the old deck	in.
t_{nd}	Thickness of the new (replaced) deck	in.
t_{nws}	Thickness of the new wearing surface	in.
t_{pt}	Time from jacking of strands to prestress transfer	days
T_{ref}	Reference temperature at which thermal strain is zero	°F
T_{tf1}	Thickness of the girder top flange at the end	in.

Symbol	Description	Units
T_{tf2}	Thickness of the girder top flange at the intersection of web and flange	in.
T_w	Thickness of girder web	in.
t_{ws}	Thickness of the old wearing surface	in.
U_h, U_c, U_S	Activation energies for moisture diffusion, drying shrinkage, and creep	J/mol
V/S	Ratio of precast member volume to surface area	mm.
w/c	Ratio of water to cement weights in the mixture (no alternative cementitious materials, such as fly ash)	
$w_{barrier}$	Weight per length of the barrier in old deck	kips/ft/side
W_{bf}	Width of the girder bottom flange	in.
W_{girder}	Distance between the girders	ft
$w_{nbarrier}$	Weight per length of the barrier in the new deck	kips/ft/side
W_{tf}	Width of the girder top flange	in.
W_{total}	Total width of the road	ft
y_b	Distance of the bottom girder fiber from the neutral axis of the non-composite girder	in.
y_{bc}	Distance between the centroid of the composite section and the bottom of a girder	in.
y_{bd}	Distance of the bottom deck fiber from the neutral axis of the composite section	in.
y_{ps}	Distance of centroid of the strands from the bottom of the girder	in.
y_t	Distance of the top girder fiber from the neutral axis of the non-composite girder	in.
y_{tc}	Distance between the centroid of the composite section and the top of the girder	in.
y_{td}	Distance of the top deck fiber from the neutral axis of the composite section	in.
z_{dg}	Distance between the centroid of the slab and the centroid of the composite section (girder + slab)	in.
α	Water-cement ratio dependent exponent to calculate shrinkage in the B4 model	
α_T	Thermal coefficient of expansion for concrete	/°F
β_{Th}	Factor governing activation energies and temperature effects when calculating drying shrinkage for the B4 model	
β_{Ts}	Factor governing activation energies and temperature effects when calculating drying shrinkage for the B4 model	
γ_c	Unit weight of concrete	kcf

Symbol	Description	Units
γ_{nws}	Unit weight of the wearing surface in the new deck	kcf
γ_{ws}	Unit weight of the wearing surface in the old deck	kcf
$\Delta M_{sh,i(i-1)}$	Moment due to differential shrinkage between time t_i and t_{i-1}	kip-ft
$\Delta N_{sh,i(i-1)}$	Axial force due to differential shrinkage between time t_{i-1} to t_i	kips
ε_0	Final drying shrinkage calculated from the B4 model	
$\varepsilon_{au}(t,t_0)$	Autogenous shrinkage at time *t* in concrete removed from curing at time t_0	
$\varepsilon_{au,cem}$	Autogenous shrinkage parameter depending on cement type for the B4 model	
$\varepsilon_{au\infty}$	Final autogenous shrinkage in the B4 model	
ε_{cem}	Empirical shrinkage parameter depending on cement type for the B4 model (360×10^{-6} for normal; 860×10^{-6} for rapid hardening; 410×10^{-6} for slow-hardening cement)	
$\varepsilon_{cr}(t,t')$	Total creep strain at time *t* due to loading applied at *t'*	
$\varepsilon_{cr,bot}(t)$	Creep strain at the bottom fiber of the girder at time *t*	
$\varepsilon'_{cr,bot}(t_n,t_{n-1})$	Change in creep strain at girder bottom fiber from time t_{n-1} to t_n	
$\varepsilon'_{cr,cgp}(t_n,t_{n-1})$	Change in creep strain at centroid of the prestressing strands from time t_{n-1} to t_n	
$\varepsilon_{cr,cgp}(t_i,t_{i-1})$	Creep strain at the centroid of the strain between time t_{i-1} and t_i	
$\varepsilon_{cr,top}(t)$	Creep strain at the top fiber of the girder at any time *t*	
$\varepsilon'_{cr,top}(t_n,t_{n-1})$	Change in creep strain at the girder top fiber from time t_{n-1} to t_n	
$\varepsilon_{sh}(t,t_0)$	Drying shrinkage strain at time *t* in concrete removed from curing at time t_0	
$\varepsilon_{sh,cgp}(t_i,t_{i-1})$	Shrinkage strain at the centroid of the strands between time t_{i-1} and t_i	
$\varepsilon_{sh,deck}(t,t_0)$	Shrinkage of the deck at time *t*, assumed to be uniform through the deck thickness	
$\varepsilon_{sh,slab}(t)$	Shrinkage strain of the concrete deck at time *t* in the concrete removed from curing at time t_{0d}	
$\varepsilon_{sh,total}(t,t_o)$	Total shrinkage strain of girder concrete at time *t* exposed to the environment at t_0	
$\varepsilon_{sh\infty}(t_0)$	Ultimate drying shrinkage as a function of curing time t_0	
ε_{temp}	Thermal strain caused by temperature difference	
ρ	Mass density of concrete	kg/m^3

Symbol	Description	Units
σ_i	Uniaxial constant stress applied at *t'*	Mpa
τ_0	Drying shrinkage calculation factor accounting for the effects of aggregate-cement ratio, water-cement ratio, cement content, and cement type in the B4 model	
τ_{au}	Autogenous shrinkage halftime for the B4 model, representing the speed of autogenous shrinkage evolution	
$\tau_{au,cem}$	Autogenous shrinkage parameter depending on cement type for the B4 model (1.00 for normal; 41.0 for rapid hardening; 1.00 for slow-hardening cement)	
τ_{cem}	Empirical shrinkage parameter depending on cement type for the B4 model (0.016 for normal; 0.080 for rapid hardening; 0.010 for slow-hardening cement)	
τ_{sh}	Drying shrinkage halftime in the B4 model	days
Φ_w	Strength reduction factor	
Ψ_{cr} (t_i,t_{i-1})	Change in girder curvature due to concrete creep developed from time t_{i-1} to t_i	/in.

Chapter 1: Introduction

1.1 Background

Although prestressed concrete girders have an expected service life of more than 50 years, concrete decks continually experience cracking, wear from traffic, and exposure to deicing salts, causing the service life of a concrete deck to range from 20 to 40 years (Boatman, 2010; Hearn & Xi, 2007). Consequently, the supporting prestressed concrete girders of a bridge could be in good condition, while the concrete deck requires replacement. Prestressed concrete girder bridges may undergo one or more full-depth bridge deck replacements during their service life.

Kansas has a large inventory of prestressed concrete girder bridges, many of which will require deck replacement by 2030, so understanding the impacts of deck removal and the replacement process on overall bridge performance is essential. A primary concern is that deck removal could damage the girder and render it unserviceable (Li et al., 2019; Assad & Morcous, 2016). There are, however, ways to remove a deck to minimize girder damage (Chapter 2). Deck replacement may also affect the short- and long-term girder stresses, deflections, and prestress forces. It is important to make sure stresses during and after deck replacement do not exceed limits, and the replacement must result in a level deck surface. Quantifying the impact of the replacement process on girder performance can help determine whether a deck replacement is preferable to replacing the entire bridge.

The estimation of long-term prestressed concrete bridge behavior is challenging because strains and stresses change over time. The initial camber due to prestressing decreases due to short-term prestress losses, while the deck load and superimposed dead loads alter the internal stress distribution. Changes in restraint conditions due to added diaphragms and a continuous deck also affect girder stresses. In addition, long-term deformations from concrete creep and shrinkage cause girder curvature and alter internal stresses. Other factors, including changes in the modulus of elasticity of concrete, effects of unloading and reloading, daily and seasonal temperature changes, and their interactions, further complicate the problem.

This study developed a realistic structural model that accounts for time-dependent effects to assess the impacts of bridge deck replacement on bridge performance. Time-step analysis procedures were applied, wherein the design life of the structure was divided into discrete time

intervals, and then force, stress, and deformation calculations were updated at each step. The model outputs estimated girder stresses across the span and depth, girder deflections throughout the span, creep and shrinkage strains, and prestress losses over time. The model can be used to study how bridge design parameters affect long-term bridge behavior and to identify conditions under which bridge deck replacements likely cause unacceptable stresses or deflections.

1.2 Research Significance: DOT Survey Results

The research team surveyed bridge engineers at various state departments of transportation (DOTs) to document current deck removal practices. Survey (Appendix A) questions addressed the number of deck removals to date, problems encountered, long-term effects of deck replacement, and plans for re-decking existing bridges. The survey also addressed whether and how states analyze the long-term effects of deck removal on bridge behavior.

Survey responses were received from 31 state DOTs (62% response rate), of which 19 (61% of respondents) had conducted full-depth deck replacements as of April 2022 and 23 (74% of respondents) expected to conduct full-depth deck replacements soon. The responses show that bridge deck replacements are increasingly common, meaning increased understanding of the long-term implications of deck replacements is essential.

A variety of survey responses described current deck removal practices. Common practices included (1) verifying the camber and deflection profiles of the bridge by surveying and calculating load-carrying capacity before and after deck replacement, (2) taking shim shots (measurement of girder elevations using a laser level) and adjusting the grade accordingly when pouring the new deck, (3) updating the design and construction details of new bridges to facilitate future deck replacements, such as placing bond breakers at the edges of the girder top flanges to ease future deck removal, (4) intentional focus on controlling the demolition process to limit damage, and (5) use of commercial structural analysis software and engineering judgment to assess long-term deformations due to deck replacement.

Survey respondents also identified problems encountered during deck removal, such as: (1) damage to the top flanges of the prestressed girder, (2) girder cracking, (3) damage to the

horizontal shear reinforcement linking the girder to the deck, and (4) constructability issues due to greater-than-expected girder camber rebound, which complicates the placement of deck formwork.

Although 61% of survey respondents have performed deck replacements and 74% expect to soon, only three DOTs (13% of respondents) have plans to analyze the long-term effects of deck replacements. Therefore, research is needed to increase understanding of the long-term effects of deck replacements on prestressed concrete girders. The proposed model will help determine whether, and under what conditions, deck replacements may be problematic.

1.3 Objectives

The objective of this study was to build a model to assess the effects of removing and replacing a damaged concrete deck over prestressed concrete girders. The main research tasks included the following:

1. Review the literature on the deck removal process, prestressed concrete girders, prestress losses, and long-term deformations in concrete.
2. Survey engineers at state DOTs to document deck replacement practices in the United States.
3. Develop and validate a model to evaluate the long-term performance of a prestressed concrete girder, including the calculation of stresses/strains and camber/deflection throughout the service life.
4. Apply the model to a prestressed concrete girder bridge to illustrate the effects of deck replacement on bridge behavior.

1.4 Scope

This study developed a detailed analytical model to simulate bridge superstructure behavior to analyze prestressed concrete I-girder bridges with bonded tendons. The product of this study is an analytical tool to estimate the camber, deflection, rebound, effective prestressing, stresses, and strains at any time throughout the service life of a bridge. A parametric study was also conducted to show the influence of design variables, loadings, and environmental parameters on an example bridge. The study was limited to linear and elastic material behavior in response to load; it does not consider temperature variations or gradients, damage caused during deck replacement, live

load effects, concrete deterioration, or reinforcement corrosion. Several assumptions were also made for model development, as described in Chapter 3, and the model is applicable only to cases where the enumerated underlying assumptions are reasonable. The results of this study will help the Kansas Department of Transportation (KDOT) determine the suitability of deck replacements for existing bridges.

Chapter 2: Literature Review

2.1 Creep and Shrinkage

Creep, the gradual deformation of concrete over time under sustained load, results from changes to the concrete microstructure and the hydration of unhydrated cement particles (Bažant & Jirásek, 2018). Concrete creep consists of basic creep and drying creep. Basic creep occurs at constant moisture content, whereas drying creep is a result of moisture movement in the concrete (Bažant & Jirásek, 2018). The impacts of creep on a prestressed concrete girder include increased deformation under sustained loads, redistribution of stresses when continuity diaphragms limit girder-end rotation, and prestressing losses (Granata et al., 2013). Bažant (2001) contains a detailed description of mechanisms that cause and influence creep, physical phenomena involved, mathematical estimation models, and computational approaches.

Shrinkage is the contraction of concrete caused by moisture loss from drying and cement hydration. Specifically, "drying shrinkage is caused by compressive stresses in the microstructure that balance variations in capillary tension, surface tension, and disjoining pressure in adsorbed water layers in nanopores in concrete". Autogenous shrinkage is caused by self-desiccation as water is consumed by the cement hydration reaction (Bažant et al., 2015). Shrinkage strain in concrete can cause the girder length to decrease, resulting in decreased initial tension force in the prestressing strands, leading to prestress loss. Concrete shrinkage impacts prestress loss, camber, and long-term deformation of the girder.

2.1.1 Accurate Estimation of Creep and Shrinkage

Despite extensive research, accurate estimation of the effects of creep and shrinkage is challenging due to the limited availability of long-term experimental studies on creep and shrinkage for model calibration and verification, the time-varying nature of creep and shrinkage, the variability of material properties of concrete constituents (aggregate, cement, water), and structural complexity that affects the degree of restraint and internal distribution of stresses. Inaccurate creep and shrinkage estimates can lead to inaccurate estimates of prestress losses, leading to uneconomical or unsafe bridge designs (Kamatchi et al., 2014). Bažant et al. (2015, 2012a, 2012) investigated damage in prestressed concrete structures caused by creep and

shrinkage, including excessive deflections, excessive cracking, prestress losses, and long-term deterioration. The failure of the Koror-Babeldaob (KB) bridge in Palau is an example of creep underestimation leading to excessive deflection of the bridge (Bažant et al., 2012a, 2012b). Bažant et al. (2011) argued that the main cause of underestimation is the use of inaccurate creep and shrinkage models and obsolete beam-type creep analysis programs. Other studies have shown that the magnitude of creep and shrinkage can vary significantly depending on the selected model (Menkulasi et al., 2018).

2.1.2 Selection of Creep and Shrinkage Model

The selection of an accurate model for creep and shrinkage is essential to obtain reasonable estimates of long-term bridge behavior (Granata et al., 2013; Menkulasi et al., 2018). ACI 209R-92 (2008) recommends sensitivity analyses and short-term testing of concrete to determine the suitability of any model. Criteria for model selection are also described in Bažant and Jirásek (2018). Calibration against tests of sample concrete was not applicable to this study because the research objective was to develop a general model applicable to most bridges, not one specific bridge. However, several models were considered for creep and shrinkage, including ACI 209R-92 (1997), B3 (Bažant et al., 1995), GL2000 (Gardner & Lockman, 2001), B4 (Wendner et al., 2013; Bažant et al., 2015), and the AASHTO LRFD (2012) models.

Previous studies have compared results from various creep and shrinkage models and evaluated their estimations of concrete behavior, proving that the choice of model for creep and shrinkage has a considerable effect on calculated values (Granata et al., 2013; Menkulasi et al. 2018; Robertson 2005). Figure 2.1 shows calculated creep compliance values, or creep strain per unit of stress, from the ACI 209R-92, CEB MC90-99 (1993), B3, GL2000, and AASHTO LRFD models. As shown in the figure, models B3 and GL2000 provide the highest creep coefficient and hence higher prestress loss and larger deflection. The AASHTO LRFD model provided the highest estimate of shrinkage.

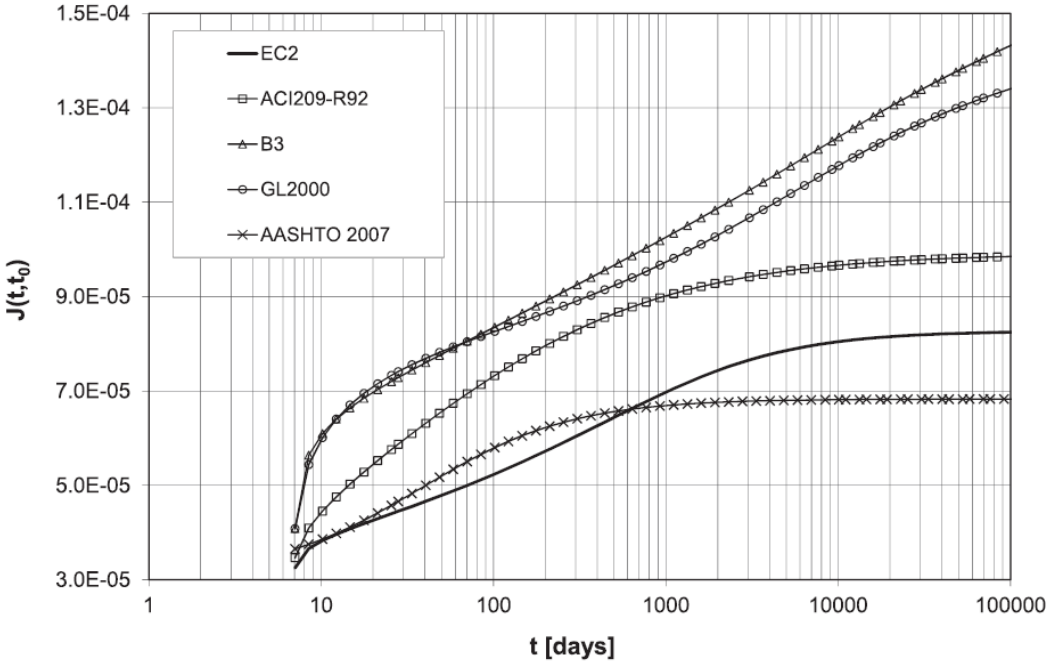

Figure 2.1: Comparison of Creep Compliance (per MPa) for Various Creep Models
Source: Granata et al. (2013)

In a similar comparison, Menkulasi et al. (2018) used the ACI 209R-92, CEB MC90-99, B3, GL2000, and AASHTO LRFD models to highlight variations of creep coefficient estimates of 1.2 to 6.2 and shrinkage strains of 300 to 780 microstrain. The creep coefficient is the ratio of creep strain to the elastic strain. The model rankings for highest to lowest calculated creep strains were GL2000, B3, CEB MC90-99, ACI209R-92, and AASHTO LRFD. Similarly, the model rankings for highest to lowest calculated shrinkage strains were ACI 209R-92, B3, CEB MC90-99, GL2000, and AASHTO LRFD.

Robertson (2005) studied a long-span prestressed concrete bridge for nine years to determine long-term deformations and strains. Creep and shrinkage tests were performed on concrete cylinders made from concrete used in the instrumented bridge. Test results were compared to estimates obtained from the ACI 209R-92, CEB MC90-99, B3, and GL2000 models. Analysis results showed that the B3 model (Bažant et al., 1995) provided the most accurate long-term estimate of creep and that the GL2000 model (Gardner & Lockman, 2001) provided the most accurate estimate of shrinkage. Bažant and San (1994), however, identified several limitations of the GL2000 model, including lack of a final asymptotic value of shrinkage, disagreement between

the initial shrinkage curve and diffusion theory, and negative initial shrinkage values. ACI 209R.2-08 performed a statistical comparison of results from several models to a database of creep and shrinkage test results and concluded that the B3 model is most accurate relative to test data.

2.1.2.1 Criteria for Model Selection

This study reviewed the ACI 209R-92 (1997), B3 (Bažant et al., 1995), GL2000 (Gardner & Lockman, 2001), B4 (Wendner et al., 2013; Bažant et al., 2015), and AASHTO LRFD (2012) models for this research. Although long-term in-situ data from bridges would have been ideal for model assessment, these data were unavailable. Therefore, the models were compared against the following evaluation criteria for creep and shrinkage models recommended in ACI 209R-92 (1997):

1. The model should account for ambient relative humidity, age at loading, duration of drying, duration of loading, specimen size, and description of concrete as either mixture proportions or mechanical properties.
2. The model should allow for changes in relative humidity.
3. Drying shrinkage and drying creep should not increase indefinitely with time.
4. Shrinkage and creep models should be compared with data from a database that is suitable for model conditions. Certain experimental data may not be suitable for evaluating a particular model. Experimental data from concrete with a low water-cement ratio, for instance, may not accurately estimate creep and shrinkage in concrete with a high water-cement ratio.
5. The model should produce creep values in terms of compliance or specific creep rather than a creep coefficient. Compliance is the total strain (elastic + creep) per unit of stress applied, specific creep is the rate of strain per unit stress applied, and creep coefficient is the ratio of the creep strain to the elastic strain. Creep compliance accounts for total deformation that occurs over time, including instantaneous and delayed deformation, whereas the creep coefficient only provides a measure of rate of deformation at a given

time. Creep compliance is a more reliable measure of the long-term behavior of concrete structures under load.

6. Shrinkage and creep equations should be applicable to concrete with admixtures.
7. Recovery of creep strain under complete unloading should not exceed the creep strain from loading and should asymptotically approach a constant value.
8. The equation used to describe creep and shrinkage should extrapolate the behavior of the material beyond the range of experimental data used to develop the equations.
9. The equations should be simple to use, and small variations in the input parameters should not greatly affect the accuracy of the estimated values.
10. The trend of the shrinkage and creep curves should align with the trend of individual test results across a broad range of time frames.
11. Creep expressions should account for drying before loading.

2.1.2.2 B4 Model for Creep and Shrinkage Calculation

The previous studies, especially Robertson (2005), showed that the B3 model provides the most accurate estimate for concrete creep. The B3 model also complies with all previously listed selection criteria. Therefore, the B4 model (Wendner et al., 2013; Bažant et al., 2015), which is an updated version of the B3 model, was selected for use in this study for both creep and shrinkage strain estimates. The B4 model has the following additional features, relative to B3 (according to Wendner et al., 2015): (1) the B4 model is based on a larger dataset, so it has a larger range of applicability than the B3 model. For example, the B4 model is applicable to high-performance concrete with admixtures, (2) the B4 model is calibrated to the Northwestern University (NU) database, with creep and shrinkage data collected over a longer loading period than used for the B3 model, and (3) shrinkage strain in the B4 model is split into a sum of drying shrinkage and autogenous shrinkage, whereas the B3 model does not account for autogenous shrinkage separately (autogenous shrinkage has a different physical mechanism than drying shrinkage and is essential

for high-performance concrete with admixtures, additives, and low water-cement ratios per Hubler et al., 2015).

The B4 model, which is based on the solidification theory and the micro-prestress theory, is based on the NU database that includes test results from approximately 1,400 creep specimens and 1,800 shrinkage specimens as well as data from 69 excessively or strongly deflecting large-span prestressed segmentally erected box-girder bridges (Wendner et al., 2013, 2015). This dataset advantageously includes results from large-span prestressed concrete bridges; other models for creep and shrinkage primarily are based on databases comprised of creep and shrinkage test data from six years or less (Bažant & Li, 2008). Use of models based on relatively short creep and shrinkage tests can lead to inaccurate estimates of long-term creep and underestimations of deflections and prestress loss that, according to Bažant et al. (2012a, 2012b), were major factors in the failure of the Koror-Babeldaob (KB) bridge in Palau. The B4 model aims to address these limitations and provide more accurate estimates of multi-decade behavior in concrete. Chapter 3 describes parameters of the B4 model, including concrete composition, aggregate and cement type, relative humidity and temperature, duration of curing, age of loading, specimen size, admixtures, and concrete strength. These parameters allow model application to high-performance concrete and account for differences in mixture design without requiring concrete samples for calibration. The B4 model distinguishes the creep into basic and drying creep (Wendner et al., 2013).

2.1.2.3 Age-Adjusted Effective Modulus

Age-adjusted effective modulus (AAEM) historically has been a common method to account for the effect of creep in structural analysis. Trost and Marsh (1967) introduced the concept of the aging coefficient to account for the effect of creep in concrete, and Bažant (1972) combined the aging coefficient with the effective modulus method to develop the AAEM, which estimates increased concrete deformation and decreased stress over time due to creep effects.

Briefly, concrete strain is calculated at age t due to (1) a stress $\sigma_c(t_0)$ introduced at age t_0, sustained during the period of $(t-t_0)$; (2) a stress increment initially zero at t_0, increasing gradually to the final value of $\Delta\sigma_c(t)$ at age t; and (3) free shrinkage, $\varepsilon_{cs}(t, t_0)$, occurring during $(t-t_0)$ (Ghali et al., 2018):

$$\varepsilon_c(t) = \sigma_c(t_0)\frac{1 + \varphi(t,t_0)}{E_c(t_0)} + \frac{\Delta\sigma_c(t)}{E_c(t,t_0)} + \varepsilon_{cs}(t,t_0) \qquad \textbf{Equation 2.1}$$

The AAEM, $E_c(t,t_0)$, in Equation 2.1 is a function of the aging coefficient, χ, the creep coefficient due to stress applied at t_0 and sustained to time t,$\varphi(t,t_0)$, and elastic modulus of concrete at age t_0, $E_c(t_0)$, as shown below:

$$E_c(t,t_0) = \frac{E_c(t_0)}{1 + \chi\varphi(t,t_0)} \qquad \textbf{Equation 2.2}$$

The primary advantage of the AAEM is that stresses and deformation are only calculated at the initial time, t_0, and then AAEM is applied to estimate these effects at any time t, thus limiting time-consuming calculations and improving efficiency (Wang & Gong, 2019). The disadvantage of the method is that it does not account for variable loads (Khazanovich, 1990). Although AAEM can be useful for structures with low sensitivity to creep deformations, the B4 model is reportedly more appropriate for sensitive structures (Bažant et al., 2015). Based on the project requirements and scope, the B4 model was selected for this study instead of the AAEM method.

2.1.3 Creep Recovery

When a load is removed from a structure, creep caused by the load is released gradually rather than abruptly. Superposition can be used to simulate this effect by adding a negative load to the structure instead of removing the existing load (Gilbert, 1988; Lockman, 2002; ACI 209R-92, 2008). The effects of each change in load, positive or negative, are then calculated separately and summed at each time-step. If superposition is used to estimate creep recovery, ACI209.2R-08 (2008) states that the basic and drying creep compliance functions must be parallel in time, meaning that the rate of change of compliance functions with time should be the same to produce consistent compliance after unloading. Lockman (2002) notes that drying creep caused by moisture expulsion from concrete cannot be recovered, indicating that 100% of creep cannot be recovered with the removal of load. As a result, superposition tends to overestimate the recovery. Although no method calculates recovery via superposition in a drying environment (ACI 209R-92, 2008), Lockman (2002) conducted tests on sealed normal strength concrete specimens loaded at 7 days

and unloaded at 107 days to and showed that the GL2000 and B3 models provided realistic creep recovery when superposition is applied. Only these models resulted in decreased strain and a constant value of strain following load removal after a certain period of time. In other models, such as Atlanta 97 (Gardner & Zhao, 1994), CEB MC 90, and ACI 209, the creep initially decreased upon load removal but eventually increased, which is not realistic, as shown in Figure 2.2.

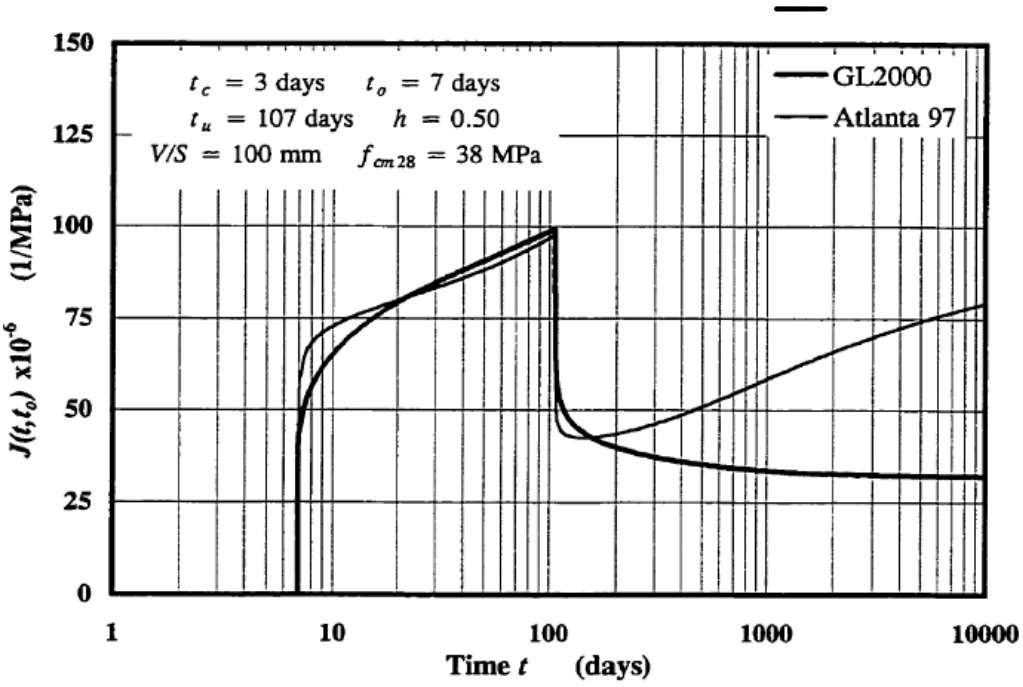

Figure 2.2: Creep Recovery of Sealed Concrete for GL2000 and Atlanta 97 Models
Source: Lockman (2002)

According to Wendner et al. (2015), the B4 model efficiently calculates creep recovery via superposition and satisfies the non-divergence condition that ensures creep recovery by applying the principle of superposition, which is always monotonic, with no possibility of recovery reversal. In other words, the creep strain recovery function must converge to a single value as the duration of load approaches infinity. Therefore, this study used superposition to estimate creep recovery from deck removal and replacement.

2.1.4 Differential Shrinkage

Concrete girders and decks are made with concretes having different properties that are placed at different times. For example, prestressed concrete girders are commonly constructed off-site, whereas most concrete decks are cast-in-place, meaning girder concrete shrinkage has already

mostly occurred when the deck concrete is placed and begins to shrink. The resulting differential shrinkage between the deck and the girder causes downward deflection of the girder (Birkeland, 1960). Shrinkage in the slab is restrained by the deck reinforcement and interface between the bottom of the deck and the girder top flange. This interaction causes tensile stress in the bottom of the slab and compressive stress in the top flange. When tensile stress in the deck exceeds the cracking limit, the deck begins to crack and stresses at those locations are released. Kasera (2014) showed that the older the girder is when the slab is cast, the higher the tensile stress and the sooner deck cracking occurs.

This current study simulated deck shrinkage by applying a fictitious external load to the composite non-transformed section as recommended by PCI (1997). The external force was calculated using AASHTO LRFD (2012) equations based on the deck shrinkage strain, as discussed in Chapter 3. Kovach (2008) and Saha (1984) provide details on differential shrinkage, but the magnitude of simulated external force was difficult to accurately estimate because of deck cracking. Therefore, a differential shrinkage strain equal to 50% of the deck shrinkage was used to account for the deck cracking, as recommended by PCI (1997).

2.1.5 Non-linear Creep and Non-uniform Shrinkage

Concrete creep can be non-linear due to humidity and temperature variation, strain-softening, cyclic loading, unloading, high stress, and multiaxial viscoplasticity (Bažant & Jirásek, 2018; Bažant 1988). Creep is linearly proportional to applied stress and can be described by linear viscoelasticity for service stress levels up to 60% of ultimate strength and at constant moisture levels (Atrushi, 2003). Non-linear creep was therefore neglected in this study because service-level stresses should remain below 60% of ultimate strength, and large-amplitude stress and moisture cycles are not typically anticipated in practice.

Non-uniform shrinkage refers to uneven shrinkage through the cross-section of a structure that occurs when various parts of the material shrink at different rates due to non-uniform moisture distributions, temperature gradients, or variations in concrete properties. Birhane et al. (2020) studied the impact of non-uniform shrinkage on the long-term deflection of a prestressed concrete bridge and found that only axial shortening is induced by uniform shrinkage, whereas non-uniform

shrinkage can induce a curvature. This current study assumed uniform moisture distribution, temperature gradient, and concrete properties throughout the cross-section of the girder, so the impacts of non-uniform shrinkage were not considered. Consequently, the creep was assumed to behave linearly, and the shrinkage was assumed to be uniform throughout the girder.

2.1.6 Creep in Compression and Tension

Although many previous studies have investigated concrete creep in compression, minimal research has studied concrete creep in tension. Rossi et al. (2013) studied the relationship between creep in compression, tension, and bending under drying conditions for normal-strength concrete and found that drying conditions, which include environmental conditions with moisture evaporation from concrete, have axial tensile creep that is greater than or equal to axial compressive creep. Bending creep is less than axial tensile creep and greater than axial compressive creep. In the bending test, the compressive bending creep strains were similar in magnitude to the tensile bending creep strains (Rossi et al., 2013). In contrast, for sealed concrete where moisture evaporation is not possible, axial compressive creep and bending creep were shown to be greater than axial tensile creep (Atrushi, 2003). Bažant and Jirásek (2018) asserted that no difference can exist between creep in tension and compression within the range of applicability of linear constitutive models, while Wendner et al. (2015) advised that the creep compliance function of the B4 model applies to both tensile and compressive loading and that cracking damage likely causes the difference in tensile and compressive creep observed in tests. Therefore, this study used the B4 model for both tensile and compressive creep.

2.2 Prestress Losses

The prestress loss, or decrease, in force in the strands of a prestressed concrete girder over time includes short-term or long-term losses. Short-term losses include anchor set losses and losses due to elastic shortening that occur immediately after the transfer of prestress force to the concrete. Long-term losses occur continuously throughout the life of the girder due to the creep and shrinkage of concrete and the relaxation of steel.

2.2.1 Short-Term Prestress Losses

Anchor set loss occurs due to slip in the strand anchors that hold the strand in an elongated position before the transfer of prestresses. According to AASHTO LRFD (2012), a common value of anchor set is 0.375 in., although values as low as 0.0625 in. can be appropriate depending on the type of anchorage device used. This study assumed that the amount of anchorage slip was accounted for in the initial jacking force and was therefore not included in the loss calculation.

Elastic shortening loss, which occurs during the transfer of prestress from the strands to the concrete, causes the girder to shorten, thereby affecting the tendon bonded to the concrete, leading to reduced strain and decreased force in the strands. Elastic shortening losses are strongly affected by the strand reinforcement ratio and elastic modulus of the concrete, which is a function of concrete strength, aggregate type, and aggregate quantity, among other variables (Garber et al., 2016). In post-tensioned girders that use unbonded tendons within ducts, friction between the strands and ducts also contributes to short-term prestress losses. Friction losses are not addressed by the proposed model, which is intended for use with prestressed girders.

2.2.2 Long-Term Prestress Losses

Long-term losses are complex and time-dependent and vary with the amount of time since concrete was placed or load was applied. Concrete creep and shrinkage are primarily responsible for long-term prestress losses. At the level of the strands, concrete is typically subjected to compression stresses, meaning creep and shrinkage cause the concrete at the level of the strands to shorten over time and, as the strands are bonded to the concrete, the strands shorten simultaneously, reducing the prestressing force. Both creep and shrinkage effects are highest early in the girder lifespan and decrease with time. Prestress losses due to creep and shrinkage are therefore impacted by all variables that affect creep and shrinkage, including ambient relative humidity, elastic modulus of the concrete, and the type and quantity of coarse aggregate, age of curing, temperature, and cement type (Gedam, 2019; Garber, 2015).

In addition to the creep and shrinkage of concrete, steel relaxation of strands also causes prestress loss and contributes to long-term deformation. Relaxation of steel refers to reduced stress in steel due to creep within the steel under prolonged strain. The magnitude of relaxation depends

on the value of initial stress. Force in the tendons also decreases because of concrete creep and shrinkage, thereby decreasing steel relaxation. Like creep and shrinkage, relaxation occurs most rapidly when the strand is first tensioned; approximately 90% of relaxation occurs within the first two years after the strands are tensioned (Buckler & Scribner, 1985). According to an analysis by Garber et al. (2012), prestress loss due to relaxation contributes minimally (approximately 5%) to the total long-term prestress loss (Figure 2.3). Therefore, long-term deformations due to steel relaxation were not considered in this study.

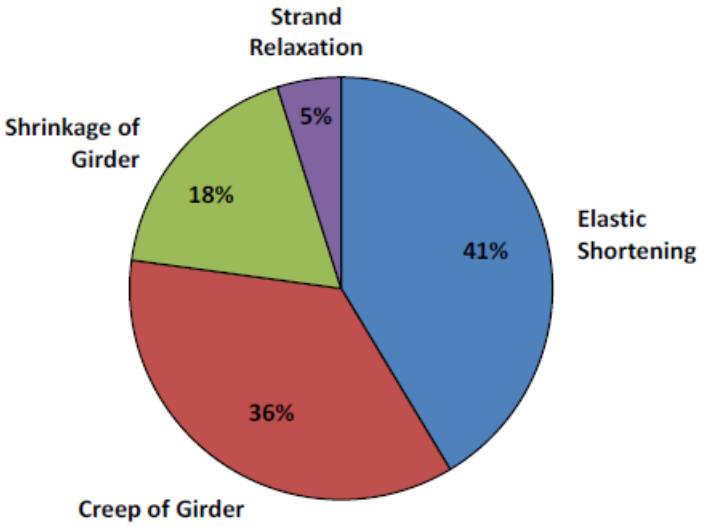

Figure 2.3: Relative Contributions of Mechanisms to Prestress Loss
Source: Garber et al. (2012)

2.2.3 Prestress Loss Estimation

The accurate estimation of prestress losses is crucial for analyzing girder behavior over time. Underestimation of prestress losses can result in more in-situ cracking and deflection than expected, while overestimation of prestress losses can cause excessive in-situ camber and an uneconomical design (Kamatchi et al., 2014). Garber et al. (2016) summarized the methods for estimating prestress losses, including transformed-section, gross-section, and iterative gross-section methods for short-term losses and the PCI simplified approach, the AASHTO LRFD approximation method, the AASHTO LRFD detailed method, and the incremental time-step method for long-term losses.

To calculate short-term prestress loss in the transformed-section approach, concrete stress at the level of prestressing strands due to prestressing force and girder weight is determined using properties of the transformed section. This stress is then converted into the stress in the strands, resulting in elastic shortening loss. Comparatively, the gross-section approach assumes that 10% of the prestressing force is lost due to elastic shortening when calculating the concrete stress at the level of prestressing strands. This stress is then converted into the stress in the strands to obtain the actual value of elastic-shortening loss. In the iterative gross-section approach, an initial prestressing force is assumed to calculate the elastic-shortening loss, which is used to revise the value of initial prestressing force. The process is iterated until a steady value of initial prestressing force and elastic shortening is reached.

When estimating long-term losses, the PCI simplified approach is a lump-sum method for calculating long-term prestress loss due to creep, shrinkage, and relaxation using equations proposed by PCI (2020). The AASHTO LRFD approximation method is another lump-sum approach that uses equations in AASHTO LRFD (2020) to calculate total long-term loss. The AASHTO LRFD detailed method more accurately captures the effects of girder creep, girder shrinkage, strand relaxation and deck shrinkage by dividing the girder life into two timespans (before deck placement and after deck placement) and using equations in AASHTO LRFD (2020) for the calculations. The incremental time-step method, a more advanced and rigorous method than any previous method, divides the life of the girder into a number of time intervals, and stresses and losses are calculated at each time step. Stresses determined in the previous time step are used to calculate losses in the succeeding time step.

Since short-term losses are dependent on the initial prestressing force, which is itself is the jacking force minus the short-term losses, an iterative approach is required. Therefore, this study used the iterative gross-section approach to estimate short-term losses and the time-step method for long-term losses to capture the effects of load and boundary condition changes, concrete deformations, and time-varying effective prestress over time.

2.3 Continuity Diaphragms and Restraint Moments

The structural behavior of bridges is commonly enhanced by casting continuity diaphragms between girder ends at supports. A continuity diaphragm consists of concrete placed between girder ends and a continuous, cast-in-place reinforced concrete deck. The deck reinforcement usually provides the tensile force in the couple resisting negative moment, while positive moment connections are due to the extension of prestressing strands into the diaphragm or by embedding reinforcing bars from the girder end into the diaphragm (Miller et al., 2004). Ma et al. (1998) includes additional information about various types of positive and negative connections.

Diaphragms advantageously enhance the riding surface for vehicles and improve durability by eliminating joints at the support and providing redundancy for extreme loads (Mirmiran, 2001). Continuity diaphragms also cause the girders to act continuously, thereby resisting beam-end rotation and developing beam-end moments, or restraint moments. AASHTO LRFD (2012) indicates that time-dependent effects, such as shrinkage, creep, or temperature gradients, cause restraint moments to develop in response to any beam curvature that occurs after continuity is established.

Ma et al. (1998) showed that the construction sequence impacts the magnitude of the restraint moment. Three possible sequences include (1) deck and diaphragm placed at the same time, (2) diaphragm placed before the deck, or (3) deck placed before the diaphragm, which is unlikely since the diaphragm is located below the deck. Hastak et al. (2003) surveyed DOT engineers and found that 50% of the respondents typically place the deck and diaphragm concrete simultaneously, whereas 32% place the diaphragm concrete first and then the deck concrete. Because KDOT engineers typically place the deck and diaphragm concrete at the same time, the model in this study assumed that the deck and diaphragm concrete are placed simultaneously.

2.3.1 Degree of Continuity of Connection

Diaphragm and deck cracking can limit how effectively the continuity diaphragm limits beam-end rotations. AASHTO LRFD (2012) considers a connection to be fully effective (i.e., act similar to a continuous girder) if the age of the precast girder is at least 90 days when continuity is established and longitudinal stresses at the bottom of the continuity diaphragm due to a

combination of superimposed loads, creep, shrinkage, settlement, 50% of live load, and temperature gradients are compressive. If these requirements are not met, the joint is considered partially effective, meaning that the diaphragm cannot completely transfer forces and moments between adjacent bridge girders. As diaphragm cracking develops, the girders act like simply-supported beams. For example, if a diaphragm cracks near the bottom of the girders, the girders are simply-supported for any gravity loads applied to the structure until the cracks are closed. Once the diaphragm cracks are closed, the diaphragm provides some resistance to beam-end rotation, so girders behave as though they are continuous and resist additional loads.

2.3.2 Restraint Moment

Restraint moments are caused by a change in support conditions. When a simple-span structure is made continuous by a continuity diaphragm, restraint moment develops as the diaphragm resists beam-end rotations caused by creep and other time-dependent deformations (Kytölä & Laaksonen, 2018). Restraint moments can be positive or negative. Positive moments are caused by creep due to prestressing and positive temperature gradient, while negative moments are caused by creep due to the self-weight of the beam and deck, differential shrinkage, and negative temperature gradients, as shown in Figure 2.4.

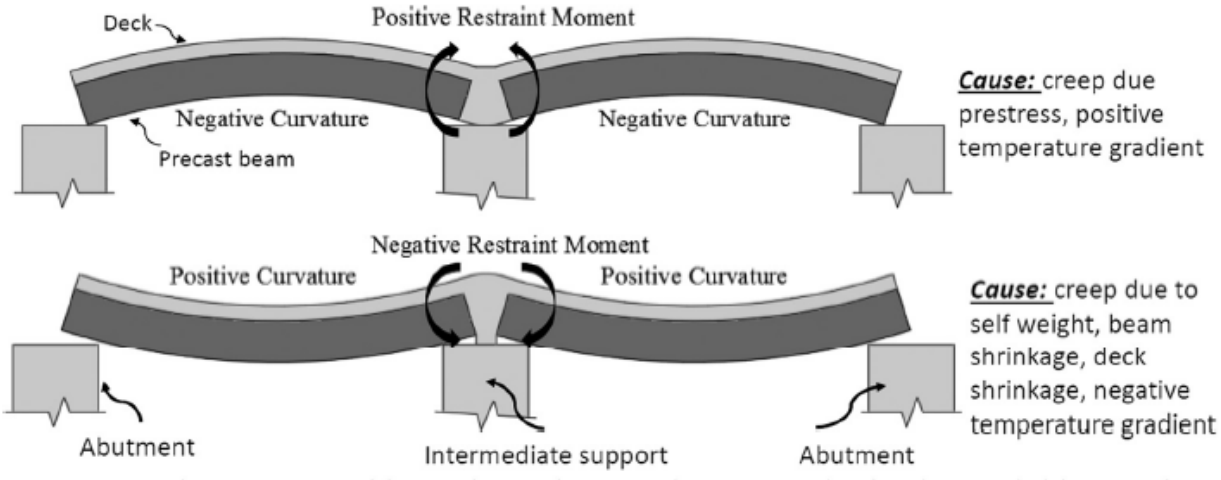

*Arrows indicate orientation of beam-end moments balancing the restraint moments

Figure 2.4: Causes of Positive and Negative Restraint Moment with Continuity Diaphragm
Source: Menkulasi et al. (2018)

A parametric study (Ghimire, 2014) identified girder age at the establishment of continuity, span length ratios between adjacent girder spans, and the ratio of the diaphragm-to-girder stiffness as key variables that affect the restraint moment magnitude. Higher restraint moments were observed for lower girder ages at the establishment of continuity. Other studies have proposed requiring a minimum girder age when continuity is established to limit diaphragm cracking (Menkulasi et al., 2018; AASHTO LRFD, 2012; Miller et al., 2004). Higher positive restraint moments were observed when the ratio between adjacent girder span lengths increased. Lower negative final restraint moments were observed for higher diaphragm-to-girder stiffness ratios when the girder age at continuity was higher. However, higher positive restraint moment values were achieved for the same diaphragm-to-girder ratios when the girder's age at continuity was lower. Other factors affecting the magnitude of restraint moment include the properties of the girder and slab concrete, the geometry of the bridge and girder, and the construction sequence of the deck and diaphragm. The magnitude of calculated restraint moment also depends on the creep and shrinkage model selected. Creep and shrinkage strain vary based on the model used for analysis, as shown in Figure 2.1.

Restraint moment is also affected by temperature variations in girders. A temperature gradient between the top and bottom of the girder induces thermal stresses and curvature that leads to additional restraint moment and stresses. Ghimire (2014) suggested that thermal gradients contribute up to one-third of the total developed restraint moment, while creep and shrinkage account for the remainder, highlighting the necessity to account for temperature effects in structural design and analysis. While acknowledging the significance of temperature effects, the current study did not consider daily or seasonal temperature variations because the research focus was modeling long-term behavior of prestressed concrete girders and thermal variations are transient in nature. Also, it would be difficult to obtain multi-decade records of temperature variation for the study.

2.3.2.1 Methods for Calculating Restraint Moment

Various methods have been proposed to calculate restraint moment. The PCA method, first introduced by Freyermuth (1969), is one of the oldest methods, and the CTL method, proposed by

Miller et al. (2004), improves on that original method. A simple method, known as the P-method, was proposed by Peterman and Ramirez (1998). Menkulasi et al. (2018) provides a detailed discussion of the advantages and limitations of these methods as well as a method for calculating the restraint moment based on restrained curvatures and strains, which are calculated by multiplying initial strains and curvatures at mid-span and at the ends by the applicable creep coefficient. The shrinkage strain, strain due to thermal gradient, and the elastic and creep strain due to initial stresses and stress changes are summed to calculate the time-dependent strains, and these strains are then converted to time-dependent curvatures that are used in the force method of analysis to determine restraint moment. Menkulasi et al. (2018) used the AAEM to account for the effects of creep and shrinkage in the concrete.

The current study used the B4 model (Wendner et al., 2013) to estimate creep and shrinkage, as discussed in Section 2.2.2. The calculated creep and shrinkage strains were then converted to girder curvature to obtain beam-end rotations using the moment-area method. Restraint moments were then calculated as the end-moment necessary to eliminate rotation, thereby simulating a fixed-end condition. This process is described in greater detail in Chapter 3. The restraint moment resulting from thermal gradients was not included in this study, but additional information about the calculation of thermal-induced secondary restraint moment is included in Ghimire (2014) and Hossain et al. (2021). The restraint moment caused by steel relaxation was also ignored since this study neglects prestress losses due to the relaxation of steel. Menkulasi et al. (2018) provides an example of a calculation restraint moment due to steel relaxation.

Since uniform shrinkage typically is assumed throughout the length and depth of the girder, beam shrinkage does not cause the development of restraint moment. However, because concrete girders and bridge decks are constructed at separate times, differential shrinkage occurs between the girder and the deck. This differential shrinkage results in the development of negative restraint moments that were considered in this study.

2.3.2.2 Limiting the Restraint Moment

Because a beam cannot develop an end moment greater than the beam-end moment strength, the magnitude of the restraint moment is limited by the diaphragm strength and moment strength of the girder ends. The literature was reviewed to understand typical values of beam-end moment strength at diaphragms (Mirmiran et al., 2001). The effects of various levels of positive moment diaphragm reinforcement were investigated, with moment strengths taken as varying fractions of the beam-end cracking moment (Mirmiran et al., 2001). The results suggest that adding reinforcement so the positive moment strength is greater than $1.2M_{cr}$ does not enhance the performance of the diaphragm, so this might be considered an upper bound for restraint moment. KDOT commonly reinforces diaphragms to provide positive moment strengths of approximately $0.6M_{cr}$ (KDOT Bridge Design Manual, 2021).

In this study, girder ends were assumed to crack when the restraint moment reached 60% of the cracking strength of the girder end ($0.6M_{cr}$), after which the restraint moment remained constant at $0.6M_{cr}$ as end rotations increased (Mirmiran et al., 2001). Ghimire (2014) proved that girder ends and diaphragms crack in the field, so these assumptions were reasonable. Use of this limiting value for restraint moment also diminished the need to consider effects of temperature gradients and steel relaxation on restraint moment, so these effects were neglected in this study.

2.4 Long-Term Deflections

The initial elastic deflection that a girder experiences due to load application is followed by a long-term deflection caused primarily by the creep of concrete under sustained load. Unloading and reloading during deck replacement may also affect long-term girder deflection. In general, long-term deflections can be estimated using one of two approaches: the simplified prediction approach or incremental time-step analysis (Naaman, 1982). Some of the simplified prediction approaches mentioned in Naaman (1982) include the American Concrete Institute (ACI) code multiplier method, Branson's multiplier method, Martin's multiplier method, and the heuristic or rule of thumb method. Long-term deflections are obtained from the simplified prediction approaches by multiplying instantaneous elastic deflection with a multiplication factor based on the selected method. The incremental time-step analysis discretizes time and then

calculates incremental changes in deflection for each time step and superimposes them at the start of the time step (Birhane et al., 2020; Rodriguez-Gutierrez & Aristizabal-Ochoa, 2007).

The literature revealed several models for calculating long-term deformations in concrete structures. Rodriguez-Gutierrez and Aristizabal-Ochoa (2007) proposed a model to calculate short-term and long-term deflection in beams with generalized end conditions, including the effects of creep, shrinkage, and tension stiffening in concrete and the relaxation of prestressing steel as well as rotational restraints at the beam ends, presence of non-prestressed reinforcement, and composite material, such as fiber-reinforced polymers. Another approach, described by Birhane et al. (2020), used an equivalent load approach to determine the long-term deflection of prestressed concrete bridges with consideration of non-uniform shrinkage and crack propagation.

In this study, the calculated prestress losses, creep, and shrinkage strains were used to determine the corresponding curvature change and total long-term deflection in the girders. Because the B4 model provides relatively higher creep strains than other models, values of long-term deflection were higher than estimated with other models. Concrete cracking affects girder deflection because it reduces its moment of inertia and increases deflection. Effective moment of inertia, which accounts for concrete cracking, can be calculated based on ACI standards, as explained in Naaman (1982). Uncracked concrete section properties were used in this study to compute long-term deflections if the concrete remained uncracked.

2.5 Time-Step Analysis

Time-step analysis is a modeling technique that incrementally steps through time, updating calculations at each time step. This approach allows the model to account for changes in load and boundary conditions while explicitly estimating creep and shrinkage effects on prestress forces, deflections, and internal stresses over time.

Concrete creep, shrinkage, and steel relaxation are not isolated processes, but rather interdependent. Shrinkage induces internal stresses and microcracks within the concrete, which affect its behavior and impact the magnitude of creep. More details on the interaction of concrete creep and shrinkage are included in Zhang (2020). Change in the length of the concrete member due to creep and shrinkage affects the relaxation of the tendons (Gedam, 2019). The interaction

between different mechanisms of deformations complicates calculations and justifies the application of time-step analysis. Time-step analysis divides each stage of the life of a girder (where a stage is bounded by distinct changes in load or boundary conditions) into discrete time steps, calculating the girder's response at each step and updating the parameters accordingly rather than lumping all time-dependent effects into a single calculation.

Accuracy of time-step analysis can be improved by increasing the number of steps and reducing the interval between them (Nilson, 1978). However, smaller time steps require more computational effort and runtime, necessitating a trade-off between the time intervals and the desired accuracy. A sensitivity study can be performed to select the optimum time interval to be used for the computation. Nilson (1978) describes the sequence of calculations in a time-step analysis on a prestressed concrete girder, where steel stress change at each time step is determined by calculating the creep and shrinkage strain and multiplying it by the modulus of elasticity, and then adding the result to the increment of relaxation loss in strands. The change in concrete stress due to relaxation loss is determined, and corresponding strain changes are calculated. Net changes in strain are determined by subtracting the strain change obtained from the gross changes, and the corresponding curvature is determined. Finally, stresses at the end of each time interval are determined by summing the initial stresses and changes in stresses, which are then used as the initial stress in the next time step.

Swartz (2010) conducted a detailed time-step analysis of a prestressed concrete girder by discretizing it into horizontal layers representing the concrete component, with one layer representing prestressing strands. At each time step, a strain distribution satisfying compatibility and equilibrium was calculated, considering both elastic and inelastic effects (creep, shrinkage, relaxation). The corresponding prestress loss was then calculated based on the updated strain. Similarly, Gedam (2019) developed a flowchart (Figure 2.5) for incremental time-step analysis in a prestressed girder, accounting for parameters that affect time-dependent and instantaneous effects in incremental time-step analysis, such as friction, anchorage slip, elastic shortening, concrete shrinkage and creep, and steel relaxation. These studies served as references for the development of the sequence of calculation steps for time-step analysis on prestressed concrete girders in bridges with deck replacement for this study.

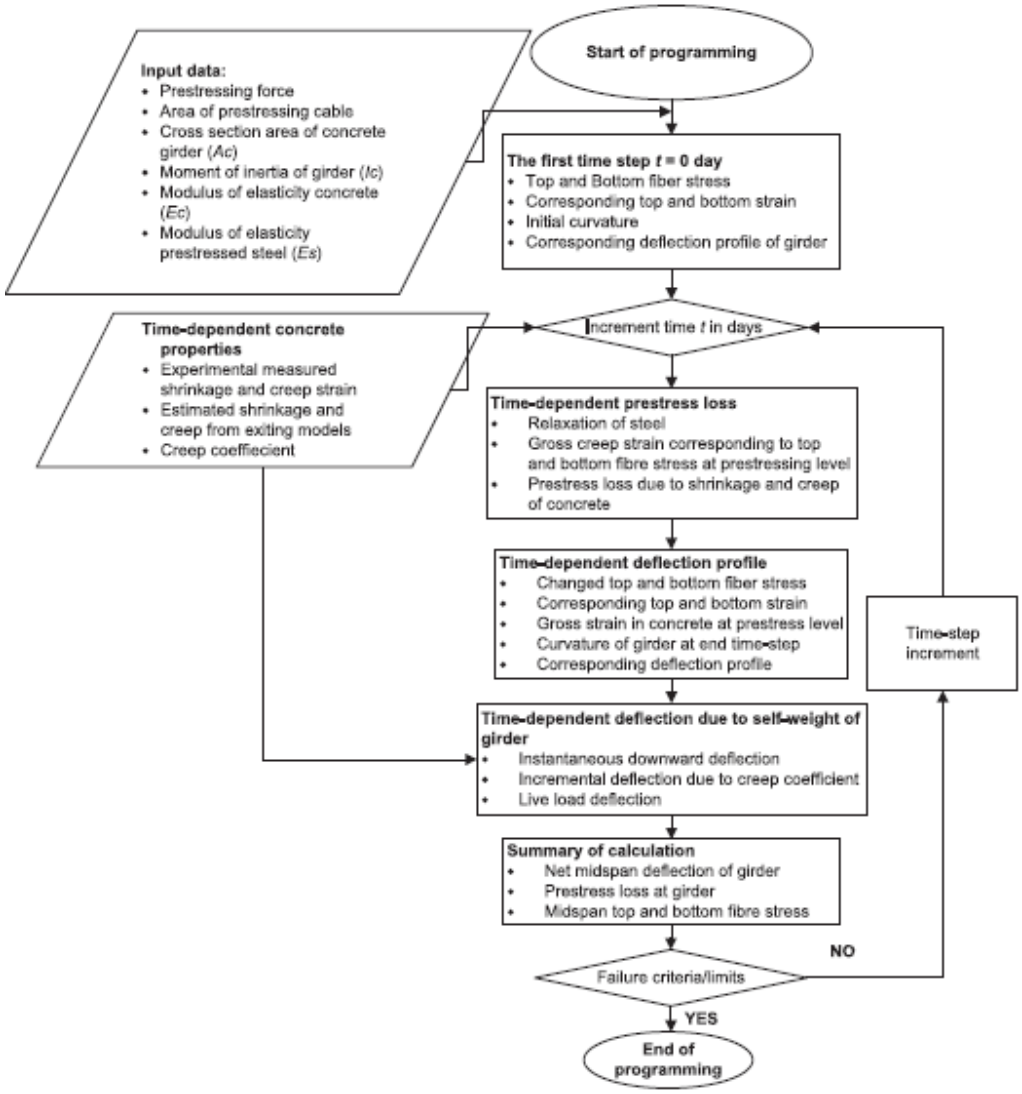

Figure 2.5: Flowchart for Incremental Time-Step Analysis for a Prestressed I-Girder
Source: Gedam (2019)

2.6 Redecking

Redecking is an alternative to bridge superstructure replacement when an existing concrete deck can no longer be repaired. Redecking requires the removal of an existing deck, repair and preparation of girders (if needed), and placement of a new deck and wearing surface. This section describes methods for deck removal and potential problems that removal can cause.

2.6.1 Deck Removal Practices

Numerous methods and equipment types can be used to remove concrete decks from bridges. Selection of the proper method and equipment depends on factors such as quantity and

quality of concrete to be removed; time available; traffic flow considerations; restrictions on vibration, noise, dust, and disposal of debris; cost of bridge closure; and availability of suitable equipment and skills (Tadros & Baishya, 1998; Manning, 1991; Phares & Shane, 2014). Although analysis of deck removal methods falls outside the scope of this study, available techniques include the following:

1. Saw-cutting: In the saw-cutting method, the bridge deck is cut into manageable pieces and then lifted by crane. This is a relatively rapid method that can cut concrete at any angle. However, removing the slab over the girders without damaging the girder or shear connectors is difficult, so other methods should be considered directly over the girders.
2. Hydro-demolition: Hydro-demolition applies high-pressure water to break the concrete. Although this process produces limited dust and vibration, proper collection and drainage of wastewater is challenging.
3. Jackhammering: This method breaks the concrete deck into small, manageable pieces using a jackhammer and then uses either a loader bucket or other construction equipment to remove the pieces. This method creates a significant amount of noise, vibration, falling material, and dust. However, when the power output of the hammer is limited, this method can be preferrable for use directly over existing girders.
4. Drilling: Drilling is used in combination with other methods such as splitting and blasting. It can also be used to remove large concrete pieces by boring overlapping small holes around the perimeter of the section (Manning, 1991).
5. Splitting: The splitting method applies tension on a predefined path either mechanically or chemically to break the concrete in a controlled way (Phares & Shane, 2014). The broken concrete is removed, and the reinforced steel is cut to free the section. The technique causes little vibration and dust, and the concrete left in place is undamaged. A major

disadvantage of this method is the time required to cut the reinforcement and remove the broken concrete.

6. Crushing: In the crushing method, opposing forces are applied to both sides of the concrete element to break the concrete and reinforced steel (Phares & Shane, 2014). Crushing is a relatively rapid method with minimal vibration and noise. However, it is difficult to use for concrete above girders, which require hand removal.
7. Peeling: Peeling is a relatively new technique in which a concrete bridge deck is removed by peeling off the concrete by applying vertical forces on the deck to break it free from the girder. Although it is a relatively rapid method, it produces significant vibration, noise, dust, and falling materials (Phares & Shane, 2014).

One method or a combination of methods listed may be used for deck removal. Detailed descriptions of each of these methods are presented in Tadros and Baishya (1998), Manning (1991), and Phares and Shane (2014).

2.6.2 Problems During Redecking

Tadros and Baishya (1998) reported several problems that typically occur due to deck removal, including (Tadros and Baishya, 1998):

1. Microcracking in girder concrete due to excessive or overly powerful jackhammering. This can generally be controlled by limiting the power of chipping and hammering equipment used directly over the prestressed girder flanges.
2. Damage due to saw-cuts in the top flange of the girders. This can generally be controlled by limiting the location and depth of saw-cuts. Saw-cuts over the girder should have a depth less than the deck depth to avoid penetrating the girder.

3. Damage in the top flange by rig-mounted breakers. Any impact equipment used to remove deck concrete should be limited in use around girder top flanges.
4. Damage to the horizontal shear reinforcement linking the deck and girders.
5. Excessive noise and vibration.

When selecting a method for deck removal, the time and cost of deck removal must be balanced against the risk of damage to supporting girders. Survey results suggest that limiting girder damage is a concern among bridge engineers, and several states aim to minimize girder damage by limiting the power of demolition hammers used for deck removal (Section 1.2).

Assad and Morcous (2016) investigated the potential for deck removal to damage girders and the effects damage to the girder top flange has on structural performance once the deck is replaced. In girders with a low span-to-depth ratio, the effect of cutting approximately 50% of the girder top flange was negligible, whereas in girders with a high span-to-depth ratio, the effect of cutting was potentially substantial. Results showed that the most cost-effective method of deck removal depends on environmental restrictions, deck dimensions, girder type, and type of shear connectors between the girder and the deck. Kamel (1996) found that specialized girder-to-deck connections may reduce deck removal effort, including connection details that use spray-on debonding agents. Another study reported that debonding of the girder-deck interface over the flanges can reduce the deck removal effort by 65% and reduce the potential for girder damage (Li et al., 2019), although such details are not useful for existing bridges.

Although no known studies examine the effects of deck replacement on long-term bridge behavior, Reybrouck et al. (2020) conducted experimental tests on prestressed concrete beams subjected to a predefined sustained load for 4.5 years, after which the beams were unloaded and observed for 6 months. The beams were then subjected to a static loading test until failure. Results showed that prestress losses in the strands during the 4.5-year period varied from 0% to 10% and from 6% to 13% during the unloading period, suggesting that loading and reloading the girders can significantly impact prestress losses and effective prestress force in the strand, leading to changes in the overall stresses in the girder. Further study is needed, however, to more accurately

quantify the effects of deck replacement on bridge performance and to increase understanding of the sensitivity of these effects to design variables.

Chapter 3: Methodology

3.1 Introduction

This study developed a time-varying analysis model to calculate girder behavior throughout its lifespan. The model, developed in Python, combines calculations for prestress losses, stress and strains, deflections, creep, and shrinkage into one incremental time-step model. This approach considers interactions between these mechanisms (e.g., prestress losses and creep) and the effects of changes in loading when calculating stresses and deflections throughout the life of the prestressed concrete girder. The model takes input from Excel and reports the outputs in .csv files. This chapter describes the model in detail, including the underlying assumptions, sign conventions, inputs, calculation steps, outputs, and the range of applicability of the model.

3.2 Assumptions

The following assumptions were made in developing the model:

1. Girder ends were assumed to be simply-supported before continuity diaphragms were placed and continuous thereafter. Supports were assumed to be located 6 in. from the girder ends.
2. Plane sections before bending were also assumed to remain plane after bending, and shear deformations were neglected.
3. Load-induced strains were assumed to be proportional to stresses, and second-order geometric effects were neglected.
4. Girders were assumed to be uncracked, so uncracked section properties were used throughout.
5. Prestress gains due to differential shrinkage between the girder and the deck were considered insignificant and neglected (PCI, 2020).
6. The principle of superposition was assumed to be valid for creep and shrinkage strains, such as when strains from creep rebound after load removal and new creep strains induced by a new load are calculated separately and summed at each time step (Wendner et al., 2015).

7. Long-term prestress loss due to relaxation was neglected because it accounted for only approximately 5% of the total prestress loss (Garber et al., 2012).
8. Unshored construction was assumed, meaning deck weight was supported by the non-composite girders.
9. Effects of live load on long-term deflections were assumed to be negligible.
10. Variation in environmental conditions over time was neglected because, although the model accounts for temperature and humidity conditions, these conditions are treated as static over the life of the bridge, thus neglecting daily, seasonal, and longer-term variation. Inputs related to environmental conditions may therefore be considered analogous to average conditions a bridge is subject to over time.
11. Haunches were neglected when developing the model for this study, resulting in a uniform thickness of bridge deck over the girder length. This simplification was made because the weight of a haunch has a minimal effect on girder moments and subsequent model outputs.
12. Damage to girders due to deck removal was not considered, nor were corrosion, spalling, and other deterioration types modeled. These would need to be considered when making decisions about a particular bridge exhibiting deterioration or damage.
13. Dead loads were assumed to be uniform along the girder length and symmetrical along the longitudinal axis of the girder. Load distribution factors and effects of loads applied eccentrically to the girder axis and were therefore neglected.
14. If present, the weight of diaphragms at the girder ends was assumed to be supported directly by bridge piers and thus neglected when the girder was analyzed.

15. Bending moments occurring during girder transport and installation were not determined; girders were assumed to remain uncracked throughout construction and service.
16. All strands within a girder were assumed to be the same diameter and subject to the same jacking force.
17. Anchorage set losses were not calculated separately because they were assumed to be accounted for in the initial jacking force value.
18. To simplify the analysis, creep that developed due to stress changes caused by restrained moment in the girder was not considered in the study.
19. Restraint moment was calculated at the continuous support by calculating girder-end rotation for a simply-supported condition to determine the moment required to bring the rotation to zero. This restraint moment was limited by the flexural strength of the girder end (Section 2.4.2). At the simple external support, where end rotations are not restrained, the restraint moment was zero.
20. Deck creep and girder creep were calculated individually, and interaction of these creep strains at the interface of the girder and deck was not accounted for.

3.3 Sign Convention

Figure 3.1 shows the sign conventions used for model development. As shown, the sign conventions were as follows:

1. Downward deflection is negative and upward deflection (camber) is positive.
2. Bending moment is positive if it causes upward concavity (sagging) and negative if it causes downward concavity (hogging).
3. In both concrete and prestressing strands, tension is positive, and compression is negative.

4. Distance is negative above the neutral axis (N.A.) and positive below the N.A.

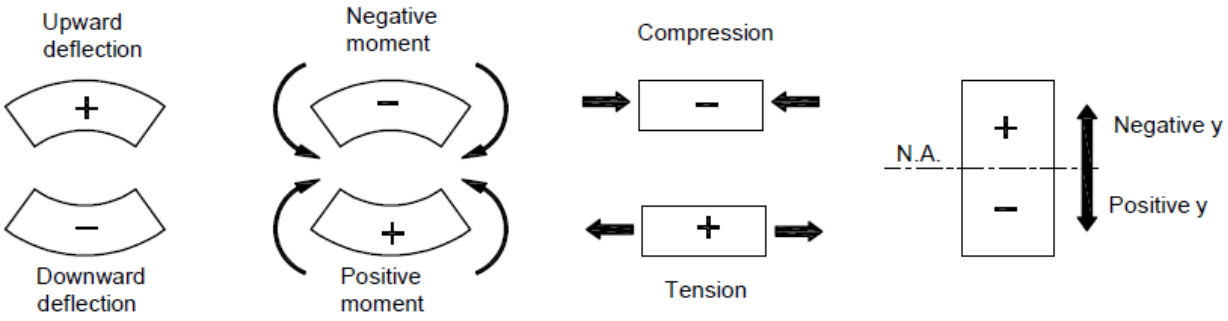

Figure 3.1: Sign Convention for Analysis

3.4 Input Parameters

Table 3.1 lists the 85 input variables required for the model. Some of these inputs are dependent on other inputs (e.g., girder section controls many dimensional variables), while others are independent of other variables. In general, the input parameters for the model describe concrete materials, dimensions, loads and material strengths, environmental conditions, and timeline. Concrete material parameters describe the composition of the concrete used for the girder, old deck, and new deck. Dimensional parameters define the bridge, girder section, prestressing strands, and deck. Load and material strength parameters include concrete and strand strengths, material unit weights, superimposed dead loads (e.g., barriers), and initial strand jacking force. Environmental condition parameters include temperature, relative humidity, and reference temperature, or the temperature at which the concrete is assumed to have zero thermal strain. Time variables include the age of the girder and deck concrete at key points in time such as: age of loading, age of drying, age of deck removal, age of new deck placement, time intervals representing construction activities, and the time steps within these intervals used in the calculation. Table 3.2 lists the units for the input variables used in the model. The Notation section contains a full list of units.

Table 3.1: Input Variables

Concrete Design Variables	Girder	*w/c, a/c, c, ctype, ρ, aggtype*
	Old deck	*w/c, a/c, c, ctype, ρ, aggtype*
	New deck	*w/c, a/c, c, ctype, ρ, aggtype*
Dimensional Variables	Bridge	L_{span}, *span*, L_{cant}, W_{girder}, N_{girder}, W_{total}
	Girder	f_1, f_2, H_w, T_{bf1}, T_{bf2}, T_{tf1}, T_{tf2}, T_w, W_{tf}, W_{bf}, H
		V/S, loc, pstype, d_s, $N_{strands}$, *sprofile,* loc_{harp} *and e*
	Old deck	t_d, t_{ws}
	New deck	t_{nd}, t_{nws}
Loads and Strength Variables	Girder	γ_c, f'_{cg}, f'_{ci}, f_{pu}, f_{py}, E_{ps}, *pstype,* P_{J1}, α_T
	Old deck	γ_c, f'_{cd}, γ_{ws}, $w_{barrier}$
	New deck	γ_c, f'_{cnd}, γ_{nws}, $w_{nbarrier}$
Environmental Variables	Bridge	*h, T,* T_{ref}
	Old deck	*h, T,* T_{ref}
	New deck	*h, T,* T_{ref}
Time Variables	Bridges	$(\Delta t)_n$, $(T_e)_n$ T_4, T_5
	Girder	t_0, T_1, T_2, *t,* T_7
	Old deck	t_{0d}, T_3, *t*
	New deck	t_{0nd}, T_6, *t*

Table 3.2: Selected Input Variables

Input Variable	Unit
Material unit weight	kips/ft^3
Compressive strength	ksi
Maximum tensile stress, yield stress and modulus of elasticity of prestressing strands	ksi
Weight of barrier	kips/ft/side
Prestressing force	kips
Cement content	lb/ft^3
Time	days
Bridge dimensions (longitudinal length, road width, deck width, cantilevered length of deck)	ft
Girder length	ft
Girder dimensions	in.
Location of prestressing strands	in.
Location of harped points (if applicable)	ft
Thickness of deck and wearing surface	in.
Diameter of strands	in.
Relative humidity	fraction
Temperature	°F
Temperature coefficient	/°F
Volume-surface area ratio	ft

3.5 Output Parameters

Model outputs are listed in Table 3.3 with their units. These outputs can be obtained for any point in time and, where appropriate, the outputs can be obtained for various sections along the girder span and throughout the composite girder depth at each section.

Table 3.3: Model Outputs with Units

Output Type	Unit
Stresses	ksi
Strains	unitless
Moments	kip-ft
Deflections	in.
Prestress force	kips
Creep and shrinkage strain	unitless

3.6 Range of Applicability

The proposed model was designed to analyze pretensioned I-girders with bonded tendons using the B4 model proposed by Wendner et al. (2013) to calculate creep and shrinkage. Consequently, the model is limited to this specific type of girder and to the following range of conditions under which the B4 model is valid, as described by Bažant et al. (2015):

1. Water-cement ratio is limited to between 0.22 and 0.87;
2. Aggregate-cement ratio is limited to between 1.0 and 13.2;
3. Concrete compressive strength is limited to between 2,070 and 10,000 psi;
4. Cement content is limited to between 12.5 and 93.6 lb/ft^3;
5. Temperature is limited to between -13 and 167 °F;
6. Curing temperature is limited to between 68 and 86 °F; and
7. Volume-to-surface area ratio is limited to between 0.039 and 0.39 ft.

3.7 Model Structure: Time-Step Analysis

This study developed a time-step analysis process to compute results. This model structure begins modeling the girder when the prestressing force is released, and then the model steps forward through time at the intervals shown in Table 3.4. The time intervals were selected so that

the time-steps are short immediately following changes in loading, when the rate of deformation is the highest, and longer after time has elapsed since a change in loading, when the rate of deformation is smallest. A sensitivity study was performed to select a sufficiently small time-step when creep and shrinkage strains are changing rapidly. Time-dependent calculations for moments, stresses, and strains were executed at each time step, and relevant computed values were then used as inputs for the next calculation step, allowing the model to develop a memory. This model structure enabled quantification of the effects of changes in load and support conditions, including effects of the timing of these changes.

The lifespan of the girder was also discretized into eight distinct time periods, or loading stages, characterized by stable bridge configuration and loading (Figure 3.2). For example, adding a bridge deck, wearing surface, and barrier walls indicated the start of a new stage that ends when the bridge deck is removed. At the start of a new stage, a short time step of 1 day was used for 50 days because creep strains change rapidly. Later within a stage, as the rate of change of creep decreased, time steps were increased accordingly to reduce the time required to execute the model. The lengths of these stages are specified at the start of the analysis (see Table 3.4). Figure 3.3 shows how stress in the concrete changed with each loading stage and how it affected the creep compliance (strain per unit of stress) developed in the concrete.

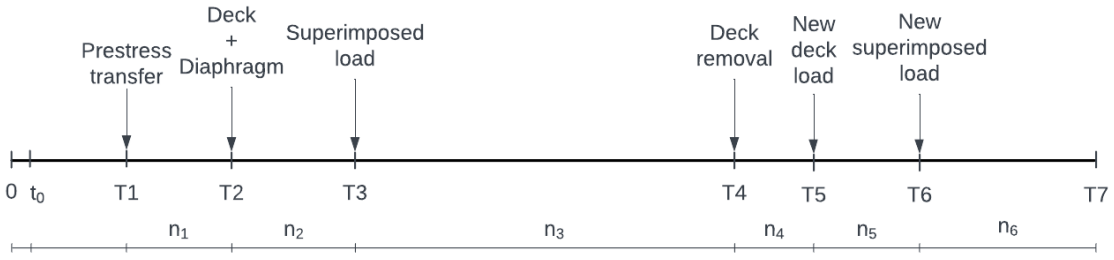

Figure 3.2: Loading Stages of a Prestressed Concrete Girder in the Model

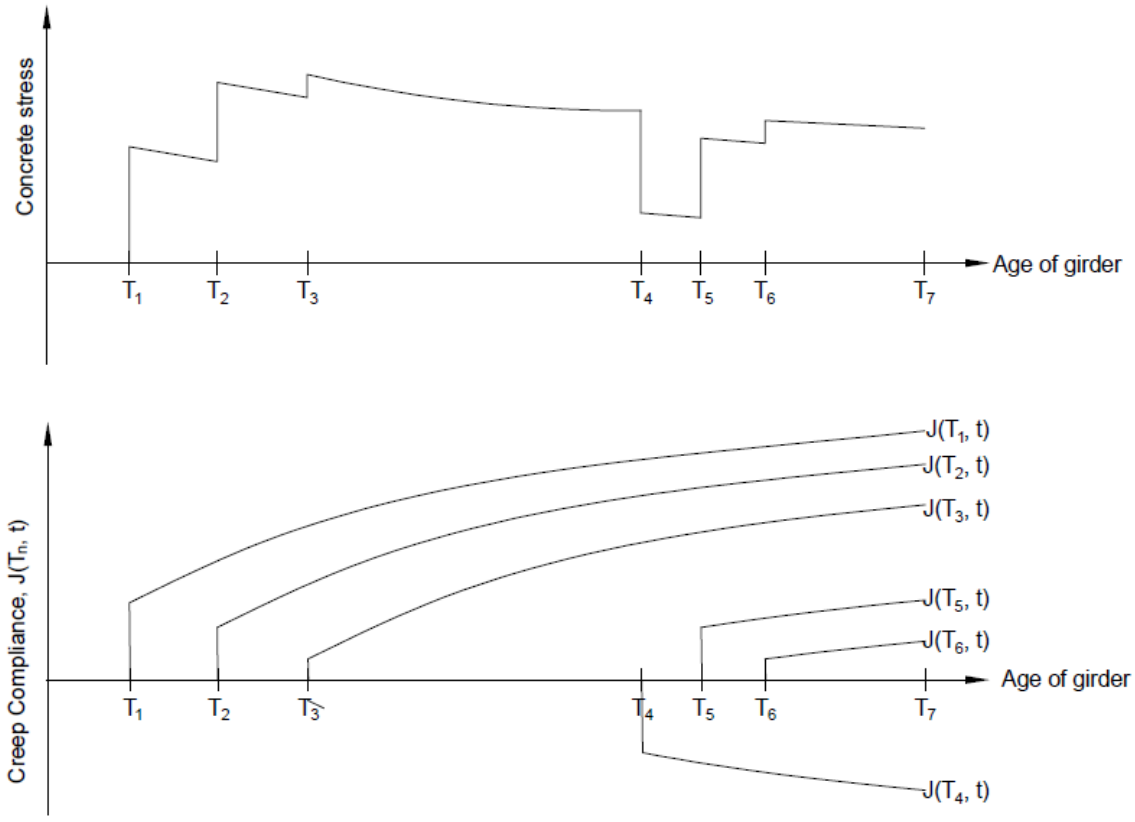

Figure 3.3: Concrete Stress and Corresponding Creep Compliance for Loading Stages

Table 3.4: Time Intervals for Prestressed Concrete Girder

Girder Age (days)		Time Interval (days)
From	To	
t_0	T_1	1
T_1	T_2	1
T_3	50	1
50	100	2
100	200	5
200	1000	20
1000	2000	200
2000	T_4	1000
T_4	T_5	1
T_5	T_6	1
T_6	T_6 + 50	1
T_6 + 50	T_6 + 100	2
T_6 + 100	T_6 + 200	5
T_6 + 200	T_6 + 1000	20
T_6 + 1000	T_6 + 2000	200
T_6 + 2000	20000	10000

The eight loading stages considered in this model are:

1. Removal from curing (at t_0):

Shrinkage of the girder concrete begins at time t_0 as the concrete is removed from curing, and relaxation of the prestressed steel occurs during the period between environmental exposure (t_0) to prestress transfer (T_1). Although shrinkage begins at t_0, it does not cause prestress loss because prestress has not yet been transferred to the concrete. The time step in this stage was set to 1 day (Table 3.4).

2. Release of prestressing strands (at T_1):

When prestress force is transferred to the concrete, the girder generally cambers upward (Figure 3.4), resulting in instantaneous prestress loss. As a result, concrete in the girder experiences stress and begins to creep. The time step in this stage was set to 1 day (Table 3.4) because changes during this stage occur rapidly. The model neglects changes in boundary conditions during transport and girder installation, instead it considers the girder to be simply-supported throughout this stage for simplicity. Just before prestress transfer at time T_1, prestressing stress was f_{PJ2} and total steel relaxation loss was Δf_{PR1}, per Section 3.8.3. After prestress transfer, elastic shortening loss was Δf_{PES}, and initial prestressing stress was f_{pi}, per Section 3.8.3.1.

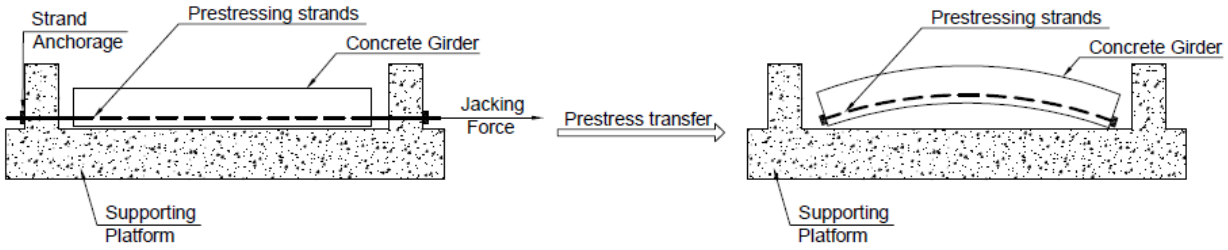

Figure 3.4: Transfer of Prestress from Prestressing Strands to Concrete

3. Addition of deck and diaphragms (at T_2):

At this stage, the deck and continuity diaphragm (if used) are placed, enabling the girders to act compositely. Figure 3.5 illustrates a two-span continuous bridge with a deck and continuity diaphragm cast monolithically. As shown, the deck load reduces the upward deflection (camber)

of the girder. Concrete creep and shrinkage between time T_1 and T_2 reduce the prestress force in the strands, and differential shrinkage between the girder and the deck slab induces additional stress and girder curvature, causing minimal prestress gain. Placement of the continuity diaphragm also changes the girder boundary conditions from simply-supported to continuous at the interior support, thereby limiting girder-end rotations and inducing restraint moments at the continuous end of the girder. Hence, the restraint moment begins to develop in the girder at T_2. The time interval between T_1 and T_2 was broken into n_1 steps. The time step in this stage was set to 1 day since the magnitude of the concrete creep and shrinkage were highest during this interval, (Table 3.4).

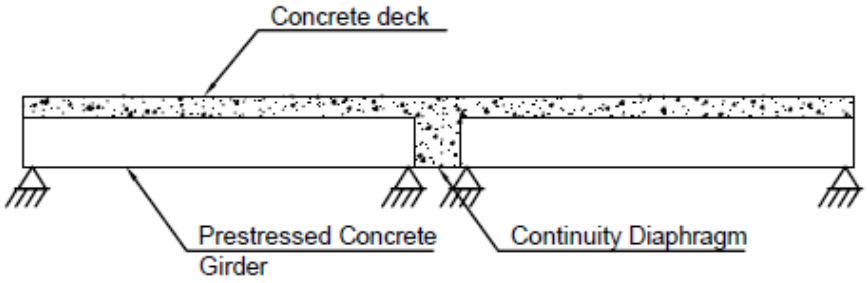

Figure 3.5: Two-Span Continuous Bridge with Cast-in-Place Deck and Continuity Diaphragm

4. Addition of superimposed dead load from barriers, curbs, and wearing surfaces at T_3:

Figure 3.6 shows a typical cross-section of a prestressed concrete bridge with concrete deck, wearing surface, and barriers. As shown in the figure, the added load causes downward deflection of the girder, and creep strains in the girder tend to increase after the application of this load. Similar to deck load, the addition of this load causes an instantaneous prestress gain in the girder. Table 3.4 shows that a time step of 1 day is used until 20 days after T_3, after which the interval is increased to two days. The time step continues to increase as time progresses to reduce computation time as the rate of creep and shrinkage slow.

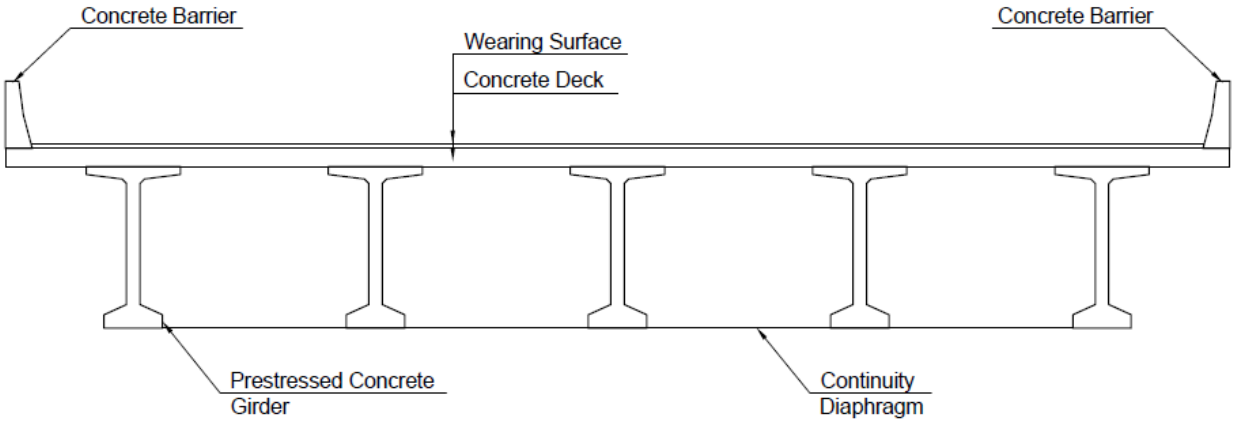

Figure 3.6: Cross-Section of a Prestressed Concrete Girder Bridge

5. Removal of deck and superimposed loads (wearing surface, barrier wall, etc.) at T_4:

The deck and superimposed loads (wearing surface, barrier wall, etc.) are removed from the bridge at T_4 when deck replacement begins. This removal reduces the load on the girder, which causes it to rebound, as shown in Figure 3.7. Since the girder has already experienced concrete deformations and prestress losses in prior stages, the girder does not rebound to its original position. For calculation purposes, instead of removing the loads, opposite loads of the same magnitude are applied to account for the effect of creep recovery due to load removal. Creep strains due to these negative loads occur after T_4. The time step in this stage is set to 1 day (Table 3.4).

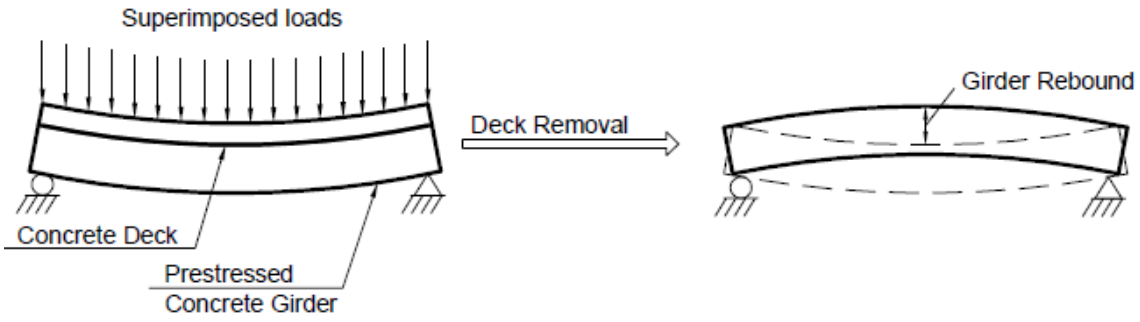

Figure 3.7: Rebound of the Girder Due to Deck Removal

6. Addition of new deck (at T_5):

Downward loads from the new deck cause the girder to deflect downward instantaneously. This new load causes an increase in creep strain and a new creep compliance calculation is introduced, as shown in Figure 3.3. The time step is 1 day in this stage (Table 3.4).

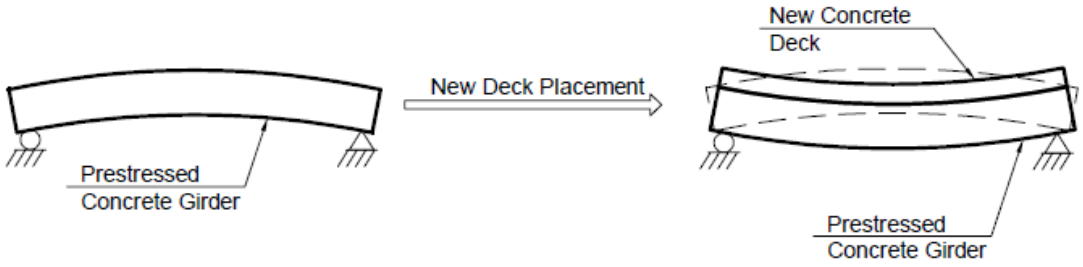

Figure 3.8: New Deck Placement on the Girder after Deck Removal

7. Addition of new superimposed dead load (at T_6):

The final stage considered for a girder with one deck replacement is the reintroduction of superimposed loads from wearing surfaces and barrier walls. From this point on, all changes in concrete stresses and strains are due to time-dependent effects. Although the reintroduction of superimposed loads increases the stress level and the creep strain, most of the creep and shrinkage would have already occurred in the girder by this age, so the change is not as significant as when it was initially loaded at time T_3. The time steps in this stage increase as the time elapsed increases (Table 3.4).

8. Final age of concrete at T_7:

The eighth stage, and the execution of the model, ends at T_7.

Figure 3.9 shows the stress distribution in the girder cross-section that occurred throughout the loading stages. The girder continued to deform and lose prestress forces until its final age, although the rate of change diminished considerably.

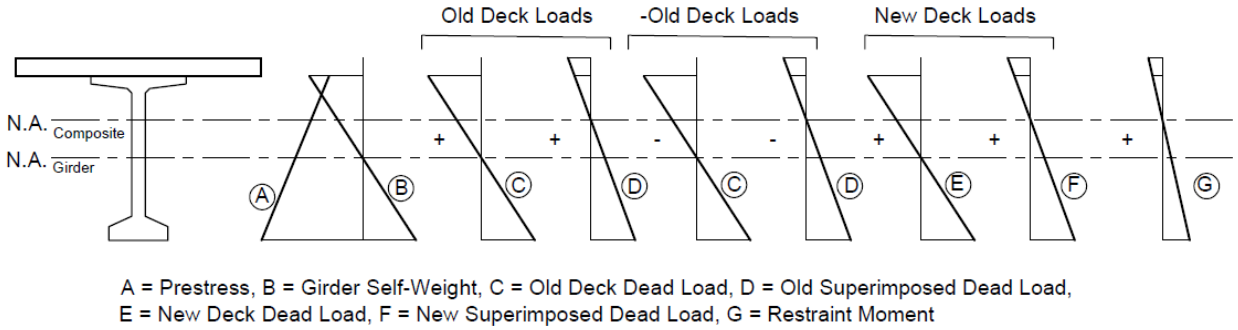

A = Prestress, B = Girder Self-Weight, C = Old Deck Dead Load, D = Old Superimposed Dead Load,
E = New Deck Dead Load, F = New Superimposed Dead Load, G = Restraint Moment

Figure 3.9: Typical Stress Distribution in a Prestressed Concrete Girder Bridge with Deck Replacement

3.8 Calculation Steps

This study developed a Python program to perform multiple calculations at sections throughout the girder length at each time step. For analysis, the girder length was divided into *n* discrete lengths, as illustrated in Figure 3.10, to account for all variations of loads, moments, and stresses. A sensitivity analysis was performed to select an appropriate value of the discrete length (*dL*). For each time step, calculations were made at *n* different locations to determine deformations throughout the length of the girder. The program followed the steps outlined in the flowchart shown in Figure 3.11; each step is described in the following sections.

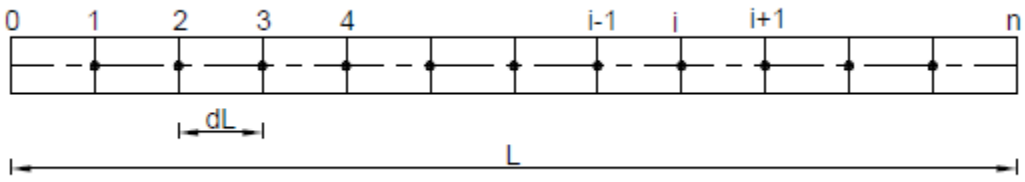

Figure 3.10: Division of Girder into Segments for Analysis

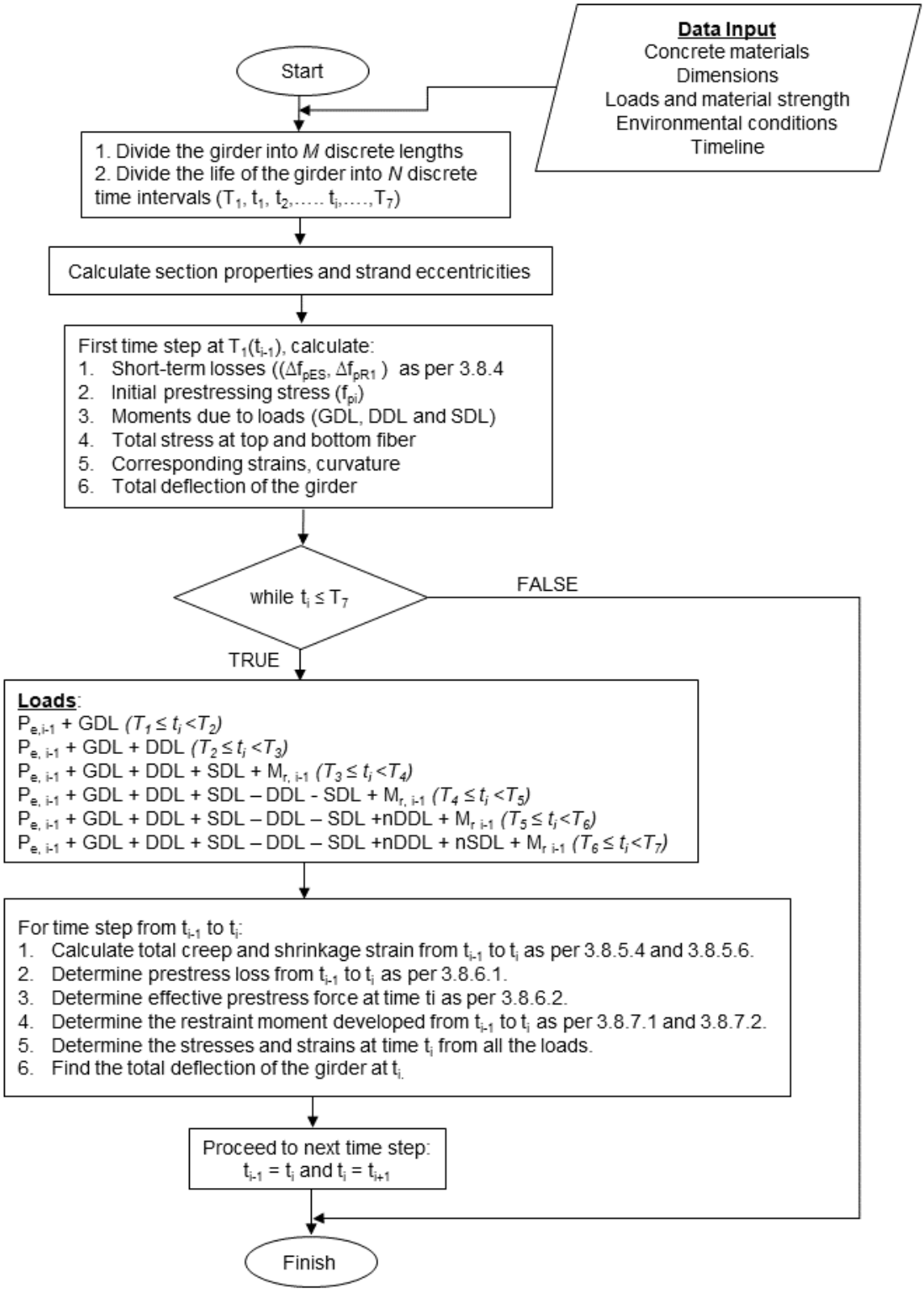

Figure 3.11: Flowchart of Analysis Steps for a Prestressed Concrete Girder

3.8.1 Section Properties and Transfer Length

Strand profile and eccentricities were determined at each location shown in Figure 3.10. Section properties, which include the area, centroids along the x-axis and y-axis, moment of inertia, and section modulus, were determined for both non-composite (girder only and deck only) and composite sections (girder plus deck) based on the input section geometries. The transformed area of the deck, calculated using a modular ratio based on the specified compressive strength of the girder concrete and the deck concrete, was used to determine the composite section properties. The prestressing force in the strands was zero at the ends and assumed to increase linearly to its full value within the transfer length. The prestressing force was constant throughout the middle portion of the span. The transfer length, l_{tr}, was calculated using Equation 3.1 based on AASHTO LRFD (2012).

$$l_{tr} = 60 \times d_s \qquad \textbf{Equation 3.1}$$

3.8.2 Loads and Stresses

Loads acting on the girder include girder self-weight, prestressing force, deck self-weight, and superimposed dead loads (SDLs). Girder dead load (GDL) and deck self-weight dead load (DDL) were determined using the unit weight of reinforced concrete (taken as 150 lb/ft^3) and the cross-sectional areas of the girder and the deck. SDLs are typically due to barrier weights and wearing surfaces. Girder-end restraint moments were considered at locations with continuity diaphragms, and restraint moments were determined based on loads applied after the continuity diaphragm was cast and effects of creep, as described in Section 3.8.6. Differential shrinkage between the deck and the girder also induced stress and curvature (Section 3.8.4.5). Unshored construction was assumed for the calculations, meaning the GDL and DDL act only on the girder and not the composite section. Superimposed loads, stresses caused by differential shrinkage between deck and girder, and restraint moments caused stress in the deck.

Stresses developed due to loads are calculated at the top and bottom fibers of the girder using the following equations:

$$f_{t,p} = -\frac{P_{e,t}}{A_c}\left(1 + e \times \frac{y_t}{r^2}\right); \quad f_{b,p} = -\frac{P_{e,t}}{A_c}\left(1 + e \times \frac{y_b}{r^2}\right) \qquad \textbf{Equation 3.2}$$

$$f_{t,gdl} = \frac{M_{gdl} \times 12}{S_{tnc}}; \quad f_{b,gdl} = \frac{M_{gdl} \times 12}{S_{bnc}} \qquad \textbf{Equation 3.3}$$

$$f_{t,ddl} = \frac{M_{ddl} \times 12}{S_{tnc}}; \quad f_{b,ddl} = \frac{M_{ddl} \times 12}{S_{bnc}} \qquad \textbf{Equation 3.4}$$

$$f_{t,sdl} = \frac{M_{sdl} \times 12}{S_{tc}}; \quad f_{b,sdl} = \frac{M_{sdl} \times 12}{S_{bc}} \qquad \textbf{Equation 3.5}$$

$$f_{t,Mr} = \frac{M_{r,t} \times 12}{S_{tc}}; \quad f_{b,Mr} = \frac{M_{r,t} \times 12}{S_{bc}} \qquad \textbf{Equation 3.6}$$

Stresses developed at the top and bottom of the deck were calculated using the following equations:

$$(f_{t,sdl})_{deck} = \frac{M_{sdl} \times 12 \times y_{td}}{I_c}; \quad (f_{b,sdl})_{deck} = \frac{M_{sdl} \times 12 \times y_{bd}}{I_c} \qquad \textbf{Equation 3.7}$$

$$(f_{t,Mr})_{deck} = \frac{M_r(t) \times 12 \times y_{td}}{I_c}; \quad (f_{b,Mr})_{deck} = \frac{M_r(t) \times 12 \times y_{bd}}{I_c} \qquad \textbf{Equation 3.8}$$

3.8.3 Short-Term Prestress Losses

This study calculated the short-term steel relaxation loss between the jacking of strands to the time of prestress transfer. First, the final jacking stress, f_{PJ2}, was calculated by subtracting anchorage set losses (f_{PA}) from prestressing stress applied to the strands in the jacking process (f_{PJ1}):

$$f_{PJ2} = f_{PJ1} - f_{PA} \qquad \textbf{Equation 3.9}$$

Short-term relaxation losses, Δf_{PR1}, were then estimated using the following equations from Naaman (1982).

For stress-relieved strands,

$$\Delta f_{PR1} = \frac{log(24t_{pt})}{10}\left[\frac{f_{PJ2}}{f_{Py}} - 0.55\right] f_{PJ2} \qquad \textbf{Equation 3.10}$$

For low relaxation strands,

$$\Delta f_{PR1} = \frac{log(24t_{pt})}{10}\left[\frac{f_{PJ2}}{f_{Py}} - 0.55\right] f_{PJ2} \qquad \textbf{Equation 3.11}$$

Elastic shortening loss was calculated using the "accurate" method for pretensioned construction via an iterative approach (Naaman, 1982). The initial prestressing stress after strand

release, f_{pi}, was the prestressing stress obtained by subtracting short-term losses (Δf_{PR1} and Δf_{pES}) from the jacking stress, f_{pJ2}. Since the calculation of elastic shortening loss, Δf_{pES}, depends on the initial prestressing stress, f_{pi}, it is an iterative process. The elastic shortening loss, Δf_{pES} , was initially assumed to be zero, and the initial prestressing stress, f_{pi}, was calculated using Equation 3.12. This value of f_{pi} was then used to calculate Δf_{pES} using Equation 3.13, which calculated the new f_{pi}. This process was repeated until convergence.

$$f_{pi} = f_{pJ2} - \Delta f_{pR1} - \Delta f_{pES} \quad \textbf{Equation 3.12}$$

$$\Delta f_{pES} = n_{pi} \times \left(\frac{f_{pi}}{f_{PJ2}} \times f_{Fj} + f_G \right) \quad \textbf{Equation 3.13}$$

3.8.4 Concrete Deformations

Shrinkage and creep strains were calculated using the B4 model (Wendner et al., 2013; Bažant et al., 2015), which individually estimates drying shrinkage and autogenous shrinkage strains and calculates creep as creep compliance. The B4 model uses SI units for calculation (Table 3.5). Rather than converting every equation, the model in this study converted inputs to SI units before executing calculations with the B4 model.

Table 3.5: Units for B4 Model Inputs

Input Parameters	Units
Concrete compressive strength (f'$_c$)	MPa
Cement content (c)	kg/m^3
Temperature	°C
Volume-to-surface ratio (V/S)	mm
Density of concrete (ρ)	kg/m^3

3.8.4.1 Calculation of Drying Shrinkage

Drying shrinkage at time t for concrete removed from curing at time t_o was calculated based on the ultimate drying shrinkage, $\varepsilon_{sh\infty}(t_0)$, modified based on humidity, k_h, and time, $S(t)$:

$$\varepsilon_{sh}(t, t_o) = \varepsilon_{sh\infty}(t_0) k_h S(t) \quad \textbf{Equation 3.14}$$

The ultimate drying shrinkage, $\varepsilon_{sh\infty}(t_0)$, which is a function of temperature, concrete mixture proportions, concrete constituent materials, and shape, was calculated as

$$\varepsilon_{sh\infty}(t_0) = -\varepsilon_0 k_{\epsilon a} \frac{E_c(7\beta_{Th} + 600\beta_{Ts})}{E_c(t_0 + \tau_{sh} \times \beta_{Ts})} \quad \textbf{Equation 3.15}$$

$$\varepsilon_0 = \varepsilon_{cem} \left(\frac{a/c}{6}\right)^{p_{\epsilon a}} \left(\frac{w/c}{0.38}\right)^{p_{\epsilon w}} \left(\frac{6.5c}{\rho}\right)^{p_{\epsilon c}} \quad \textbf{Equation 3.16}$$

$$\beta_{Ts} = exp\left[\frac{U_s}{R}\left(\frac{1}{293} - \frac{1}{T + 273}\right)\right] \quad \textbf{Equation 3.17}$$

$$\beta_{Th} = exp\left[\frac{U_h}{R}\left(\frac{1}{293} - \frac{1}{T_{cur} + 273}\right)\right] \quad \textbf{Equation 3.18}$$

A value of 4,000 K was used in the model instead of U_h/R and U_s/R as recommended in Bažant et al. (2015).

The humidity-dependent factor, k_h, was based on the relative humidity of the environment, h:

$$k_h = 1 - h^3 \quad if\ h \leq 0.98 \quad \textbf{Equation 3.19}$$

$$k_h = 12.94(1 - h) - 0.2 \quad if\ 0.98 \leq h \leq 1 \quad \textbf{Equation 3.20}$$

The modification factor to account for time since removal from curing was then calculated based on τ_{sh}, the drying shrinkage halftime (Wendner et al., 2013).

$$S(t) = tanh\sqrt{\frac{t - t_0}{\tau_{sh}}} \quad \textbf{Equation 3.21}$$

The drying shrinkage halftime, or the time for drying strain to reach half its final value, depends on factors related to concrete mixture proportions, constituent materials, and shape (see Notation).

$$\tau_{sh} = \tau_0 \times k_{\tau a} \times \left(k_s \frac{D}{1mm}\right)^2 \quad \textbf{Equation 3.22}$$

$$\tau_0 = \tau_{cem} \left(\frac{a/c}{6}\right)^{p_{\tau a}} \left(\frac{w/c}{0.38}\right)^{p_{\tau w}} \left(\frac{6.5c}{\rho}\right)^{p_{\tau c}} \quad \textbf{Equation 3.23}$$

$$D = 2 \times (\mathrm{V/S}) \quad \textbf{Equation 3.24}$$

3.8.4.2 Calculation of Autogenous Shrinkage

Autogenous shrinkage typically begins at the time of the first set, $t = 0$, whereas drying shrinkage begins after the concrete is exposed to the environment at time t_0 (Bažant et al., 2015). Autogenous shrinkage, which is a function of concrete mixture proportions and cement type, was calculated using the B4 model as follows:

$$\varepsilon_{au}(t, t_0) = \varepsilon_{au\infty}\left[1 + \left(\frac{\tau_{au}}{t + t_0}\right)^{\alpha}\right]^{r_t} \quad \textbf{Equation 3.25}$$

$$\tau_{au} = \tau_{au,cem}\left(\frac{w/c}{0.38}\right)^{r_{\tau w}} \quad \textbf{Equation 3.26}$$

$$\varepsilon_{au\infty} = -\varepsilon_{au,cem}\left(\frac{a/c}{6}\right)^{r_{\epsilon a}}\left(\frac{w/c}{0.38}\right)^{r_{\epsilon w}} \quad \textbf{Equation 3.27}$$

$$\alpha = r_{\alpha}\left(\frac{w/c}{0.38}\right) \quad \textbf{Equation 3.28}$$

The Notation section contains values of modification factors.

3.8.4.3 Calculation of Creep Compliance

Creep compliance includes both elastic and creep strains, and creep strains include basic creep and drying creep. Basic creep occurs at constant moisture content, while drying creep occurs when the concrete is drying while under load. Because elastic strain was calculated separately in this model, the model eliminated elastic strain from the creep compliance calculated from the B4 model (Bažant et al., 2015). The resulting creep compliance function, neglecting elastic strains, was

$$J(t, t') = R_T C_0(t, t') + C_d(t, t', t_0) \quad \textbf{Equation 3.29}$$

The first term, representing basic creep, was calculated using the following equations, which are a function of the current age of the concrete, t, and the concrete age at the time of loading, t':

$$C_0(t, t') = q_2 Q(t, t') + q_3 ln\left[1 + \left(\frac{t - t'}{1\ day}\right)^{0.1}\right] + q_4 ln\left(\frac{t}{t'}\right) \quad \textbf{Equation 3.30}$$

$$Q(t, t') = Q_f(t')\left(1 + \left(\frac{Q_f(t')}{Z(t, t')}\right)^{r(t')}\right)^{\frac{1}{r(t')}} \quad \textbf{Equation 3.31}$$

$$Q_f(t') = \left[0.086\left(\frac{t'}{1\ day}\right)^{\frac{2}{9}} + 1.21\left(\frac{t'}{1\ day}\right)^{\frac{4}{9}}\right]^{-1} \quad \textbf{Equation 3.32}$$

$$r(t') = 1.7\left(\frac{t'}{1day}\right)^{0.12} + 8 \quad \textbf{Equation 3.33}$$

$$Z(t.t') = \left(\frac{t'}{1day}\right)^{-0.5} ln\left[1 + \left(\frac{t-t'}{1day}\right)^{0.1}\right] \quad \textbf{Equation 3.34}$$

The constants q_2, q_3, and q_4 are semi-empirical parameters for various components of creep and shrinkage calibrated to a database of test results (Bažant et al., 2015; Wendner et al., 2015). They are a function of cement type and concrete mixture proportions:

$$q_2 = \frac{p_2}{1GPa}\left(\frac{w/c}{0.38}\right)^{p_{2w}} \quad \textbf{Equation 3.35}$$

$$q_3 = p_3 q_2 \left(\frac{a/c}{6}\right)^{p_{3a}} \left(\frac{w/c}{0.38}\right)^{p_{3w}} \quad \textbf{Equation 3.36}$$

$$q_4 = \frac{p_4}{1GPa}\left(\frac{a/c}{6}\right)^{p_{4a}} \left(\frac{w/c}{0.38}\right)^{p_{4w}} \quad \textbf{Equation 3.37}$$

Drying creep compliance is a function of concrete mixture proportions; relative humidity; drying shrinkage halftime, τ_{sh}; concrete age at the time of loading, *t'*; and concrete age when removed from curing, t_0. It was calculated using

$$C_d(t,t',t_0) = q_5\langle exp[-p_{5H}H(t,t_0)] - exp[-p_{5H}H_c(t'_0,t_0)]\rangle^{0.5} \quad \textbf{Equation 3.38}$$

$$H_c(t,t_0) = 1 - (1-h)tanh\sqrt{\frac{t'_0 - t_0}{\tau_{sh}}} \quad \textbf{Equation 3.39}$$

$$H(t,t_0) = 1 - (1-h)tanh\sqrt{\frac{t - t_0}{\tau_{sh}}} \quad \textbf{Equation 3.40}$$

$$q_5 = \frac{p_5}{1GPa}\left(\frac{a/c}{6}\right)^{p_{5a}} \left(\frac{w/c}{0.38}\right)^{p_{5w}} |k_h \epsilon_{sh\infty}(t_0)|^{p_{5\epsilon}} \quad \textbf{Equation 3.41}$$

3.8.4.4 Creep and Shrinkage Strain

Creep compliance obtained from the B4 model was converted to creep strain. To determine the creep strain resulting from different loads applied at different points in time, the principle of superposition was applied (Table 3.6). Once creep compliance was obtained, the creep strain at any point could be calculated at time *t* as

$$\varepsilon_{cr}(t, t') = J(t, t') \times \sigma_i \qquad \textbf{Equation 3.42}$$

Stresses in the girder were calculated at the top and bottom fibers at various sections throughout the length of the girder. The corresponding creep strains due to these stresses were then computed using Equation 3.42. Because different loads were applied at different points in time, the creep strains developed by these loads were calculated separately and then summed (Section 3.7.1). Some loads, such as prestressing force, change over time as the concrete creeps. Therefore, creep induced by prestressing forces must account for changes in force with time. Modeling of the interconnectedness of creep and effective prestress force is discussed in Section 3.8.5.2.

Table 3.6 presents the formulas used to calculate the creep strains at various stages in this study. When the deck was removed at time T_4, the load due to deck self-weight and superimposed loads no longer acted on the girder, resulting in changes in the creep strains in the girder. To account for creep recovery resulting from the removal of the load, deck removal was simulated by adding a load equal to the deck weight acting in the direction opposite gravity, as discussed in Section 2.2.3. The new deck was then cast at time T_5, and a new sustained load was introduced to the structure. Finally, superimposed loads were reapplied to the new deck at time T_6. The girder continued to creep and shrink until the final age, T_7.

Table 3.6: Formulas for Calculating Creep Strain

From time T_1 to T_2:	
$\varepsilon_{cr,top}(t) = J(t,T_1).\left[f_{t,p} + f_{t,gdl}\right]$	**Equation 3.43**
$\varepsilon_{cr,bot}(t) = J(t,T_1).\left[f_{b,p} + f_{b,gdl}\right]$	**Equation 3.44**
From time T_2 to T_3:	
$\varepsilon_{cr,top}(t) = J(t,T_1).\left[f_{t,p} + f_{t,gdl}\right] + J(t,T_2).\left[f_{t,ddl} + \Delta f_{t,dsh}(t)\right]$	**Equation 3.45**
$\varepsilon_{cr,bot}(t) = J(t,T_1).\left[f_{b,p} + f_{b,gdl}\right] + J(t,T_2).\left[f_{b,ddl} + \Delta f_{b,dsh}(t)\right]$	**Equation 3.46**
From time T_3 to T_4:	
$\varepsilon_{cr,top}(t) = J(t,T_1).\left[f_{t,p} + f_{t,gdl}\right] + J(t,T_2).\left[f_{t,ddl} + \Delta f_{t,dsh}(t)\right] + J(t,T_3).f_{t,sdl}$	**Equation 3.47**
$\varepsilon_{cr,bot}(t) = J(t,T_1).\left[f_{b,p} + f_{b,gdl}\right] + J(t,T_2).\left[f_{b,ddl} + \Delta f_{b,dsh}(t)\right] + J(t,T_3).f_{b,sdl}$	**Equation 3.48**
From time T_4 to T_5:	
$\varepsilon_{cr,top}(t) = J(t,T_1).\left[f_{t,p} + f_{t,gdl}\right] + J(t,T_2).\left[f_{t,ddl} + \Delta f_{t,dsh}(t)\right] + J(t,T_3).f_{t,sdl} - J(t,T_4).\left[f_{t,ddl} + \Delta f_{t,dsh}(t) + f_{t,sdl}\right]$	**Equation 3.49**
$\varepsilon_{cr,bot}(t) = J(t,T_1).\left[f_{b,p} + f_{b,gdl}\right] + J(t,T_2).\left[f_{b,ddl} + \Delta f_{b,dsh}(t)\right] + J(t,T_3).f_{b,sdl} - J(t,T_4).\left[f_{b,ddl} + \Delta f_{b,dsh}(t) + f_{b,sdl}\right]$	**Equation 3.50**
From time T_5 to T_6:	
$\varepsilon_{cr,top}(t) = J(t,T_1).\left[f_{t,p} + f_{t,gdl}\right] + J(t,T_2).\left[f_{t,ddl} + \Delta f_{t,dsh}(t)\right] + J(t,T_3).f_{t,sdl} - J(t,T_4).\left[f_{t,ddl} + \Delta f_{t,dsh}(t) + f_{t,sdl}\right] + J(t,T_5).\left[f_{t,nddl} + \Delta f_{t,ndsh}(t)\right]$	**Equation 3.51**
$\varepsilon_{cr,bot}(t) = J(t,T_1).\left[f_{b,p} + f_{b,gdl}\right] + J(t,T_2).\left[f_{b,ddl} + \Delta f_{b,dsh}(t)\right] + J(t,T_3).f_{b,sdl} - J(t,T_4).\left[f_{b,ddl} + \Delta f_{b,dsh}(t) + f_{b,sdl}\right] + J(t,T_5).\left[f_{b,nddl} + \Delta f_{b,ndsh}(t)\right]$	**Equation 3.52**
From time T_6 to T_7:	
$\varepsilon_{cr,top}(t) = J(t,T_1).\left[f_{t,p} + f_{t,gdl}\right] + J(t,T_2).\left[f_{t,ddl} + \Delta f_{t,dsh}(t)\right] + J(t,T_3).f_{t,sdl} - J(t,T_4).\left[f_{t,ddl} + \Delta f_{t,dsh}(t) + f_{t,sdl}\right] + J(t,T_5).\left[f_{t,nddl} + \Delta f_{t,ndsh}(t)\right] + J(t,T_6).f_{t,nsdl}$	**Equation 3.53**
$\varepsilon_{cr,bot}(t) = J(t,T_1).\left[f_{b,p} + f_{b,gdl}\right] + J(t,T_2).\left[f_{b,ddl} + \Delta f_{b,dsh}(t)\right] + J(t,T_3).f_{b,sdl} - J(t,T_4).\left[f_{b,ddl} + \Delta f_{b,dsh}(t) + f_{b,sdl}\right] + J(t,T_5).\left[f_{b,nddl} + \Delta f_{b,ndsh}(t)\right] + J(t,T_6).f_{b,nsdl}$	**Equation 3.54**

Creep strain at the centroid of the prestressing strands was then calculated from the top fiber and bottom fiber strains obtained from the above equations as

$$\varepsilon_{cr,cgp}(t) = \varepsilon_{cr,bot}(t) - \left[\varepsilon_{cr,bot}(t) - \varepsilon_{cr,top}(t)\right] \times y_{ps}/H \quad \textbf{Equation 3.55}$$

The incremental creep strain at the centroid of the prestressing strand between time t_{i-1} and t_i was

$$\varepsilon_{cr,cgp}(t_i, t_{i-1}) = \varepsilon_{cr,cgp}(t_i) - \varepsilon_{cr,cgp}(t_{i-1}) \quad \textbf{Equation 3.56}$$

Total shrinkage strain at time t was the sum of drying and autogenous shrinkage (Sections 3.8.4.1 and 3.8.4.2):

$$\varepsilon_{sh,total}(t, t_0) = \varepsilon_{sh}(t, t_0) + \varepsilon_{au}(t, t_0) \quad \textbf{Equation 3.57}$$

Shrinkage was assumed to be uniform throughout the girder depth. To calculate the shrinkage strain at the centroid of the strands between t_{i-1} and t_i, the shrinkage strain that developed between time t_0 and t_{i-1} was subtracted from the strain that developed between time t_0 and t_i, in which t_{i-1} and t_i are sequential time steps. The shrinkage strain between t_{i-1} and t_i was

$$\varepsilon_{sh,cgp}(t_i, t_{i-1}) = \varepsilon_{sh,total}(t_i, t_0) - \varepsilon_{sh,total}(t_{i-1}, t_0) \quad \textbf{Equation 3.58}$$

3.8.4.5 Differential Shrinkage

Because bridge girders and decks typically are made with different concrete placed at different times, they develop different magnitudes of shrinkage after the deck concrete sets. However, the calculation of differential shrinkage is complicated by deck cracking that develops due to girder restraint. PCI (1997) recommends estimating differential shrinkage as 50% of the deck shrinkage. This study used deck shrinkage, not the difference between deck and girder shrinkage, because girder shrinkage after deck placement is much smaller in magnitude than deck shrinkage (due to the relative difference in concrete ages), and the 50% factor for cracking is already relatively rough. The effects of differential shrinkage were therefore calculated based on 50% of the shrinkage calculated for the deck concrete (Section3.8.4.4), as shown in Figure 3.12. The effects of this strain were simulated as an external moment acting on the girder cross-section according to AASHTO LRFD (2012) recommendations.

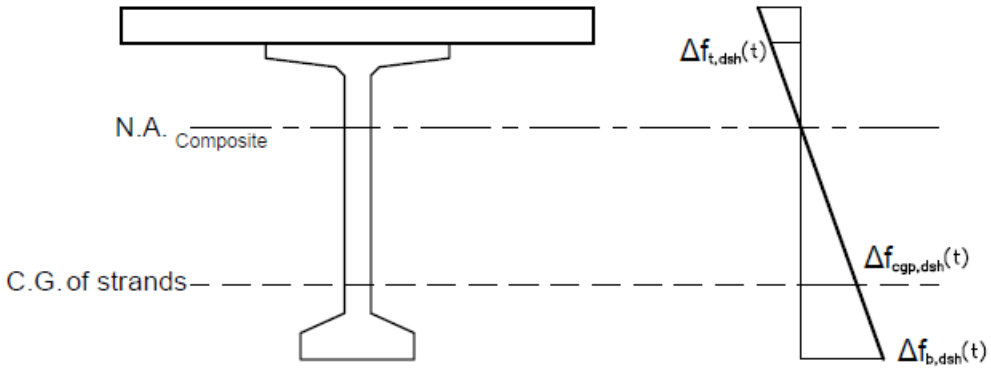

Figure 3.12: Stresses Caused by Differential Shrinkage

The stresses induced by differential shrinkage shown in Figure 3.12 were calculated as

$$\Delta f_{t,dsh}(t) = 0.5 \times \varepsilon_{sh,deck}(t,t_0) \times A_d \times E_{cd} \times \left(\frac{1}{A_c} - \frac{y_{tc}e_d}{I_c}\right) \quad \textbf{Equation 3.59}$$

$$\Delta f_{b,dsh}(t) = 0.5 \times \varepsilon_{sh,deck}(t,t_0) \times A_d \times E_{cd} \times \left(\frac{1}{A_c} - \frac{y_{bc}e_d}{I_c}\right) \quad \textbf{Equation 3.60}$$

$$\Delta f_{cgp,dsh}(t) = 0.5 \times \varepsilon_{sh,deck}(t,t_0) \times A_d \times E_{cd} \times \left(\frac{1}{A_c} - \frac{e_{pc}e_d}{I_c}\right) \quad \textbf{Equation 3.61}$$

3.8.4.6 Temperature-Induced Strains

As mentioned previously, daily, seasonal, and longer-term temperature variations were not considered for this analysis. The only temperature-induced strains considered in the model arise from differences between a reference temperature, when the concrete is setting and assumed to have zero strain, and the ambient environmental temperature, assumed to be constant over time. Temperature-induced strains were calculated as

$$\varepsilon_{temp} = \alpha_T \times \Delta T \quad \textbf{Equation 3.62}$$

3.8.5 Determination of Prestressing Forces

Prestress losses and subsequent effective prestress force are a function of calculated creep and shrinkage strains. Using the AASHTO LRFD equations for converting the creep and shrinkage strains in each time step to incremental prestress losses within that time step (Section 3.8.5.1), effective prestress force at time t_i was calculated by subtracting the incremental prestress losses

from the effective prestress force at time $t_{(i-1)}$. As the effective prestress force changes, the resulting concrete stresses and creep change, which again alters the effective prestress force. Section 3.8.5.2 describes the algorithm and calculation sequence to account for the interdependence between creep and prestress losses over time.

3.8.5.1 Prestress Losses

The incremental prestress loss due to concrete creep between time t_{i-1} and t_i was based on $\varepsilon_{cr,cgp}(t_i, t_{i-1})$, calculated with Equation 3.58, concrete elastic modulus, girder cross-sectional area, and a transformed section coefficient, K_{id}, to account for reinforcement ratio, modular ratio, and strand eccentricity:

$$\Delta P_{cr,t(i)(i-1)} = E_{ps} \times \varepsilon_{cr,cgp}(t_i, t_{i-1}) \times K_{id} \times A_{ps} \qquad \textbf{Equation 3.63}$$

The transformed section coefficient was calculated as follows:

$$K_{id} = \frac{1}{1 + \frac{E_p}{E_{ci}} \frac{A_{ps}}{A_g} \left(1 + \frac{A_g {e_{pg}}^2}{I_g}\right) [1 + 0.7\psi_b(t_f, t_i)]} \qquad \textbf{Equation 3.64}$$

Equation 3.64, from AASHTO LRFD (2012), includes a term in the denominator to account for time-dependent interaction between the concrete and bonded steel. The aging term, [*1+ 0.7* $\psi_b(t_f,t_i)$], was set to 1 in this study because the time-step analysis explicitly accounts for changes over time.

Prestress loss due to shrinkage of the girder concrete between time t_{i-1} and t_i was calculated as

$$\Delta P_{sh,t(i)(i-1)} = E_{ps} \times \varepsilon_{sh,cgp}(t_i, t_{i-1}) \times K_{id} \times A_{ps} \qquad \textbf{Equation 3.65}$$

Equation 3.65 is based on $\varepsilon_{sh,cgp}(t_i, t_{i-1})$, calculated with Equation 3.58, concrete elastic modulus, girder cross-sectional area, and K_{id}.

After neglecting the interdependence of prestress loss and creep/shrinkage, the total loss of prestress between time t_{i-1} and t_i was

$$\Delta P_{t(i)(i-1)} = \Delta P_{sh,t(i)(i-1)} + \Delta P_{cr,t(i)(i-1)} \qquad \textbf{Equation 3.66}$$

3.8.5.2 Interdependence of Creep and Effective Prestress Force

Creep and effective prestress force change over time, and each affects the other. Theoretically, resolving this requires iteration within each time step to balance the incremental creep and prestress loss. To reduce computation time, the model in this study did not iterate. Instead, the algorithm in Table 3.7 was used with a sufficiently small time interval to minimize error. In the algorithm, effective prestress force at the start of a time step is used to estimate incremental creep during the time step (Section 3.8.4.4). The incremental creep and the shrinkage strains are then used to estimate incremental change in prestress force within the time step (Section 3.8.5.1), which is then subtracted from the effective prestress force at the start of the time step to obtain the effective prestress force at the end of the time step:

$$P_{e,t_{(i+1)}} = P_{e,t_i} - \Delta P_{t_{i+1}t_i} \qquad \textbf{Equation 3.67}$$

Because creep is a function of a stable force and the time it was imposed, the model accounted for the time-varying nature of prestress force by considering the incremental prestress loss in each interval as a separate force acting at the end of the time interval. With this algorithm, the effective prestress force and prestress losses in the girder were profiled throughout the girder lifespan.

Table 3.7: Algorithm to Calculate Prestress Losses and Effective Prestress Force

Step no.	Process
Step 1:	Calculate the initial prestressing force P_i from 3.8.2
Step 2:	Determine: $\varepsilon_{cr,cgp}(t_1)$, $\varepsilon_{sh,total}(t_1, t_0)$ from t_{ptg} to t_1 from a and b
Step 3:	Convert the creep and shrinkage strain from step 2 to prestress force loss ($\Delta P_{t_1 t_0}$) using 3.8.5.1
Step 4:	Determine the total effective prestress force at time t_1 using Equation 3.67: $$P_{e,t_1} = P_{e,t_0} - \Delta P_{t_1 t_0}$$
Step 5:	Determine the change in creep strain from t_1 to t_2: Determine the change in creep strain from t_1 to t_2 due to initial prestressing force (P_i) and all other loads: $$\varepsilon'_{cr,top}(t_2, t_1) = \varepsilon_{cr,top}(t_2) - \varepsilon_{cr,top}(t_1)$$ **Equation 3.68** $$\varepsilon'_{cr,bot}(t_2, t_1) = \varepsilon_{cr,bot}(t_2) - \varepsilon_{cr,bot}(t_1)$$ **Equation 3.69** $$\varepsilon'_{cr,cgp}(t_2, t_1) = \varepsilon'_{cr,bot}(t_2, t_1) - [\varepsilon'_{cr,bot}(t_2, t_1) - \varepsilon'_{cr,top}(t_2, t_1) \times \frac{y_{ps}}{H}$$ **Equation 3.70** Determine the stress caused by $\Delta P_{t_1 t_0}$ at the centroid of the prestressing strand ($f_{cgp,\Delta P_{t_1 t_0}}$) as per 3.8.5.1 Determine the creep strain developed at time t_2 caused by $\Delta P_{t_1 t_0}$ applied at time t_1: $$\Delta\varepsilon_{cr,cgp}(t_2) = J(t_2, t_1) \times f_{cgp,\Delta P_{t_1 t_0}}$$ **Equation 3.71** Total creep strain developed from time t_1 to t_2 is $$d\varepsilon_{cr,cgp}(t_2, t_1) = \varepsilon'_{cr,cgp}(t_2, t_1) + \Delta\varepsilon_{cr,cgp}(t_2)$$ **Equation 3.72** Total shrinkage strain developed from time t_1 to t_2 is $$d\varepsilon_{sh,total}(t_2, t_1) = \varepsilon_{sh,total}(t_2, t_0) - \varepsilon_{sh,total}(t_1, t_0)$$ **Equation 3.73**
Step 6:	Convert the shrinkage ($d\varepsilon_{sh,total}(t_2, t_1)$) and creep strain ($d\varepsilon_{cr,cgp}(t_2, t_1)$) from step 5 to prestress loss ($\Delta P_{t_2 t_1}$) using 3.8.5.1
Step 7:	Determine the effective prestress force at time t_1: $$P_{e,t_2} = P_{e,t_1} - \Delta P_{t_2 t_1}$$ **Equation 3.74**
Step 8:	Repeat the procedure for another time step: For time step t_{n-1} to t_n : $$\varepsilon'_{cr,top}(t_n, t_{n-1}) = \varepsilon_{cr,top}(t_n) - \varepsilon_{cr,top}(t_{n-1})$$ **Equation 3.75** $$\varepsilon'_{cr,bot}(t_n, t_{n-1}) = \varepsilon_{cr,bot}(t_n) - \varepsilon_{cr,bot}(t_{n-1})$$ **Equation 3.76** $$\varepsilon'_{cr,cgp}(t_n, t_{n-1}) = \varepsilon'_{cr,bot}(t_n, t_{n-1}) - [\varepsilon'_{cr,bot}(t_n, t_{n-1}) - \varepsilon'_{cr,top}(t_n, t_{n-1}) \times \frac{y_{ps}}{H}$$ **Equation 3.77** Determine the creep strain developed from time t_{n-1} to t_n caused by $\Delta P_{t_1 t_0}$, $\Delta P_{t_1 t_n}$ … $\Delta P_{t_{n-1} t_{n-2}}$ applied at time t_1, t_2, … t_{n-1}

Step no.	Process	
	$\Delta\varepsilon_{cr,cgp}(t_n) = J(t_n, t_{n-1}) \times f_{cgp,\Delta P_{(n-1)(n-2)}} + \sum_{i=1}^{n-2} \left([J(t_n, t_i) - J(t_{n-1}, t_i)] \times f_{cgp,\Delta P_{t_i t_{i-1}}} \right)$	**Equation 3.78**
	Total creep strain developed from time t_{n-1} to t_n is $d\varepsilon_{cr,cgp}(t_n, t_{n-1}) = \varepsilon'_{cr,cgp}(t_n, t_{n-1}) + \Delta\varepsilon_{cr,cgp}(t_n)$	**Equation 3.79**
	Total shrinkage strain developed time t_{n-1} to t_n is $d\varepsilon_{sh,total}(t_n, t_{n-1}) = \varepsilon_{sh,total}(t_n, t_0) - \varepsilon_{sh,total}(t_{n-1}, t_0)$	**Equation 3.80**
Step 9:	Convert the shrinkage ($d\varepsilon_{sh,total}(t_n, t_{n-1})$) and creep strain ($d\varepsilon_{cr,cgp}(t_n, t_{n-1})$) from step 5 to prestress loss using 3.8.5.1	
Step 10:	Determine the effective prestress force at time t_n: $P_{e,t_n} = P_{e,t_{n-1}} - \Delta P_{t_n t_{n-1}}$	**Equation 3.81**

3.8.6 Determination of Restraint Moment

The method proposed by Menkulasi et al. (2018) served as the basis for calculating restraint moments at the ends of a simply-supported girder made continuous with diaphragms, but modifications were made to accommodate the research objectives. Creep compliance obtained from the B4 model was used to determine the creep strain instead of the AAEM in Menkulasi et al. (2018). Similarly, shrinkage of the deck and girder were calculated with the B4 model to determine the restraint moment due to differential shrinkage. Girder curvature was then obtained from the calculated strains, and the moment-area method was used to calculate girder deflections and girder-end rotations. The time-step method was then used to calculate the restraint moment at each time step. The mid-span moment due to end restraint was approximately one-tenth of the mid-span moments due to applied loads. Therefore, the effects of restraint moment on creep strains were minimal compared to the total mid-span moment, so they were not considered in the study for the purpose of simplification.

3.8.6.1 Restraint Moment Due to Creep

Girder curvature in a simply-supported girder due to creep strain was calculated at each section along the span length as

$$\varphi_{cr}(t_i, t_{i-1}) = (d\varepsilon_{cr,bot}(t_i, t_{i-1}) - d\varepsilon_{cr,top}(t_i, t_{i-1}))/H \quad \textbf{Equation 3.82}$$

Assuming that diaphragms fully restrain girder-end rotation and girder elongation, the axial force and moment at the centroid of the girder cross-section were calculated at discrete lengths throughout the girder. The axial force $N_{gcr}(t_i, t_{i-1})$ that developed between time t_{i-1} and t_i depended on the creep change during that time period. Similarly, the moment $M_{gcr}(t_i, t_{i-1})$ that developed between time t_{i-1} and t_i depended on the curvature due to creep between that time period, $\varphi_{cr}(t_i, t_{i-1})$, axial force calculated before, $N_{gcr}(t_i, t_{i-1})$, and distance between the centroid of the girder to the centroid of the transformed section (concrete + reinforcement), or d_{gt} (considered zero in our case). The axial forces and moments at the center of gravity of the girder due to concrete creep were

$$N_{gcr}(t_i, t_{i-1}) = d\varepsilon_{cr,cgp}(t_i, t_{i-1}) \times E_c \times A_c \quad \textbf{Equation 3.83}$$

$$M_{gcr}(t_i, t_{i-1}) = \varphi_{cr}(t_i, t_{i-1}) \times E_c \times I_{cg} + N_{gcr}(t_i, t_{i-1}) \times d_{gt} \quad \textbf{Equation 3.84}$$

Time-dependent change in curvature due to girder concrete creep from any time t_{i-1} to t_i was

$$\delta\varphi_{cr}(t_i, t_{i-1}) = \frac{M_{gcr}(t_i, t_{i-1})}{E \times I_c} \quad \textbf{Equation 3.85}$$

The curvature profile of the girder was obtained by calculating the time-dependent curvature at various sections throughout the length of the girder. Changes in the end rotations ($\theta_{t_i t_{i-1}}$) were then determined from the curvature profile using the moment-area method. The resulting end rotation ($\theta_{t_i t_{i-1}}$) was used to determine the restraint moment developed on the girder between time t_{i-1} to t_i. According to Alberta Technical Services Branch (2018), restraint moment at the end support for end spans is

$$M_{r,cr}(t_i, t_{i-1}) = 0 \quad \textbf{Equation 3.86}$$

And restraint moment at the continuous support is

$$M_{r,cr}(t_i, t_{i-1}) = -\frac{3E_c I_c \theta_{t_i t_{i-1}}}{L} \quad \textbf{Equation 3.87}$$

For middle spans, Alberta Technical Services Branch (2018) calculates restrained moment at the left support as

$$M_{r,cr}(t_i, t_{i-1}) = \frac{2E_c I_c \theta_{t_i t_{i-1}}}{L}$$ **Equation 3.88**

And restrained moment at the right support as

$$M_{r,cr}(t_i, t_{i-1}) = -\frac{2E_c I_c \theta_{t_i t_{i-1}}}{L}$$ **Equation 3.89**

Total restraint moment developed due to creep until time t_i is given by

$$M_{r,cr}(t_i) = \sum_{n=1}^{n=i-1} M_{r,cr}(t_n, t_{n-1})$$ **Equation 3.90**

3.8.6.2 Restraint Moment Due to Shrinkage

In this study, uniform shrinkage was assumed throughout the length and depth of the girder, meaning that shrinkage of the girder did not cause the restraint moment. However, differential shrinkage between the deck and the girder resulted in girder curvature and negative restraint moment. Therefore, deck and girder shrinkage were calculated using the B4 model, with only 50% of the deck shrinkage considered to account for deck cracking, as recommended by PCI (Section 3.8.4.5). According to Kytölä and Laaksonen (2018), the equations used to calculate the restrained force due to differential shrinkage between the slab and girder are

$$N_{sh}(t) = \Delta\varepsilon_{sh}(t).A_d.E_{cd}$$ **Equation 3.91**

$$\Delta\varepsilon_{sh}(t) = 0.5\varepsilon_{sh,deck}(t, t_{0d}) - \varepsilon_{sh,total}(t, t_0)$$ **Equation 3.92**

And the restrained force between time t_i and t_{i-1} is

$$\Delta N_{sh,i(i-1)} = N_{sh}(t_i) - N_{sh}(t_{i-1})$$ **Equation 3.93**

Similarly, moment due to differential shrinkage between time t_i and t_{i-1} is

$$\Delta M_{sh,i(i-1)} = \Delta N_{sh,i(i-1)}.z_{dg}$$ **Equation 3.94**

And total restraint moment due to differential shrinkage until time t_i is

$$M_{r,sh}(t_i) = \sum_{n=1}^{n=i-1} \Delta M_{sh,i(i-1)}$$ **Equation 3.95**

3.8.6.3 Calculation of Cracking Moment

The effectiveness of the continuity diaphragm at limiting girder-end rotations decreases when the continuity diaphragm or the girder ends begin to develop cracks (Mirmiran et al., 2001). Strength calculations suggest that girder ends are likely to crack before the diaphragm, although this depends on the reinforcement detailing and diaphragm configuration. Once the girder ends crack in bending, the flexural strength of the girder at the face of the diaphragm limits restraint moments. Studies suggest that typical bridge details provide beam-end moment strengths that are 0.6 to 1.2 times the cracking moment strength. For simplicity, this study assumed that the restraint moments did not exceed the girder-end cracking moment, which is typically computed with gross girder composite section properties, the effective width of the composite deck slab, if any, and the material properties of the concrete in the concrete girder (AASHTO LRFD, 2012). The elastic modulus of concrete was based on the specified 28-day concrete strength and assumed to remain constant over time; any increase in elastic modulus due to an increase in compressive strength of concrete over time was neglected. The increase in modulus of rupture (f_r) due to increased concrete strength over time was also neglected.

The cracking moment of the girder at any section was calculated using the following equation (Ghimire, 2014):

$$M_{cr} = \frac{I_c}{y_{bc}}\left[\frac{P_e}{A_c}\left(1 + \frac{e.y_b}{r^2}\right) + f_r\right] \qquad \textbf{Equation 3.96}$$

Since the prestressing force at the ends of the girders was equal to zero, P_e was taken as zero, reducing Equation 3.96 to:

$$M_{cr} = \frac{I_c.f_r}{y_{bc}} \qquad \textbf{Equation 3.97}$$

According to Naaman (1982), the modulus of rupture of the girder concrete is

$$f_r = 7.5\sqrt{f'_c(psi)} \qquad \textbf{Equation 3.98}$$

3.9 Stress Limits

Stresses in the girder developed at any time were compared against the stress limits determined using AASHTO LRFD (2012). Stress limits for the prestressing tendons and concrete are listed in Tables 3.8 and 3.9, respectively.

Table 3.8: Stress Limits for Prestressing Tendons according to AASHTO LRFD (2012)

Conditions	Tendon Type	
	Stress-Relieved Strand	Low Relaxation Strand
Immediately before transfer (f_{pbt})	$0.70f_{pu}$	$0.75f_{pu}$
At service limit state after all losses (f_{pe})	$0.80f_{py}$	$0.80f_{py}$

Table 3.9: Stress Limits for Concrete according to AASHTO LRFD (2012)

Location	Compressive Stress Limit	Tensile Stress Limit
Other than segmentally constructed bridges, due to the sum of effective prestress and permanent loads	$0.45f'_{cg}$	$0\ to\ 0.19\sqrt{f'_{cg}}$
Segmentally constructed bridges, due to the sum of effective prestress and permanent loads	$0.45f'_{cg}$	$0\ to\ 0.0948\sqrt{f'_{cg}}$
Due to the sum of effective prestress, permanent loads, and transient loads as well as during shipping and handling	$0.60\Phi_w f'_{cg}$	NA

Chapter 4: Results

This chapter describes the application of the model described in Chapter 3 to the example bridge in Design Example 9.1a of the *PCI Bridge Design Manual* (3rd edition) to (1) validate the model outputs against published bridge design calculations and (2) show how varying model inputs affects bridge behavior over time. Details of the bridge and girders and the parameters used for the calculations are summarized, and the chapter includes the results from a parametric study that highlighted the influence of input parameters on girder behavior during and after deck replacement.

4.1 Example Bridge

The bridge in *PCI Bridge Design Manual* Example 9.1a has six 120-ft single-span AASHTO BT-72 girders supporting an 8-in. thick concrete deck. The girders are spaced 9 ft apart, resulting in a total roadway width of 51 ft, including a 3-ft cantilever slab on each side, as shown in Figure 4.1. The cross-section of the girder and the deck is shown in Figure 4.2. Prestressing strands are doubly harped at 0.4L from the ends, where L is the length of the prestressed girder. Additional assumptions were made to define the support conditions, environmental conditions, and mixture proportions to supplement the provided information. The relevant input information is provided in Tables 4.1 to 4.6. The following differences were observed between the design example and the analysis inputs:

1. The bridge is described as single-span in the design example, but a two-span bridge is considered in the analysis to show the calculation of continuity diaphragm effects and restraint moment.
2. In the design example, long-term prestress loss is calculated using equations 5.9.5.4.3a to d in AASHTO LRFD (2012). The model uses time-step analysis to explicitly calculate the interaction of creep, shrinkage, elastic deformations in response to load, and prestress force.
3. The design example lacks some inputs required for the model, so assumptions were made where necessary.

4. Unlike the example, the model neglects live loads because the focus of this is on long-term bridge behavior.

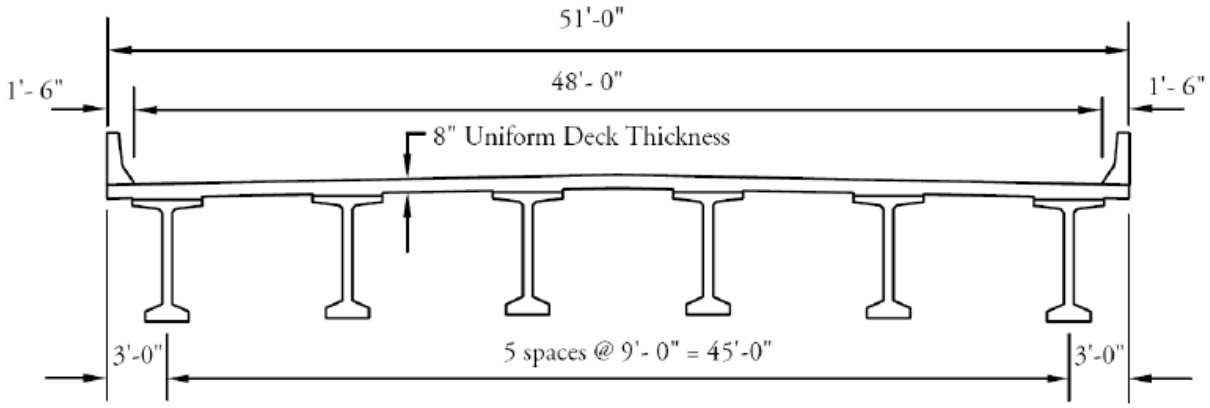

Figure 4.1: Cross-Section of Example Bridge
Source: Example 9.1a of PCI (2020)

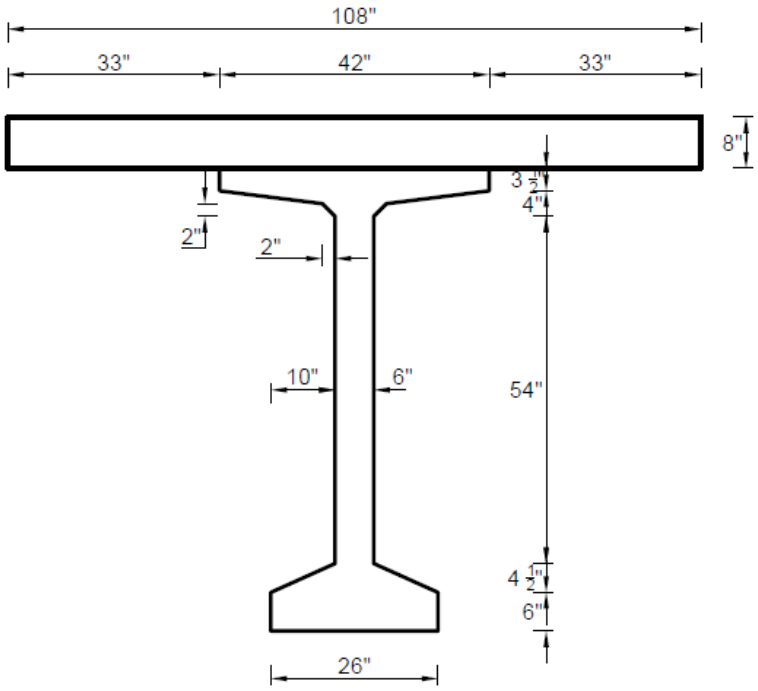

Figure 4.2: Composite (Girder + Deck) Section for Example Bridge
Source: Example 9.1a of PCI (2020)

Table 4.1: Loads and Material Strength Inputs

	Parameter	Variable	Value
Concrete	Compressive strength of girder concrete, ksi	f_{cg}	6.5
	Initial compressive strength of girder concrete, ksi	f_{ci}	5.8
	Compressive strength of old deck concrete, ksi	f_{cd}	4
	Compressive strength of new deck concrete, ksi	f_{cnd}	4
	Unit weight of concrete, kcf	γ_c	0.15
Strands	Ultimate tensile strength of strands, ksi	f_{pu}	270
	Yield strength of strands, ksi	f_{py}	243
	Modulus of elasticity of strands, ksi	E_{ps}	28500
Superimposed Loads	Unit weight of wearing surface, kcf	γ_{ws}	0.15
	Unit weight of barrier, kips/ft/side	γ_b	0.3
	Unit weight of future wearing surface, kcf	γ_{fws}	0.15

Table 4.2: Timeline Inputs

Parameters	Variable	Value
Age of girder at the end of curing, days	t_0	0.5
Age of girder during transfer, days	T_1	1.0
Age of girder at deck placement, days	T_2	28
Age of girder during the addition of superimposed loads, days	T_3	33
Age of deck at the end of curing, days	t_{0d}	0.5
Age of girder at deck removal, days	T_4	7305
Age of girder at deck replacement, days	T_5	7325
Age of new deck at the end of curing, days	t_{0nd}	0.5
Age of girder during addition of new superimposed loads, days	T_6	7330
Age of girder at final time-step, days	T_7	20000

Table 4.3: Concrete Mixture Proportion Inputs

Parameters	Variables	Girder	Old deck	New deck
Water-cement ratio	*wc*	0.4	0.5	0.5
Cement content, lb/ft^3	*c*	13.7	13.7	13.7
Cement type	*ctype*	Normal	Normal	Normal
Density of concrete, lb/ft^3	*ρ*	146.7	146.7	146.7
Aggregate-cement ratio	*ac*	7	7	7
Aggregate type	*aggtype*	Unavailable	Unavailable	Unavailable
Volume-to-surface ratio, ft	*V/S*	0.25	0.31	0.31

Table 4.4: Dimensional Data Inputs

Parameters	Variable	Value
Properties of the bridge		
Bridge span, ft	L'	121
Design span of the girder, ft	L_{span}	120
Distance between girders, ft	S	9
Overhang length, ft	L_{cant}	3
Total width of the road, ft	W_{total}	51
Properties of the girder		
Girder type		AASHTO BT-72
Total girder height, in.	H	72
Girder cross-sectional area, in.^{2}	A_c	767
Prestressing strand diameters, in.	d_s	½
Number of strands	$N_{strands}$	48
Profile of strands	*sprofile*	Doubly harped
Strand eccentricity at ends, in.	e_{end}	17.2
Strand eccentricity at harping points, in.	e_{harped}	29.7
Properties of old deck		
Deck thickness, in.	t_d	8
Deck cross-sectional area, in.^{2}	A_d	864
Properties of new deck		
Deck thickness, in.	t_{nd}	8
Deck cross-sectional area, in.^{2}	A_{nd}	864

Table 4.5: Environmental Variables Inputs

Parameters	Variables	Girder	Old deck	New deck
Relative humidity	h	0.7	0.7	0.7
Temperature, °F	T	68	68	68
Reference temperature, °F	T_{ref}	68	68	68

Table 4.6: Geometry and Sectional Properties

Sectional Properties	Variables	Girder	Deck	Composite section
Area, in.^{2}	A	767	678	1,440
Depth of CG from the bottom, in.	y_b	36.6	4.0	55.0
Depth of CG from the top, in.	y_t	35.4	4.0	24.9
Moment of inertia, in.^{4}	I_{cg}	546,000	3,600	1,189,000
Top section modulus, in.^{3}	S_t	15,400	904	47,700
Bottom section modulus, in.^{3}	S_b	14,900	904	21,600

4.2 Sensitivity Analysis

The model in this study divided the prestressed girder span into n segments for analysis. Accuracy of results depended on the discrete length (dL) chosen because short segments produce precise calculations and a smooth deflection profile, but they increase the required computation time. Table 4.7 summarizes the results of a sensitivity analysis that was conducted to select the optimal value for dL. The deflection at various loading stages, creep strains at the end of the analysis, and effective prestress force were compared to evaluate different values of dL. Discrete lengths of 0.5 ft, 1 ft, 2 ft, 6 ft, and 12 ft were selected, which ranged from 0.4 to 10% of the girder length, L. Values obtained with dL = 0.5 ft (0.4% of L) are treated as the base case to compare other values.

Of the parameters considered, effective prestress was least sensitive to discrete length. The discrete length had the most substantial impact on girder deflection. For the bridge considered, increasing dL from 0.4% of L to 10% of L led to a change in the final deflection of approximately 10%. The girder deflection profiles plotted in Figure 4.3 also show that shorter discrete lengths resulted in a smoother deflection profile. Some discrepancy in the deflection profile was also observed at dL = 12 ft. As shown in Table 4.7, creep strain was sensitive to dL, with dL = 10% of

L producing a creep strain at 20,000 days that differed by -7.4% relative to the reference (*dL* = 0.4% of *L*). Error in the creep strain remained nearly constant regardless of the time elapsed, as shown in Table 4.7. A *dL* of 2 ft (1.7% of *L*) was selected for the study analysis to balance computation time with accuracy. Discrete lengths of 0.5, 1, and 2 ft produced similar results with a maximum discrepancy of 0.3%.

Table 4.7: Sensitivity Analysis for Incremental Length

Parameters	**Values for *dL* = 0.5 ft (0.4% of *L*) (Base case)**	**% difference from the base case**			
		1 ft (0.8% of *L*)	**2 ft (1.7% of *L*)**	**6 ft (5% of *L*)**	**12 ft (10% of *L*)**
Deflection after all loads applied (34 days)	2.38 in.	-0.05%	-0.15%	-1.17%	-5.53%
Rebound due to deck removal	2.69 in.	-0.01%	-0.10%	-1.32%	-5.38%
Deflection at 20000 days	-0.43 in.	0.07%	-0.30%	-4.02%	-9.69%
Creep strain at 100 days	-6.65×10^{-4}	-0.04%	-0.21%	-1.97%	-7.92%
Final creep strain at 20000 days	-9.20×10^{-4}	-0.04%	-0.19%	-1.83%	-7.36%
Preliminary prestress losses	141 kips	0.01%	0.03%	0.25%	1.02%
Total prestress loss	525 kips	0.01%	0.06%	0.54%	2.15%

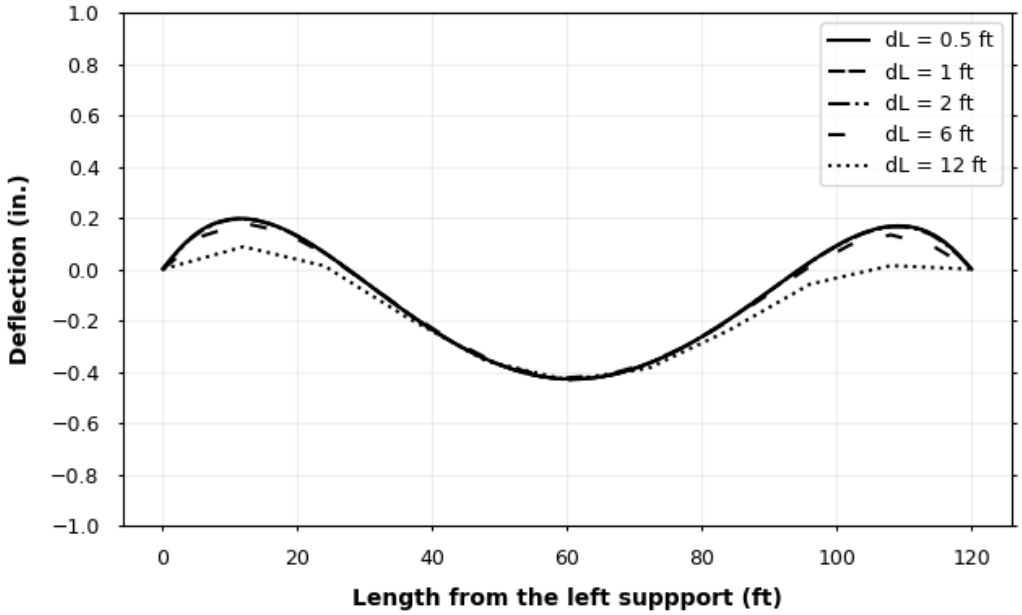

Figure 4.3: Deflection Profile of Prestressed Concrete Girder at 20,000 Days with Various Discrete Lengths

4.3 Example Bridge Analysis Results

4.3.1 Effective Prestress Force

Figure 4.4 shows the effective prestress force at midspan of the girder throughout its lifespan. As shown, most prestress loss occurred early in the girder life between points A (prestress transfer) and C (deck placement), when creep and shrinkage strains develop most rapidly. Prestress gains at points C and D in Figure 4.4 are due to the change in creep strain caused by the addition of deck and superimposed loads, respectively. The deck load and the superimposed load, which create tension at the bottom and compression at the top, opposed the prestressing force (compression at the bottom and tension at the top), leading to creep strain opposite the creep strain due to prestressing force, which resulted in prestress gain (Figure 4.4). Between D and E, which represent addition of superimposed loads and deck removal, creep and shrinkage gradually contributed to prestress loss over time. As expected, prestress force decreased as the deck was removed (at E) and increased when the deck and superimposed loads were reinstalled (F and G, respectively). Prestress gain due to initial deck placement was approximately 20 kips, whereas prestress gain for the new deck placement was approximately 3 kips. Gain during initial loading was larger because early-age concrete is more susceptible to the effects of creep and shrinkage.

Older concrete experiences less creep and shrinkage. As loads were removed at E, the prestress gain caused by the loads also diminished, resulting in a slight reduction of prestress force. If the new deck load was similar to the loads removed, the difference in prestress force due to deck replacement was minimal in this example.

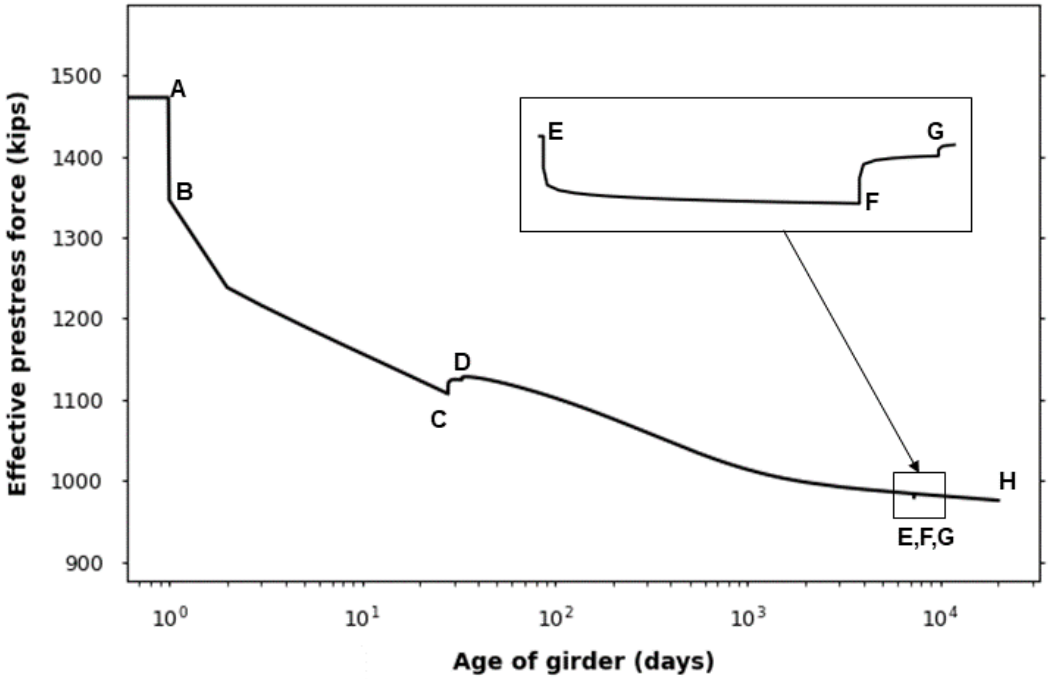

Figure 4.4: Effective Prestress at Girder Midspan Over Time

A: Prestress transfer
A-B: Elastic shortening loss
B-C: Concrete creep and shrinkage loss
C: Prestress gain due to addition of deck load
D: Prestress gain due to addition of superimposed loads
D-E: Long-term prestress loss due to concrete creep and shrinkage
E: Removal of old deteriorated deck
E-F: Loss due to concrete creep and shrinkage + creep recovery from the removal of old deck loads
F: Prestress gain due to addition of a new deck
G: Prestress gain due to addition of superimposed loads
G-H: Long-term prestress loss due to concrete creep and shrinkage
H: Age of girder = 20000 days

The primary causes of prestress loss in the prestressed concrete girder were concrete creep, concrete shrinkage, and elastic shortening. Figure 4.5 illustrates how each of these losses changed over time. Total loss is the summation of elastic shortening, creep, and shrinkage losses. The rate of creep and shrinkage loss was especially high during the initial days of construction. Figure 4.5 also shows that concrete creep was the largest contributor to prestress loss, causing approximately 60% of the total loss at 20,000 days. Previous studies (Granata et al., 2013; Meknulasi et al., 2018) showed that the B4 model produces a higher value of creep and shrinkage strain than other creep and shrinkage models, resulting in more prestress loss in the girder compared to other models.

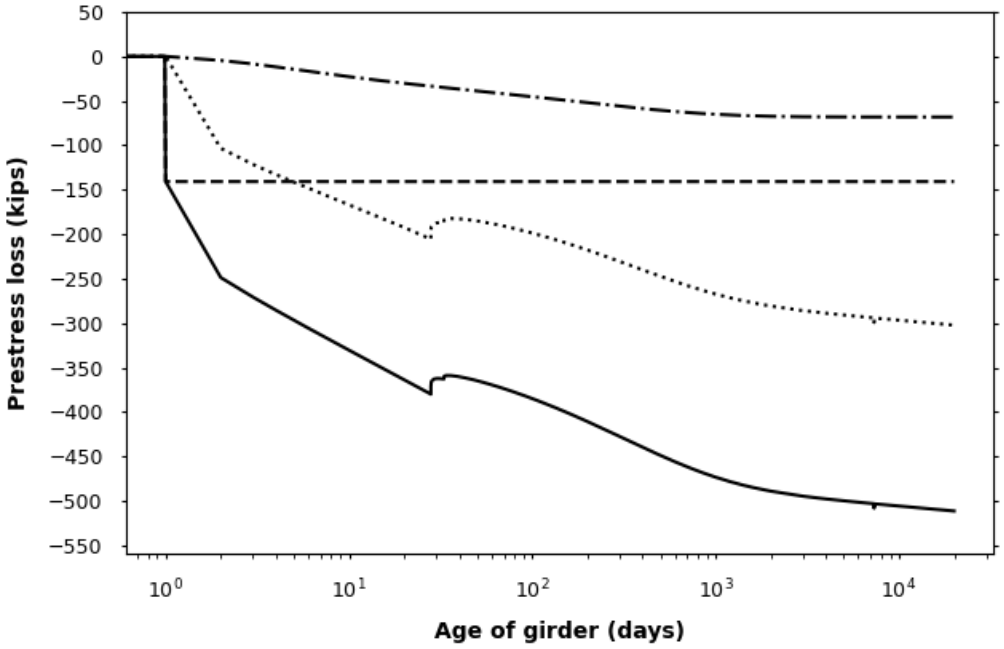

Figure 4.5: Components of Prestress Loss at Midspan

As shown in Figure 4.5, elastic shortening loss occurred at day 1 when the prestressing force was transferred to the concrete. Elastic shortening loss of the prestressed concrete girder was 141 kips at the midspan of the girder, or 9.5% of the initial jacking force. The dot-dashed line in the figure illustrates the trend of prestress loss resulting from concrete shrinkage as the girder ages, with the majority (90%) of the loss occurring within the first 400 days of construction.

Figure 4.6 shows the variation of loss percentage due to elastic shortening throughout the girder length: 0% at the ends to 9.5% at the midspan of the girder. Elastic shortening loss accounted

for approximately 25% of the total prestress loss at 20,000 days from girder construction for this example.

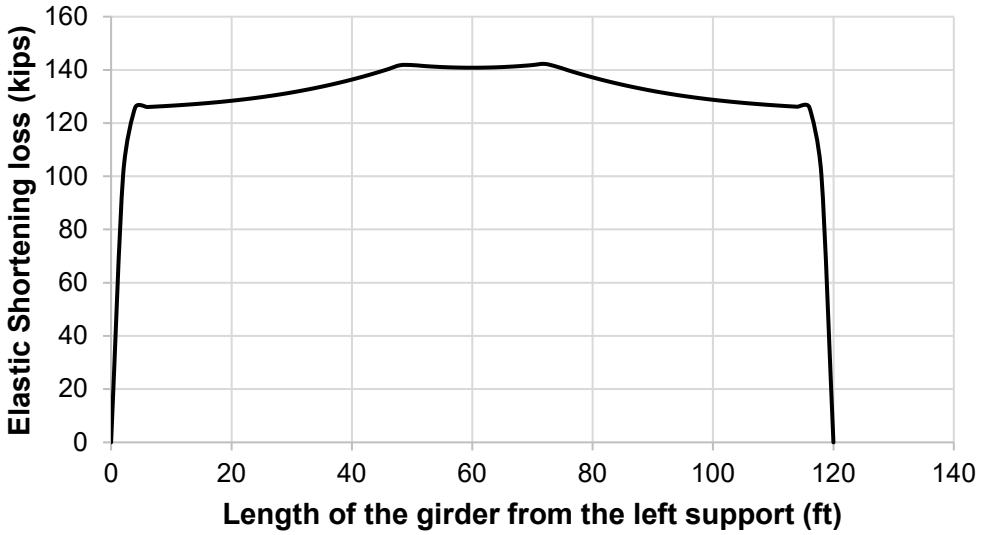

Figure 4.6: Elastic-Shortening Loss Throughout the Girder Length

Table 4.8 shows the trend of prestress force lost due to concrete creep. The rate of creep loss was highest during the initial days of construction, with a calculated rate of creep loss of 18 kips/day, diminishing to 0.01 kips/day 1000 days after girder construction. Approximately 80% of the final creep loss occurred within the first 400 days of girder construction.

Table 4.8: Effective Prestress Forces and Losses in a Prestressed Concrete Girder

Loading stages	Girder age (days)	Effective prestress (kips) [1]	Total creep loss (kips) [2]	Total shrinkage loss (kips) [3]
Before transfer	0	1487	0	0
Prestress transfer(A-B)	1	1346	0	0
After transfer (B-C)	2	1238	-103	-5
	27	1109	-204	-33
Deck placement (C)	28	1107	-206	-34
After deck placement (C-D)	29	1124	-188	-34
	32	1125	-187	-35
SDL placement (D)	33	1124	-187	-35
After all loads applied (D-E)	34	1128	-183	-35
	100	1102	-199	-45
	400	1047	-240	-59
	1000	1014	-267	-65
	7000	984	-294	-68
Deck removal (E)	7305	984	-294	-68
After deck removal (E-F)	7306	980	-298	-68
	7324	979	-299	-68
New deck placement (F)	7325	979	-299	-68
After new deck placement (F-G)	7326	982	-296	-68
	7329	982	-296	-68
New SDL placement (G)	7330	982	-296	-68
After deck replacement (G-H)	7331	983	-295	-68
	9125	982	-296	-68
	14325	978	-300	-68
	20000	976	-302	-68

[1] Effective prestress at a given time refers to the prestress force after subtracting elastic shortening, creep, and shrinkage losses. Change in the effective prestress from A to B was due to an elastic shortening loss of 141 kips. The remaining changes were due to creep and shrinkage of concrete.
[2] Total creep loss refers to the loss in prestress force due to creep of girder concrete.
[3] Total shrinkage loss refers to the loss in prestress force due to shrinkage of girder concrete.

Concrete shrinkage was shown to contribute to total prestress loss, accounting for approximately 15% of the total loss 20,000 days after girder construction. Shrinkage loss was not affected by any changes in loading conditions. As shown in Table 4.8, shrinkage loss remained

constant at 68 kips after 7,000 days of girder construction. Figure 4.7 shows that the rate of shrinkage loss decreased from 4.5 kips/per day initially to 0.1 kips/day after 100 days.

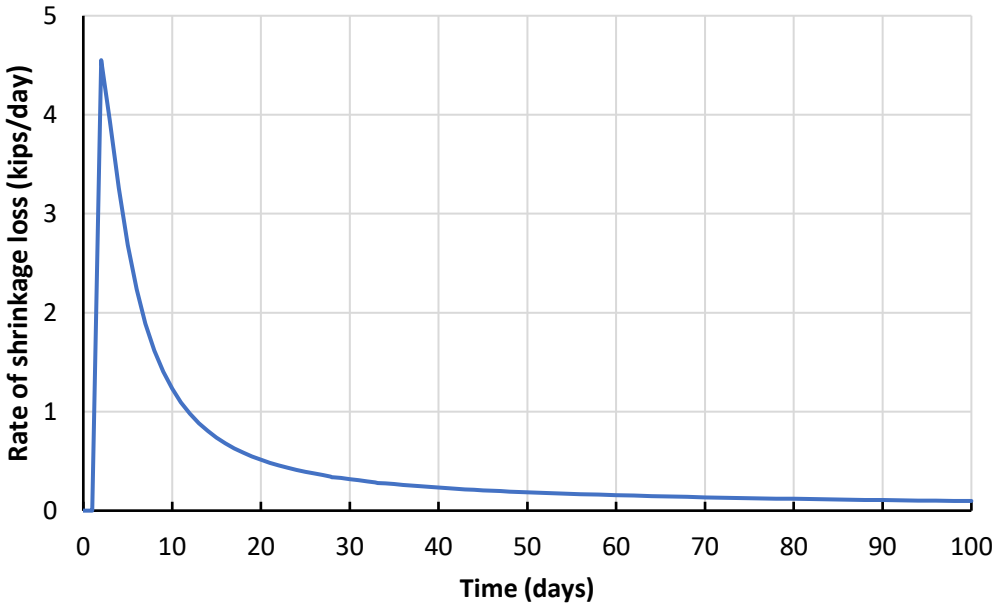

Figure 4.7: Rate of Prestress Loss Due to Girder Shrinkage During Initial 100 Days

4.3.2 Creep and Shrinkage

Figure 4.8 shows the midspan creep strains calculated over time at the top and bottom of the girder and at the top and bottom of the deck. As shown, concrete creep rates were highest during the initial days of construction, gradually decreasing over time. Creep strains were affected by changes in the loads on the girder, and the magnitude of creep in the deck was much smaller than in the girder due to lower stress levels in the deck. Figure 4.8 indicates an instantaneous increase in creep strain at day 1 that could be a limitation of the B4 model when calculating creep strains at early ages of the concrete. Creep strain at the midspan of the girder after 20,000 days was -2,240 microstrain at the bottom and -1,100 microstrain at the top. The negative slope of the creep strain throughout the figure shows that net tensile stress never occurred in the girder.

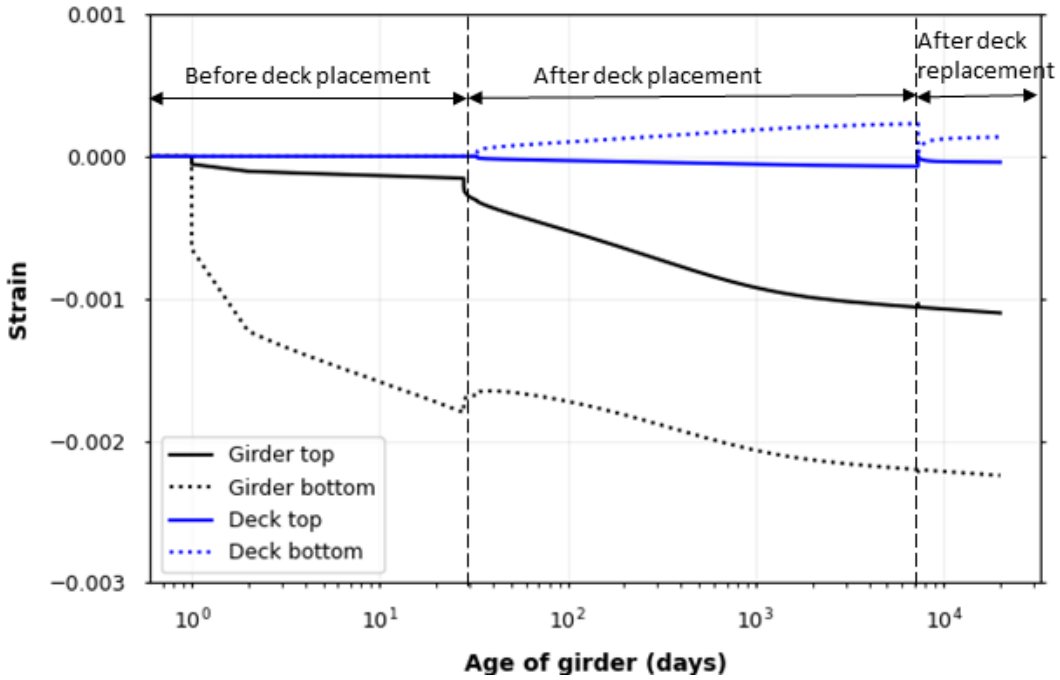

Figure 4.8: Creep Strain Along the Composite Section Over the Age of the Girder

Figure 4.9 shows a plot of shrinkage strain developed in the girder and the deck over time. Concrete shrinkage began as soon as the concrete was removed from curing, with nearly all shrinkage occurring within the first 1,000 days of construction. This study assumed uniform shrinkage along the cross-section of the girder; shrinkage strain was not influenced by changes in loading conditions or the deck replacement process. Model results showed a shrinkage strain of 350 microstrain for the girder after 1,000 days and remained nearly constant thereafter, while deck shrinkage reached -300 microstrain after 1,000 days and remained nearly constant until the old deck was removed. Deck shrinkage dropped to zero when the deck was removed and then approached the same shrinkage magnitude as the original deck. The difference in shrinkage strain of the girder and deck was due to differences in girder and deck concrete mixture proportions.

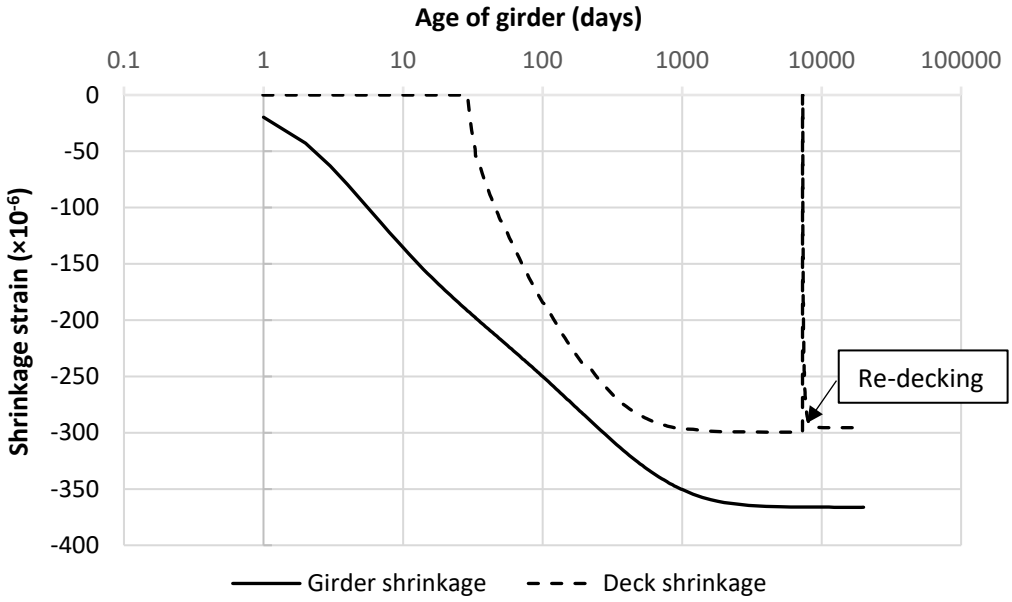

Figure 4.9: Shrinkage Strain Developed in the Girder and Deck Over Time

4.3.2.1 Differential Shrinkage

Figure 4.10 shows the corresponding stress in the girder at the level of prestressing strands at midspan and the girder end. The model represented the effects of differential shrinkage as fictitious external forces generating stress in the girder. The force was calculated considering 50% of the deck shrinkage using AASHTO LRFD (2012) Eq. 5.9.5.4.3d-2. The resulting stresses in the girder were determined from fictitious forces. Figure 4.10 shows that deck shrinkage induced a maximum stress of 0.14 ksi at midspan due to differential shrinkage between the girder and the old deck just before its removal, as well as 0.14 ksi at 20,000 days due to differential shrinkage between the girder and the replaced deck. Redecking of the girder caused decreased stress at approximately 7,300 days (Figure 4.10). When the old deck was removed, the girder was released from the stress due to shrinkage of the old deck, and when the new deck was added, shrinkage of the new deck began to exert stress on the girder over time. By the time the new deck was added, girder shrinkage had reached a constant value, so changes in girder shrinkage strain were negligible.

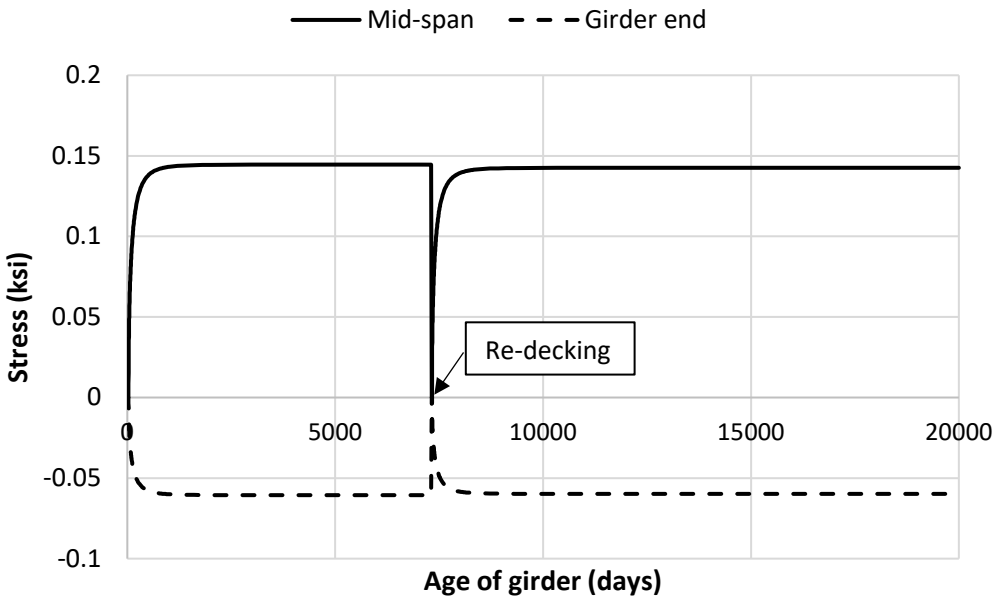

Figure 4.10: Stress at Girder CG Due to Differential Shrinkage Between Girder and Deck

4.3.2.2 Creep Recovery

When the deck is removed from the girder, a portion of creep caused by the deck loads is recovered (Section 2.2.3). To demonstrate how the model incorporated creep recovery into the calculation, a study was performed where deck loads were applied at 28 days and removed at 100 days, and left untouched thereafter. The resulting data for creep strain and creep recovery due to deck loads (SDL + DDL) are plotted in Figure 4.11. Approximately one-third of the creep was recovered, with the recovery amount based on the magnitude and duration of the load and concrete material properties, such as viscosity and elasticity. The magnitude of creep strain when the load is reapplied depends on the time elapsed since the load was removed. For example, if the load is reapplied immediately, the creep strain will go back to its pre-removal value, but if the load is reapplied after a certain time, the resulting creep strain will be smaller than it would have been if the loads were never removed. This is because the stress reduction caused by the load removal decreases the creep strain between the load removal and reapplication.

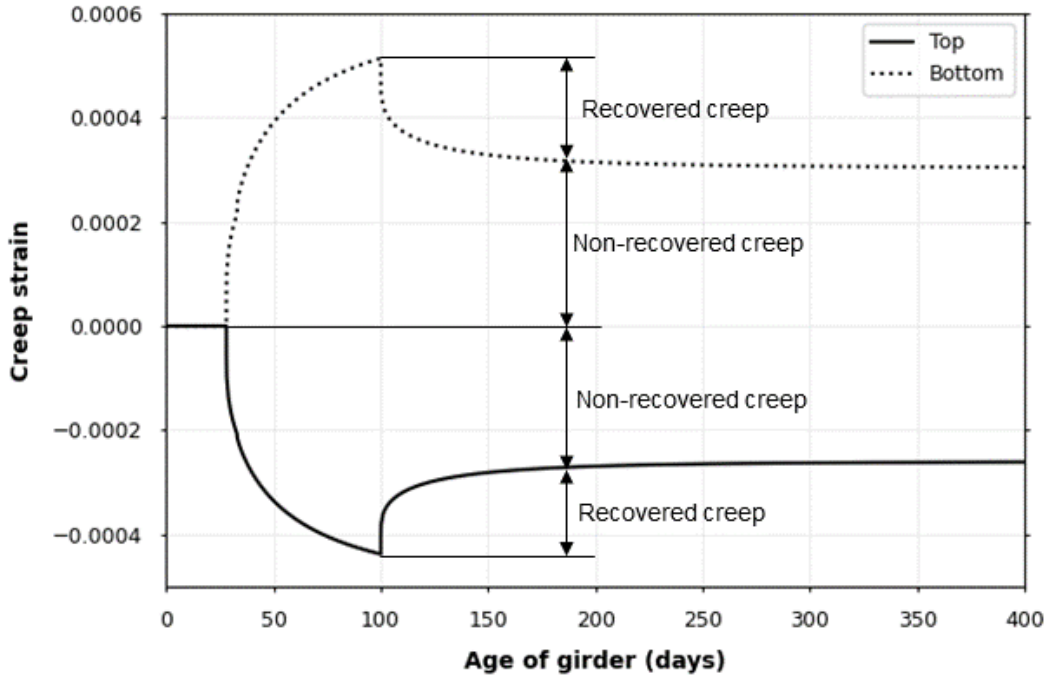

Figure 4.11: Creep Recovery Due to Deck Load Removal from the Girder

4.3.3 Deflections

Figure 4.12 is a plot of total midspan deflection of the prestressed concrete girder versus girder age. Instantaneous changes in the deflection resulted from changes in loads, whereas gradual changes in girder deflection were due to concrete deformations. In this example, long-term deflections due to DDL and SDL were similar in magnitude to the camber, resulting in small long-term deflections.

Figure 4.13 shows the relative importance of deflections due to different loads and creep. Deflection due to GDL, DDL, and SDL remained constant over time, whereas deflection due to prestress force, restraint moment, and concrete creep changed with time. When the prestress was transferred to the concrete, the girder cambered up by 2.3 in. This upward camber increased over time due to concrete creep. The maximum midspan camber of the girder was 5.80 in., or 1/248th of the girder length just prior to deck load application, which itself caused an instantaneous camber reduction of 1.7 in., followed by a further reduction of 0.3 in. due to SDL. The change in midspan deflection from 2.8 in. (after the application of SDL) to -1.1 in. (just prior to deck removal) was due to long-term concrete deformations. The girder rebounded by 2.4 in. when the deck loads were

removed. After adding the new deck and all associated loads, the midspan deflection in the girder changed to -0.6 in., indicating a short-term change in deflection of 0.5 in. due to the deck replacement process.

Figure 4.14 shows the deflection profile of the girder at various loading stages. The camber was highest when the prestress was transferred and decreased over time as additional loads were applied. The midspan deflection changed from positive (upward deflection) to a negative value (downward deflection) at approximately 680 days. As shown in the figure, the girder did not return to its original camber when the loads were released. The difference between the camber at prestress transfer and the camber after the old deck removal was approximately 3.5 in. due to concrete deformation between the time of transfer and the time of deck removal.

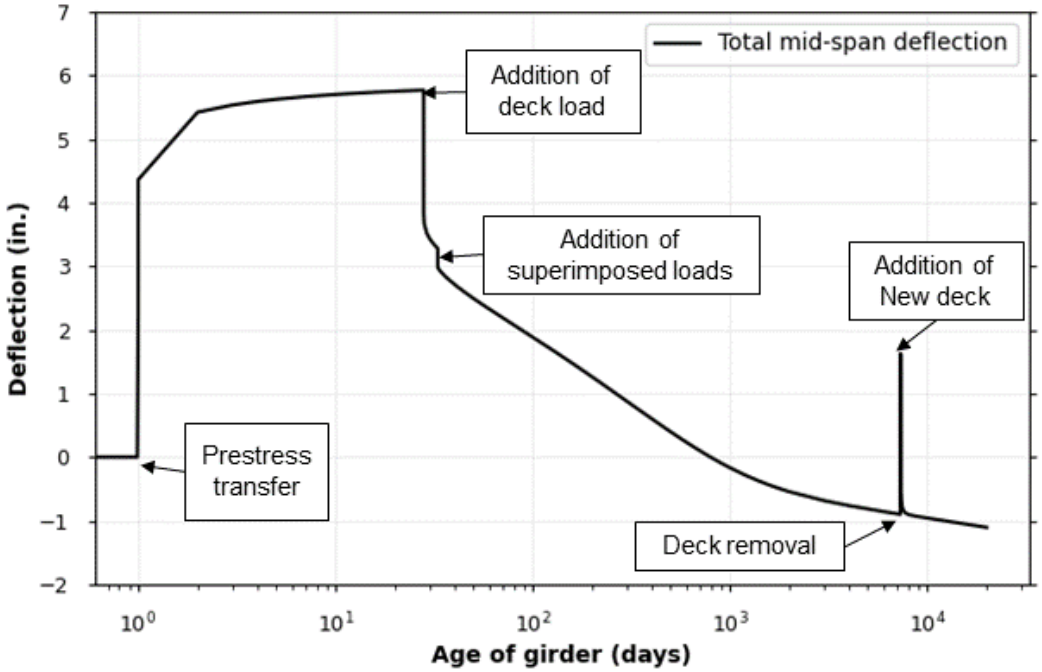

Figure 4.12: Total Midspan Deflection of the Girder

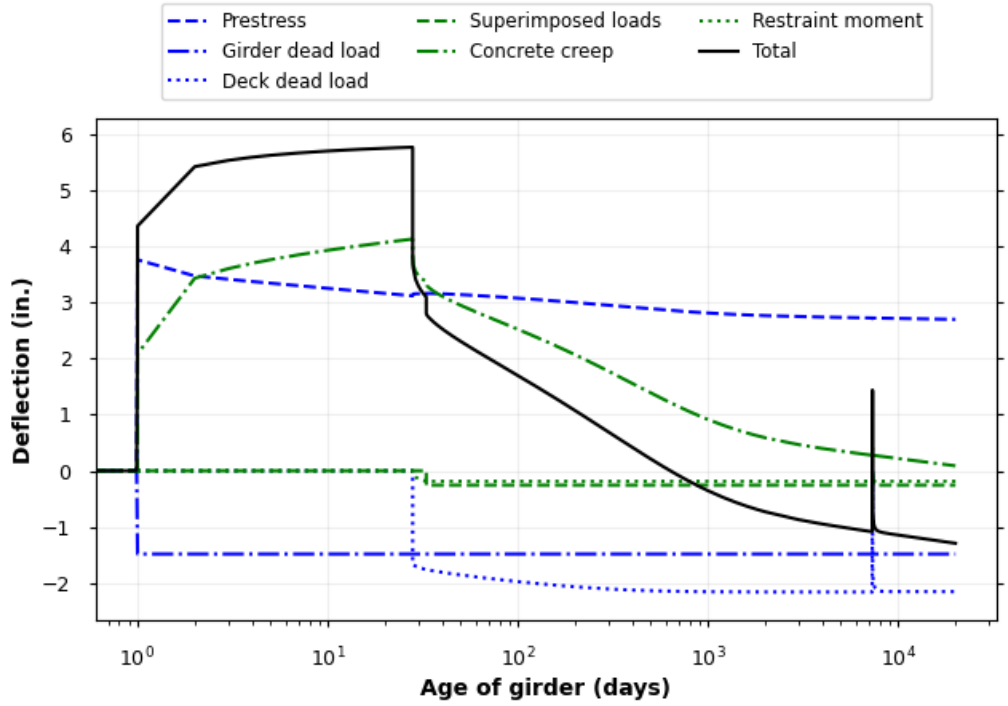

Figure 4.13: Components of Midspan Deflection Over Time

Figure 4.14: Deflection Profile of a Prestressed Concrete Girder at Loading Stages

4.3.4 Stresses

The model in this study estimated the stress response in the prestressing strands and concrete at any time during the girder lifespan. As the concrete deformed over time, the stress in the girder changed accordingly. Figure 4.15 shows midspan stress in the prestressing strands, while Figure 4.16 shows concrete stresses at the top and bottom of the girder at midspan over time; events A to H are described in Section 4.3.1.

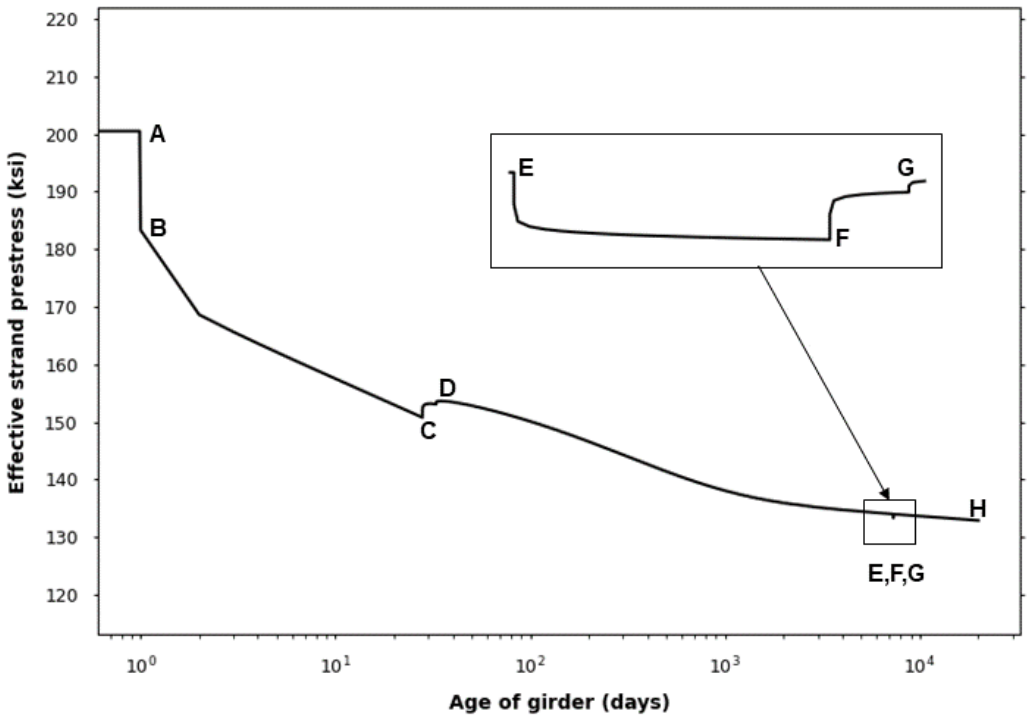

Figure 4.15: Effective Prestress Force in Prestressing Strands Over Time

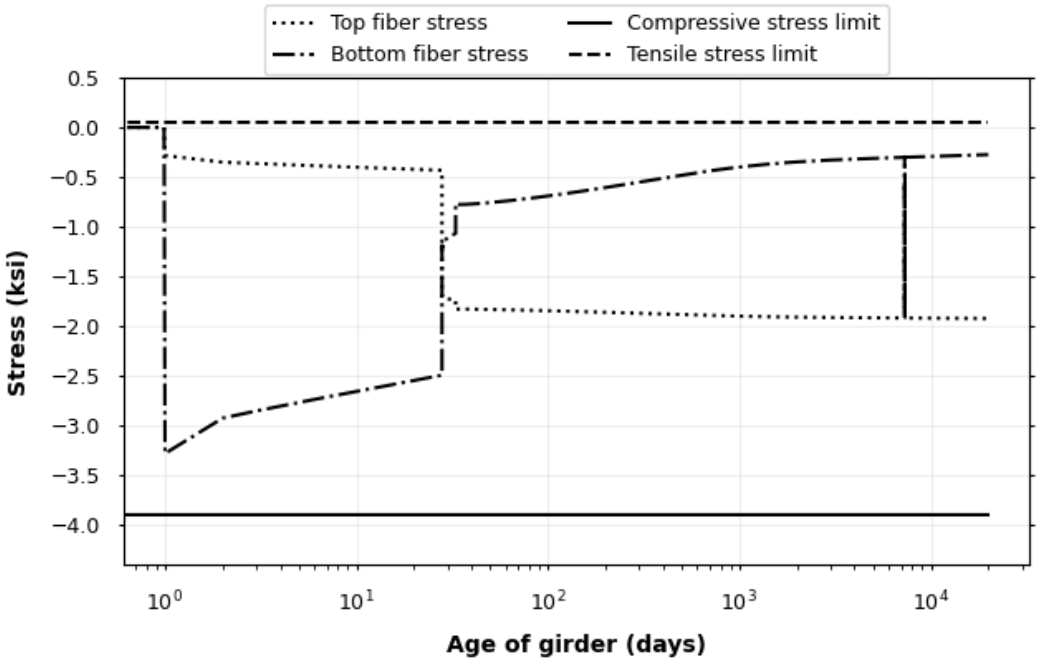

Figure 4.16: Concrete Stresses at Section Top and Bottom at Midspan with Stress Limits

Prestressing force caused the development of compressive stress of -0.3 ksi at the top of the girder and -3.2 ksi at the bottom. As shown in Figures 4.15 and 4.16, stress changed over time due to prestress loss. DDL and SDL caused tensile stresses at the girder bottom that decreased the total stress from -2.5 ksi to -0.7 ksi. Similarly, compressive stress induced at the girder top due to this load changed the stresses at the girder top from -0.5 ksi to -1.8 ksi. When the deck was removed from the girder after approximately 20 years (7,305 days), the midspan stress at the top of the girder changed from -1.9 ksi to -0.6 ksi, and midspan stress at the bottom changed from -0.3 ksi to -1.9 ksi. When the new deck was added, the girder reverted to a stress of -1.9 ksi at the top and -0.3 ksi at the bottom, given that the new deck loads were similar to the removed loads. Figure 4.16 shows that stresses that developed in the girder over time remained within the stress limits discussed in Section 3.9. Maximum compressive stress of -3.3 ksi was observed at the girder bottom immediately after the prestress force was transferred, and tensile stress was never observed throughout its life.

Figure 4.17 is a plot of stresses caused by various load types, and Figure 4.18 shows stress distribution throughout the girder depth due to these loads. As shown in Figure 4.18, on day 1, when the prestress was transferred to the concrete, the only stress in the girder was due to

prestressing and self-weight. However, the stresses changed due to changes in load and support conditions and concrete deformation over time. Stresses in the deck were due only to SDL and restraint moment (Figure 4.18).

For this example, the stresses in the girder were compressive at the top and bottom of the girder throughout the girder life, which may not necessarily be the case for other inputs. Therefore, further investigation is needed to determine behavioral changes in the girder if tensile stresses develop.

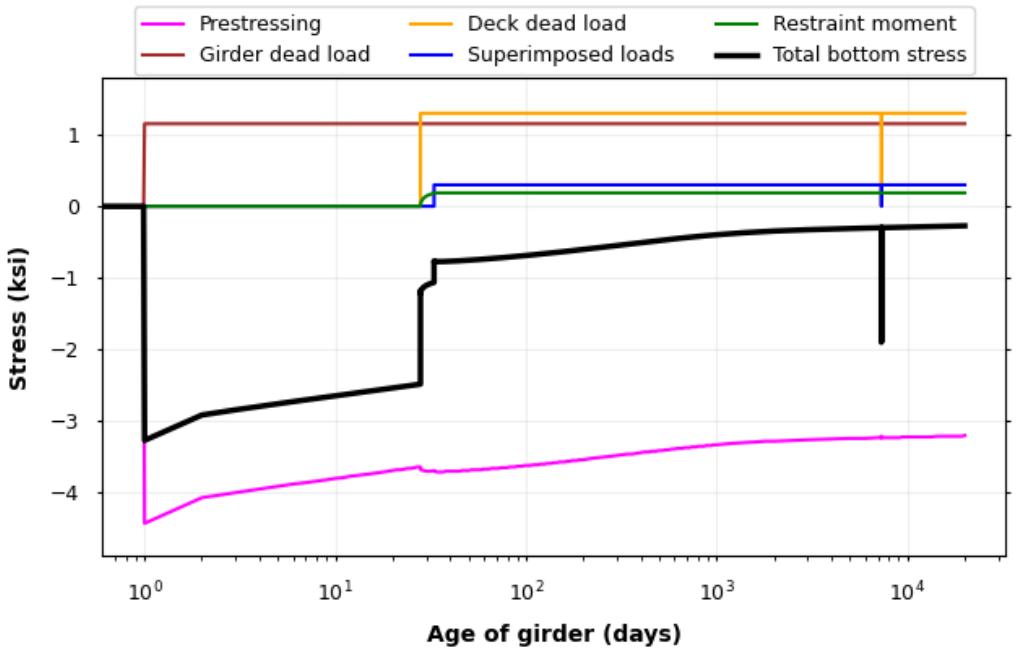

Figure 4.17: Midspan Stress at Girder Bottom for Specific Loads

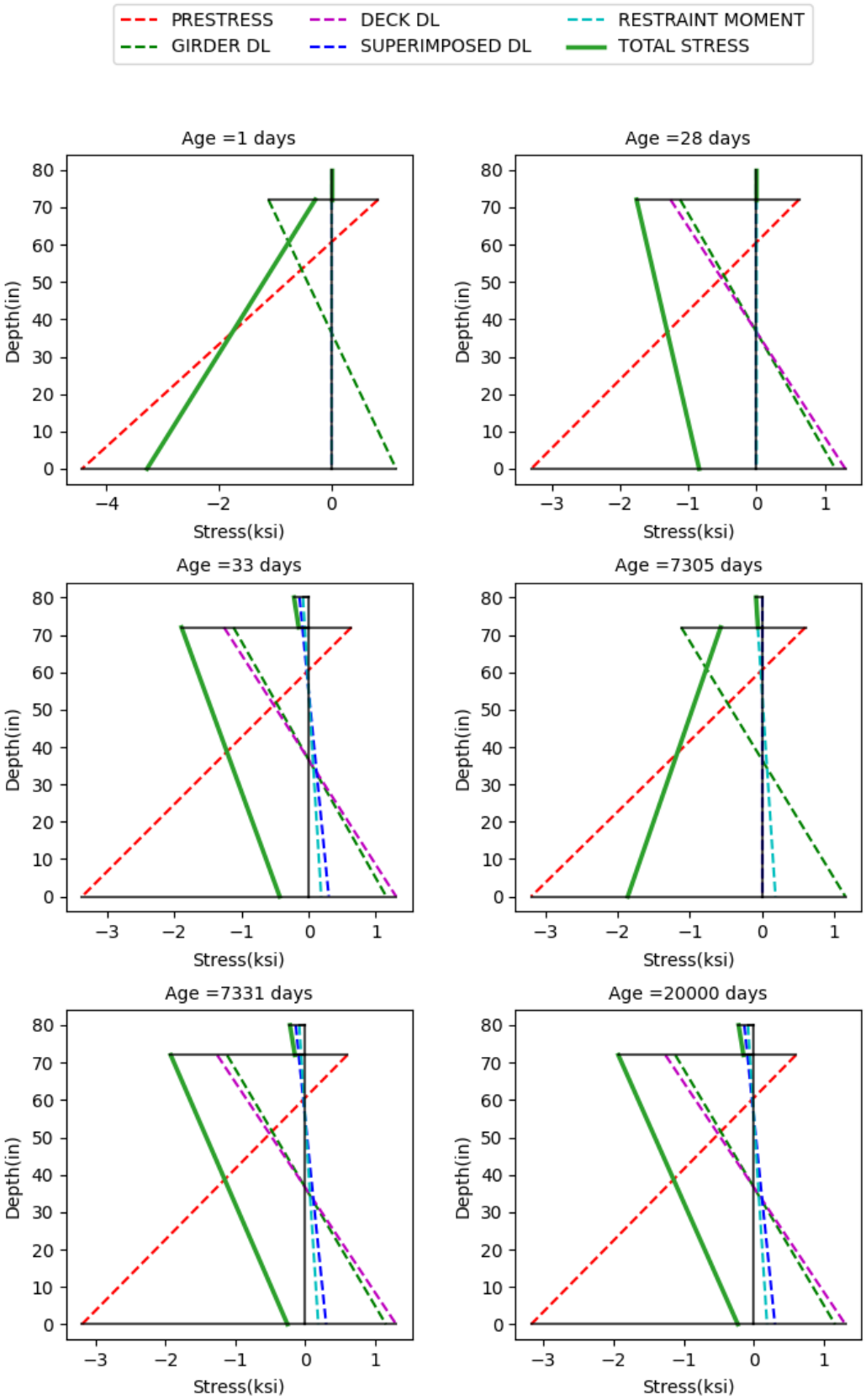

Figure 4.18: Stress Distribution Over the Girder and Deck Depth at Different Time Steps

4.3.5 Restraint Moment

Restraint moment developed in the girder because the diaphragm restrained girder-end rotations arising from creep- and shrinkage-induced deformations. One end of the girder was assumed to be simply-supported, and the other end was continuous due to a diaphragm. Although the magnitude of this restraint moment depended on the creep and shrinkage of the concrete at a given time, it was limited to no more than 0.6 times the girder-end cracking moment (650 kip-ft), as discussed in Section 2.4.2.2. Figure 4.19 shows that the restraint moment rapidly reached the 650 kip-ft limit, while Figure 4.20 shows that the deflection due to the restraint moment was -0.18 in., suggesting that the restraint moment had only a minor impact on midspan deflection. The restraint moment caused a maximum stress of -0.06 ksi at the top and 0.18 ksi at the bottom, as shown in Figure 4.18. Further investigation of the influence of restraint moment on girder behavior is described in Section 4.6.

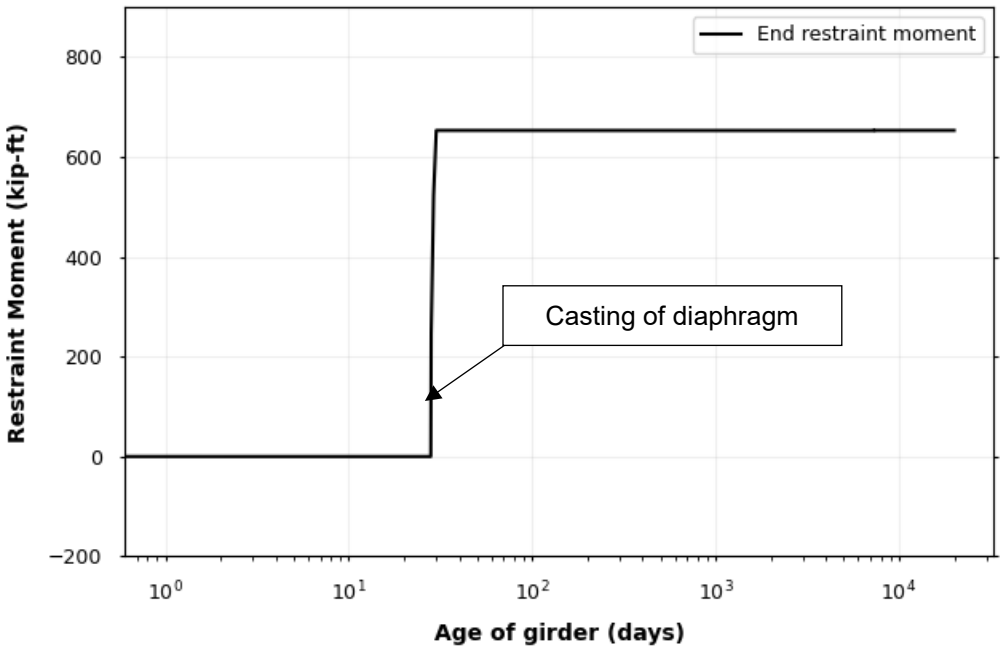

Figure 4.19: Restraint Moment in the Prestressed Concrete Girder

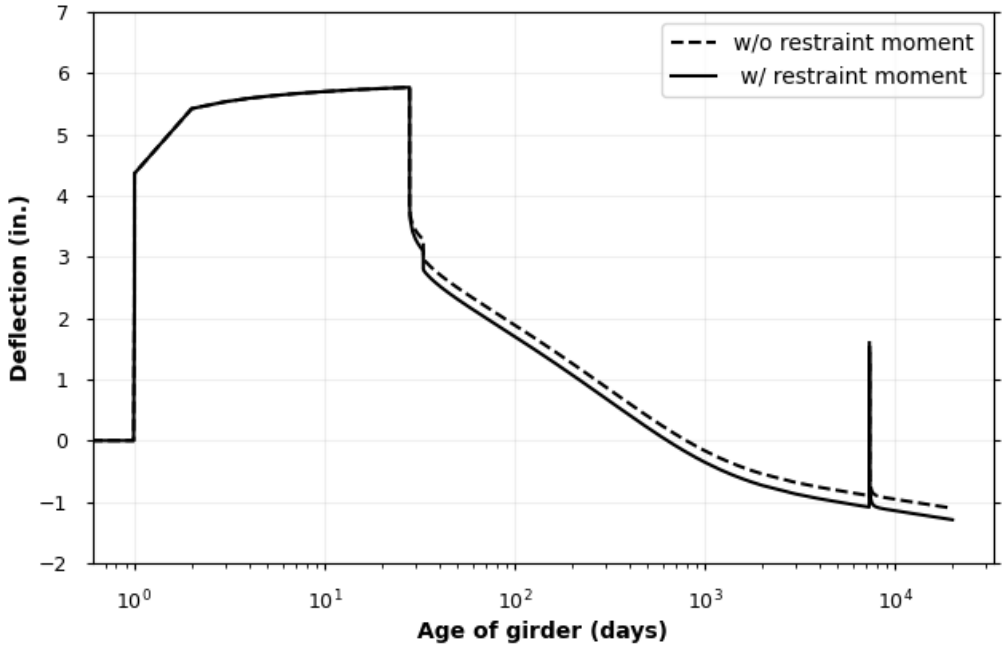

Figure 4.20: Comparison of Midspan Deflection of the Girder With and Without Restraint Moment

4.4 Model Verification

Validation of the model outputs was challenging because no known studies have applied the B4 model for creep and shrinkage to prestressed girder calculations. To verify the model, moments, stresses, initial prestressing forces, and deflections obtained from the model that did not involve creep and shrinkage calculations were compared to results from the PCI Design Example 9.1a. This verification was done for a single calculation step because the PCI Design Example does not consider time-step analysis. Table 4.9 shows results for prestress losses and initial prestressing force obtained from the design example and the model from this study. Differences were minimal for both the initial prestressing force and the sum of elastic shortening and relaxation losses.

Table 4.9: Initial Prestressing Force and Stresses from the PCI Design example and Study Model

Parameters	Units	PCI [1]	Model [2]
Elastic shortening + Relaxation loss	ksi	18.9	18.3 to 20.5
Initial Prestressing force	kips	1,348	1,352 to 1,337

[1] PCI losses are calculated only at girder midspan

[2] The range of loss values from the model is distributed throughout the length of the girder, varying slightly due to eccentricity of the strands

Midspan moments resulting from various loads as obtained from the PCI example and the model are presented in Table 4.10. The results show that the moments calculated with the model were consistent with results from the design example except for the moment due to deck loads. This discrepancy of less than 3% occurred because the model did not consider the weight of the haunch, whereas the design example included the weight due to a uniform haunch depth of 0.5 in.

Table 4.10: Comparison of Moments from the PCI Example and Study Model

Parameters	Units	PCI	Model
Moment due to DL of girder	kip-ft	1,440	1,440
Moment due to DL of deck [1]	kip-ft	1,660	1,620
Moment due to superimposed DL	kip-ft	540	540

[1] The difference in the moment obtained from the DL of deck is because the model does not consider the weight of the haunch

Stresses due to various loads obtained from both the design example and the model are presented in Table 4.11. The results show that differences between the PCI Design Example and model outputs were minor.

Table 4.11: Comaprison of Stresses from the PCI Example and Study Model

Parameters	Location	Units	PCI	Model
Stress due to DL of girder	top	ksi	-1.12	-1.11
	bottom	ksi	+1.07	+1.12
Stress due to DL of deck	top	ksi	-1.27	-1.26
	bottom	ksi	+1.22	+1.30
Stress due to superimposed dead load	top	ksi	-0.10	-0.13
	bottom	ksi	+0.30	+0.30
Stress due to prestress	top	ksi	+0.83	+0.83
	bottom	ksi	-4.40	-4.41

The study model used the moment-area method to calculate deflections from the moment-curvature relationship. To verify proper use of the moment-area method, the deflections obtained from the model were compared with those from the design example (Table 4.12). The similarity in results indicates correct application of the moment-area method and verifies model accuracy for this calculation.

Table 4.12: Comparison of Midspan Deflection from the PCI Example and Study Model

Parameters	Units	PCI	Model
Deflection due to DL of girder	in.	-1.48	-1.48
Deflection due to DL of deck	in.	-1.67	-1.67
Deflection due to superimposed dead load	in.	-0.28	-0.28
Deflection due to prestress	in.	3.65	3.74

To verify accuracy of the B4 model for calculating creep and shrinkage strains, model outputs were compared to an example calculation in Bažant et al. (2015). However, the example calculation only covers a single age of concrete, so only one data point was available for verification. Model results for this comparison were generated using the following inputs from Bažant et al. (2015): normal cement; age of loading t' = 28 days; age when drying begins t_0 = 28 days; relative humidity = 0.5; concrete compressive strength = 4 ksi; volume-to-surface area ratio = 0.0625 ft; cement content = 13.69 lb/ft^3; aggregate-cement ratio = 7; and water-cement ratio = 0.60.

Figure 4.21 shows a plot of creep compliance (basic creep + drying creep) obtained with the model over 160 days and the value reported in Bažant et al. (2015) at 112 days, excluding

elastic strain. Similarly, Figure 4.22 shows a plot of shrinkage strains obtained with the model over 160 days and the value reported in Bažant et al. (2015) at 112 days. Both the creep compliance and the shrinkage strain from the model agreed with the values reported in Bažant et al. (2015).

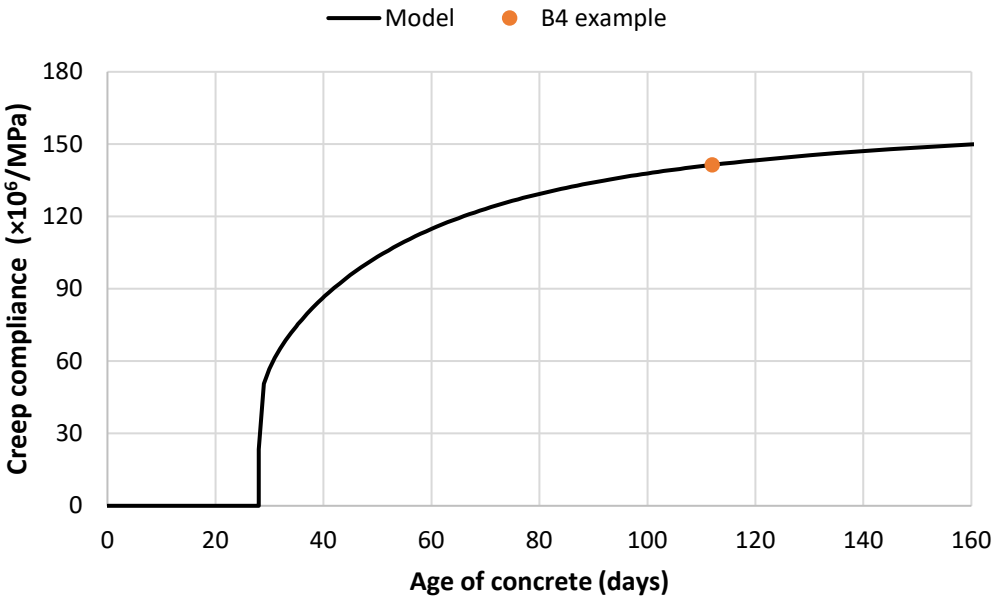

Figure 4.21: Comparison of Creep Compliance, Excluding Elastic Strains

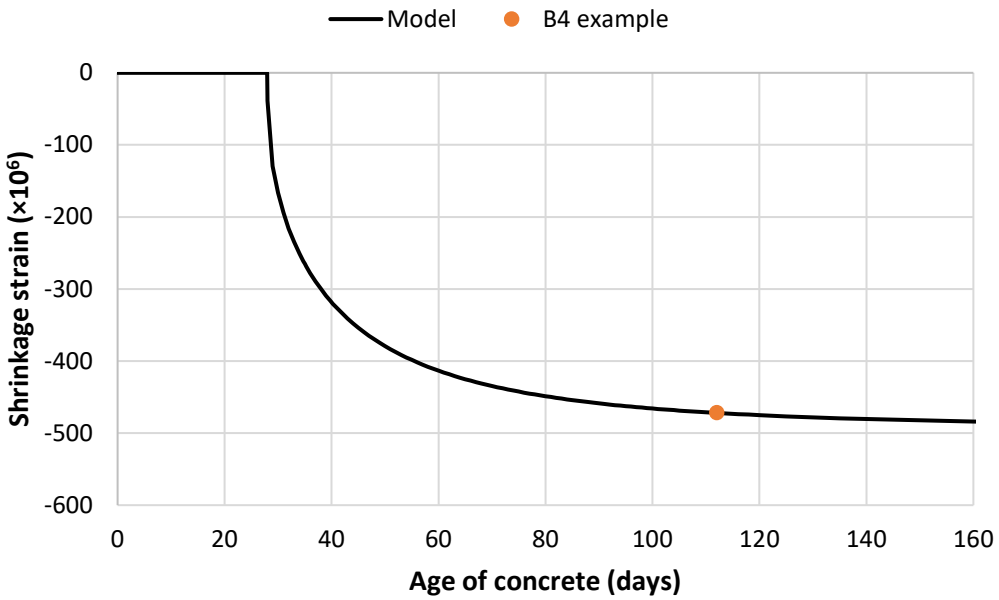

Figure 4.22: Comparison of Shrinkage Strain

Taken together, these comparisons are evidence that the model described in Chapter 3 correctly implements the equations for calculating forces, moments, stresses, deflections, and both creep and shrinkage strains. The proposed model should therefore provide results that are as valid as the assumptions and data underlying the model development.

4.5 Impact of Deck Removal

Two scenarios were analyzed to investigate the effect of deck removal on long-term girder performance: deck replacement after 20 years and no deck replacement. The deflections, stresses, strains, and prestress force of the two cases were compared (Table 4.13). Only the deflection of the girder immediately after the deck replacement (at 7,350 days) was affected by the replacement process, and total deflection at 20,000 days was nearly identical for both cases. Figure 4.23 shows the total midspan deflection of the girder for the two scenarios from 7,000 to 8,000 days. Removal of the deck loads caused the girder to rebound 2.5 in. and deflect again when the loads were re-applied, whereas no significant change was evident in the deflection of the girder without deck replacement. Replacing the deck after 20 years had minimal impact on the long-term prestress force, stresses, strains, and deflection for the considered bridge.

Table 4.13: Impact of Deck Replacement on Prestressed Concrete Girders

Parameters	Deck replacement	No deck replacement	% difference
Midspan deflection at 7,350 days, in.	0.08	-0.23	-395%
Total deflection at 20,000 days, in.	-0.43	-0.43	2%
Total bottom stress at 7,350 days, ksi	-0.25	-0.26	1%
Total bottom stress at 20,000 days, ksi	-0.23	-0.23	0%
Total top stress at 7,350 days, ksi	-1.92	-1.92	0%
Total top stress at 20,000 days, ksi	-1.93	-1.93	0%
Creep strain at 7,350 days	-2.31E-03	-2.31E-03	0%
Final creep strain at 20,000 days	-2.35E-03	-2.35E-03	0%
Total effective prestress at 20,000 days, kips	962	962	0%

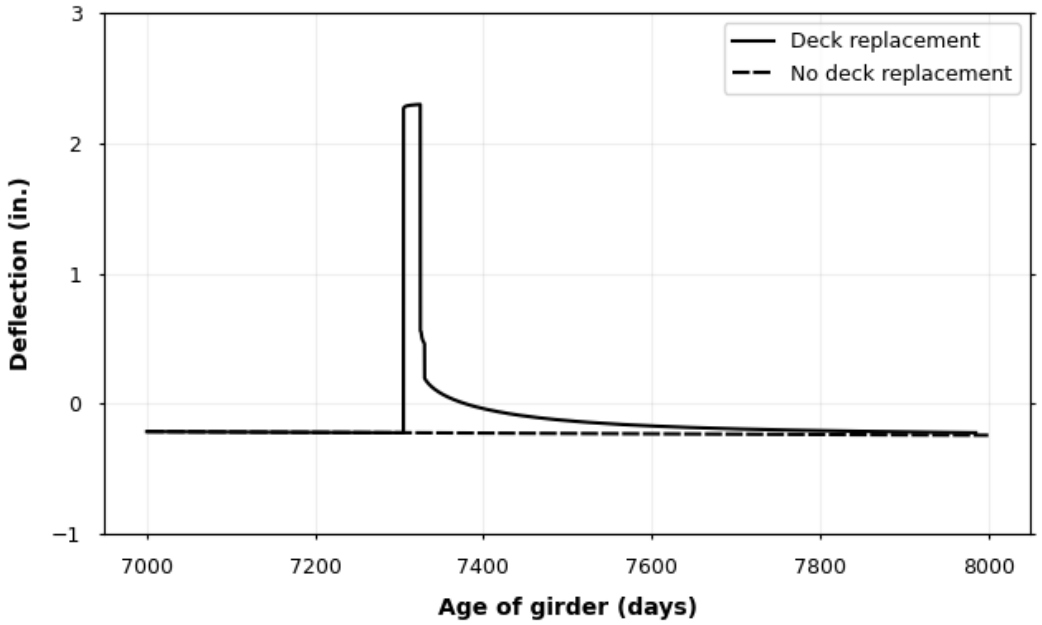

Figure 4.23: Midspan Deflection of the Girder During Deck Replacement

4.6 Impact of Diaphragm

This section describes the impact of the continuity diaphragm on the overall girder performance during the deck replacement process for the example bridge and the effect on girder

behavior of the restraint moment at the girder ends due to a continuity diaphragm. Two scenarios were considered to examine the impacts of diaphragm removal: the continuity diaphragm removed with the deck and another where only the deck was removed.

4.6.1 Impact of the Restraint Moment

Table 4.14 shows the strains, stresses, deflections, and prestress forces obtained from the model with and without the inclusion of restraint moment. These data were compared to determine if the presence of the restraint moment in the girder alters the girder behavior. Development of restraint moment caused a difference of approximately 0.19 in. in the total midspan deflection of the girder at 20,000 days between the two cases, and stresses at the bottom of the girder changed by 0.18 ksi due to the restraint moment. Although the percentage difference was large, the magnitude of the difference in deflection and stresses was not substantial enough to cause major changes in girder behavior for the bridge. Changes in the girder rebound and effective prestress due to the restraint moment were also negligible. Although the continuity diaphragm minimally impacted the overall bridge performance, its presence did not significantly affect the impact of deck replacement on the bridge.

Table 4.14: Effects of a Continuity Diaphragm at One End of the Girder

Parameters	With restraint moment	Without restraint moment	% difference
Rebound due to deck removal (in.)	2.50	2.50	0%
Δdeflection due to deck replacement (in.)	2.60	2.60	0%
Total deflection at 20,000 days (in.)	-0.43	-0.24	-44%
Final creep strain at 20,000 days	-3.85E-04	-3.85E-04	0%
Total girder top stress at 20,000 days (ksi)	-1.93	-1.87	-3%
Total girder bottom stress at 20,000 days (ksi)	-0.23	-0.41	79%
Total effective prestress at 20,000 days (kips)	962	962	0%

4.6.2 Impact of Diaphragm Removal with the Deck

To assess whether the continuity diaphragm should be removed with the damaged deck during the replacement process, two case scenarios were examined, with results shown in Table 4.15. Diaphragm removal led to a greater girder rebound and more deflection change before and after deck replacement: the girder rebound with diaphragm removal was 2.69 in. and 2.50 in. without removal. Removal of the diaphragm relieved the restraint moment that had developed at the end of the girder over time, but a new restraint moment began to develop once a new diaphragm was cast, as shown in Figure 4.24.

Table 4.15: Impact of Diaphragm Removal with the Deck

Parameters	Diaphragm removed	Diaphragm intact	% difference
Rebound due to deck removal (in.)	2.69	2.50	-6.97%
Δdeflection due to deck removal (in.)	0.61	0.42	-30.72%
Total deflection at 20,000 days (in.)	-0.43	-0.43	0.00%
Final creep strain at 20,000 days	-2.35E-03	0.00	0.00%
Total effective prestress at 20,000 days (kips)	962	962	0.00%
Restraint moment after deck removal (kip-ft)	0	652	-
Restraint moment after 10 days of new deck placement (kip-ft)	173	652	-

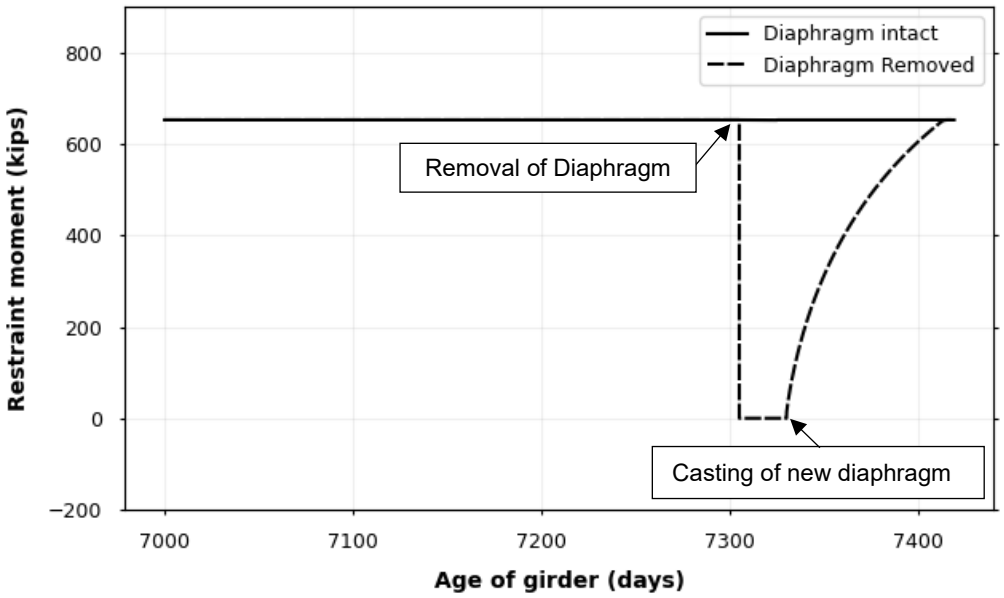

Figure 4.24: Comparison of Restraint Moment With and Without the Diaphragm During Deck Replacement

Although some differences in girder behavior were observed depending on whether the diaphragm was removed with the deck or left intact, these differences were not substantial enough to cause important changes in the structural performance for the bridge. However, removal of the diaphragm may increase the amount of effort and time required for the replacement. The decision of whether to replace the diaphragm should be made on a case-by-case basis for each bridge depending on site conditions, severity of the cracking and concrete deterioration, and constructability considerations for bridges where, like this example, the restraint moments are limited by girder cracking and thus relatively small.

4.7 Parametric Study

Results from the model in this study were dependent on factors such as concrete properties, girder and deck dimensions, properties of the prestressing strands, construction sequence and timelines, and environmental conditions. A parametric study was conducted to quantify the impact of these factors on girder performance and its response to deck replacement. One parameter was varied in each iteration and all other parameters were held constant to isolate the influence of that parameter. Table 4.16 shows the results from the parametric study performed by varying the relative humidity and concrete mixture proportions parameters. The increase or decrease in the

output based on increase/decrease of individual input parameters are shown in Table 4.17. The subsequent results from each parameter are detailed in the following sections.

Table 4.16: Results from Varying Relative Humidity and Concrete Mixture Proportion Parameters

Parameters		Pe at 20,000 days		ε_{sh} at 20,000 days		$\varepsilon_{cr,b}$ at 20,000 days		Girder rebound		Δdeflection		Deflection at 20,000 days	
		kips	% change[1]	micro-strain	% change[1]	micro-strain	% change[1]	in.	% change[1]	in.	% change[1]	in.	% change[1]
Relative humidity	0.5	847	0%	-460	0%	-2,890	0%	2.84	0%	0.74	0%	-3.44	0%
	0.7	962	14%	-385	-16%	-2,350	-19%	2.69	-5%	0.61	-18%	-0.43	-88%
	0.8	997	18%	-326	-29%	-2,230	-23%	2.57	-10%	0.51	-32%	0.36	-110%
	0.98	988	17%	-177	-62%	-2,420	-16%	2.24	-21%	0.24	-68%	1.03	-130%
Cement content	12.5 lb/ft^3	962	0%	-382	0%	-2,360	0%	2.50	0%	0.42	0%	-0.45	0%
	13.7 lb/ft^3	962	0%	-385	1%	-2,350	0%	2.50	0%	0.42	0%	-0.43	-4%
	20 lb/ft^3	965	0%	-395	3%	-2,330	-1%	2.50	0%	0.42	0%	-0.35	-22%
	40 lb/ft^3	970	1%	-415	9%	-2,290	-3%	2.50	0%	0.42	0%	-0.22	-50%
	50 lb/ft^3	971	1%	-422	11%	-2,280	-4%	2.50	0%	0.42	0%	-0.19	-58%
Cement type	Normal	962	0%	-385	0%	-2,350	0%	2.50	0%	0.42	0%	-0.43	0%
	Rapid hardening	1,100	14%	-405	5%	-1,090	-54%	2.45	-2%	0.35	-17%	-0.22	-48%
	Slow hardening	1,079	12%	-379	-2%	-1,670	-29%	2.48	-1%	0.42	-1%	1.26	-394%
Water-cement ratio	0.40	962	0%	-385	0%	-2,350	0%	2.50	0%	0.42	0%	-0.43	0%
	0.45	901	-6%	-363	-5%	-2,980	26%	2.53	1%	0.43	1%	-1.07	150%
	0.50	822	-15%	-364	-5%	-3,750	59%	2.55	2%	0.43	1%	-2.44	471%

Parameters		Pe at 20,000 days		ε_{sh} at 20,000 days		$\varepsilon_{cr,b}$ at 20,000 days		Girder rebound		Δdeflection		Deflection at 20,000 days	
		kips	% change[1]	micro-strain	% change[1]	micro-strain	% change[1]	in.	% change[1]	in.	% change[1]	in.	% change[1]
Aggregate type	NA	962	0%	-385	0%	-2,350	0%	2.50	0%	0.42	0%	-0.43	0%
	Diabase	978	2%	-452	17%	-2,370	1%	2.51	0%	0.42	0%	1.27	-396%
	Quartzite	920	-4%	-327	-15%	-2,660	13%	2.50	0%	0.42	0%	-0.55	29%
	Limestone	964	0%	-365	-5%	-2,350	0%	2.50	0%	0.42	0%	-0.85	100%
	Sandstone	990	3%	-504	31%	-2,070	-12%	2.51	0%	0.42	0%	-0.37	-13%
	Granite	976	1%	-381	-1%	-2,250	-5%	2.50	0%	0.42	0%	-0.98	128%
	Quartz Diorite	962	0%	-385	0%	-2,350	0%	2.50	0%	0.42	0%	-0.43	0%
Aggregate-cement ratio	3	746	0%	-736	0%	-3,200	0%	2.57	0%	0.43	0%	-5.41	0%
	5	892	20%	-497	-32%	-2,630	-18%	2.52	-2%	0.43	-1%	-1.78	-67%
	7	962	29%	-385	-48%	-2,350	-26%	2.50	-3%	0.42	-2%	-0.43	-92%
	9	1,004	35%	-317	-57%	-2,190	-32%	2.49	-3%	0.42	-3%	0.27	-105%
Volume-to-surface area ratio [2]	0.06 ft	962	0%	-385	0%	-2,350	0%	2.50	0%	0.43	0%	-0.43	0%
	0.1 ft	970	20%	-373	-32%	-2,290	-18%	2.50	-2%	0.43	-1%	-0.92	-67%
	0.15 ft	974	29%	-368	-48%	-2,260	-26%	2.50	-3%	0.43	-2%	-1.15	-92%
	0.2 ft	975	35%	-367	-57%	-2,250	-32%	2.50	-3%	0.43	-3%	-1.24	-105%

[1]The percentage (%) change is calculated based on the smallest value of the parameter used in the parametric study for most cases. For cement type, % change is calculated based on 'Normal' type cement. For aggregate type, it is calculated based on 'NA', which is the default option when information regarding the aggregate is not available.

Table 4.17: Impact of Changing Input Parameters on Prestressed Concrete Girder Outputs

Parameters	Deflection	Girder rebound	Creep strain	Shrinkage strain	Effective prestress
Relative humidity ↑	↓	↓	↓	↓	↑
Cement content ↑	↓	-	↓	↑	-
Water-cement ratio ↑	↑	↑	↑	↓	↓
Aggregate-cement ratio ↑	↓	↓	↓	↓	↑
Volume-surface area ratio ↑	↓	↓	↓	↓	↑

4.7.1 Relative Humidity

The effects of changing relative humidity (RH) are shown in Tables 4.16 and 4.17. Increasing RH from 0.50 to 0.98 resulted in approximately 60% less shrinkage strain and approximately 20% less creep strain at 20,000 days. Changing the RH from 0.50 to 0.98 led to a decrease in the girder rebound after deck removal of 0.6 in., and the final deflection decreased from -3.44 in. at RH of 0.50 to +1.03 in. at RH of 0.98 at 20,000 days. Overall, an RH of 0.50 had the most negative impact on girder performance.

4.7.2 Cement Content

The results in Tables 4.16 and 4.17 show that high cement content in the girder increased the shrinkage strain but decreased the creep strain. Prestress loss due to creep decreased by 16 kips, while prestress loss due to shrinkage increased by 6 kips when the cement content increased from 12.5 lb/ft^3 to 50 lb/ft^3. A high cement content therefore led to slightly less prestress loss and final deflection at 20,000 days due to decreased creep strain. Interestingly, almost no change in girder rebound and deflection due to deck removal was observed with varying cement content. Overall, cement content only minimally impacted the long-term behavior of the girder and deck replacement process.

4.7.3 Water-Cement Ratio

Results in Table 4.16 show that increasing the water-cement ratio (w/c ratio) increased the shrinkage strain and the prestress loss. Deflection of the girder increased from -0.43 in. to -2.44 in. when the w/c ratio changed from 0.40 to 0.50. According to Table 4.16, w/c ratio had very little impact on the girder rebound after deck removal and change in deflection due to deck replacement. Therefore, the w/c ratio causes a major impact on the shrinkage strain, leading to a change in prestress loss and deflection of a prestressed concrete girder.

4.7.4 Cement Type

Cement was found to significantly influence the long-term performance of the girder. Results provided by the model based on the cement type are tabulated in Table 4.16. Initially, prestress loss due to shrinkage was lowest for rapid-hardening cement, followed by normal and slow-hardening cement, but the final loss was highest for rapid-hardening cement followed by normal and slow-hardening, as shown in Figure 4.25. Prestress loss due to creep was highest for normal cement, followed by slow-hardening and rapid-hardening types, as shown in Figure 4.26. Overall, the normal cement type caused the maximum amount of prestress loss, as shown in Figure 4.27. Minimal difference was observed in the girder rebound due to cement type, but the final deflection decreased from -0.43 in. (downward) to 1.25 in. (upward) between normal and slow-hardening cement.

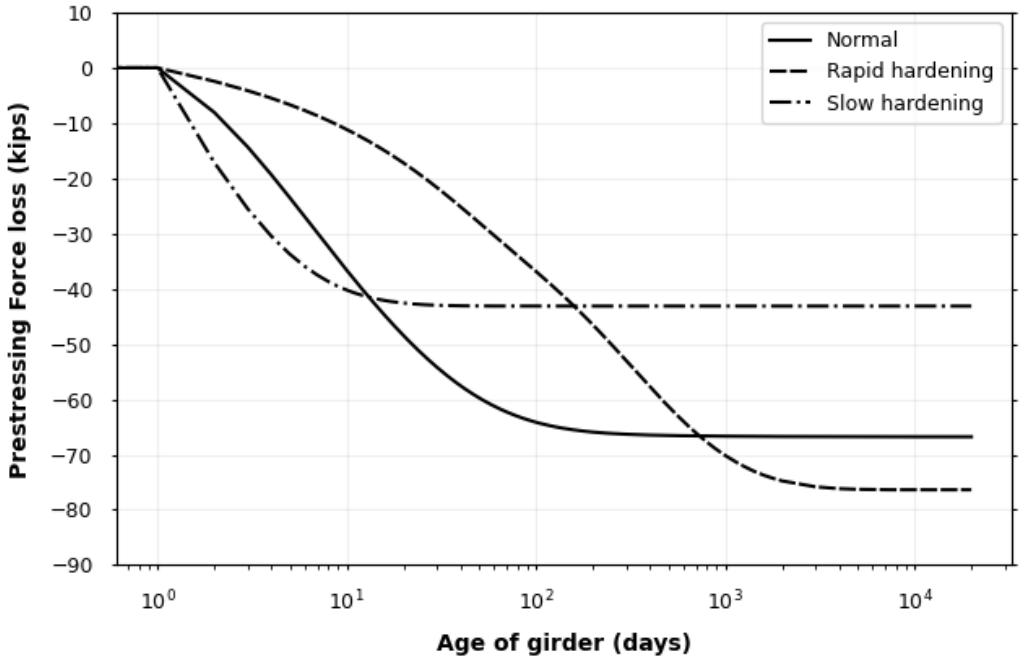

Figure 4.25: Prestress Loss Due to Shrinkage by Cement Type

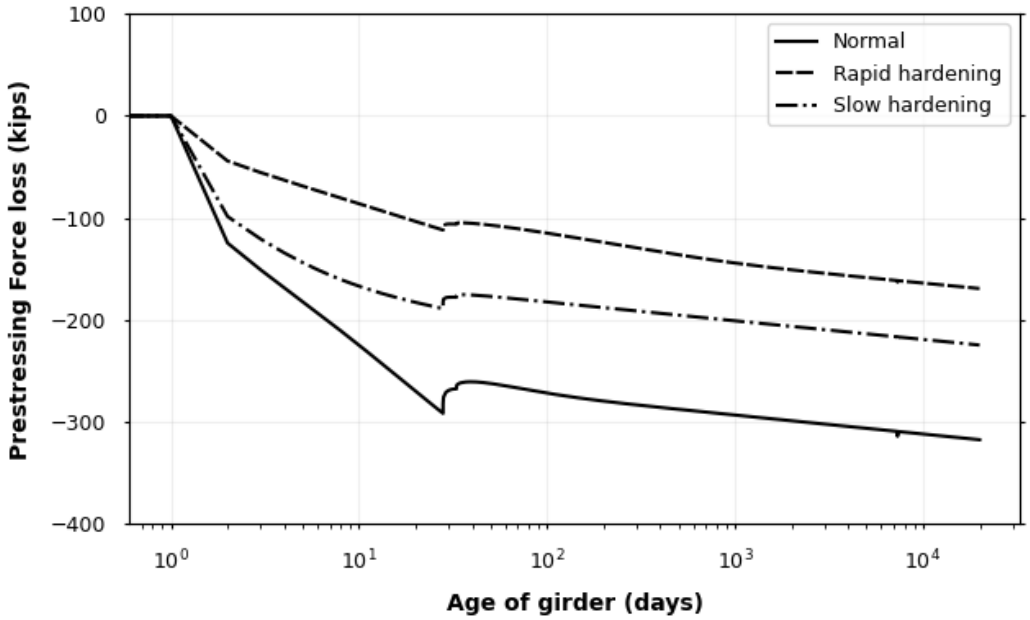

Figure 4.26: Prestress Loss Due to Creep by Cement Type

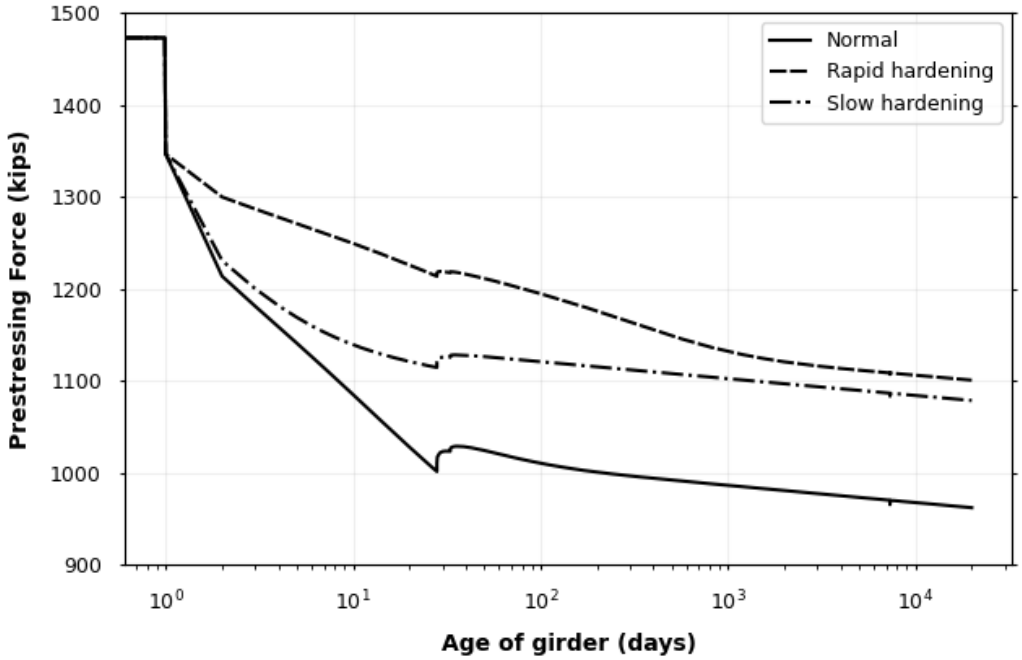

Figure 4.27: Effective Prestress Over Time by Cement Type

4.7.5 Aggregate Type

The B4 model allows for the selection of six different types of aggregate to calculate long-term deformation. When the type of aggregate is unknown, the B4 model provides a default value (NA) option. This study evaluated the behavior of prestressed concrete girders based on aggregate type, and the results, shown in Table 4.16, demonstrated that prestress loss and creep strain were highest for quartzite and lowest for sandstone, while shrinkage strain was highest for sandstone and lowest for quartzite. The plot of midspan deflection at 20,000 days by aggregate type (Figure 4.28) shows that deflection was notably different for diabase, resulting in a net upward deflection at 20,000 days while the other types resulted in downward deflection. Figure 4.29 shows the total midspan deflection of the girder, with various aggregate types, over time. Although aggregate type can substantially impact long-term girder behavior, no considerable differences were observed in the behavior during deck replacement. Only a 4% difference was observed in effective prestress at 20,000 days, and the difference in girder rebound and deflection change was less than 1% during deck replacement. Therefore, aggregate type is not a crucial factor for deck replacement but it should be considered when determining the overall performance of the girder.

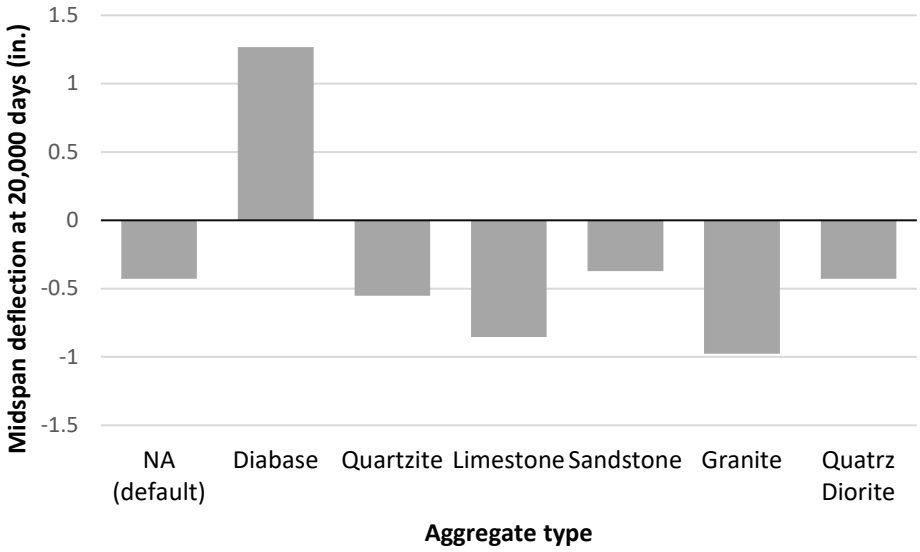

Figure 4.28: Midspan Deflection at 20,000 Days by Aggregate Type

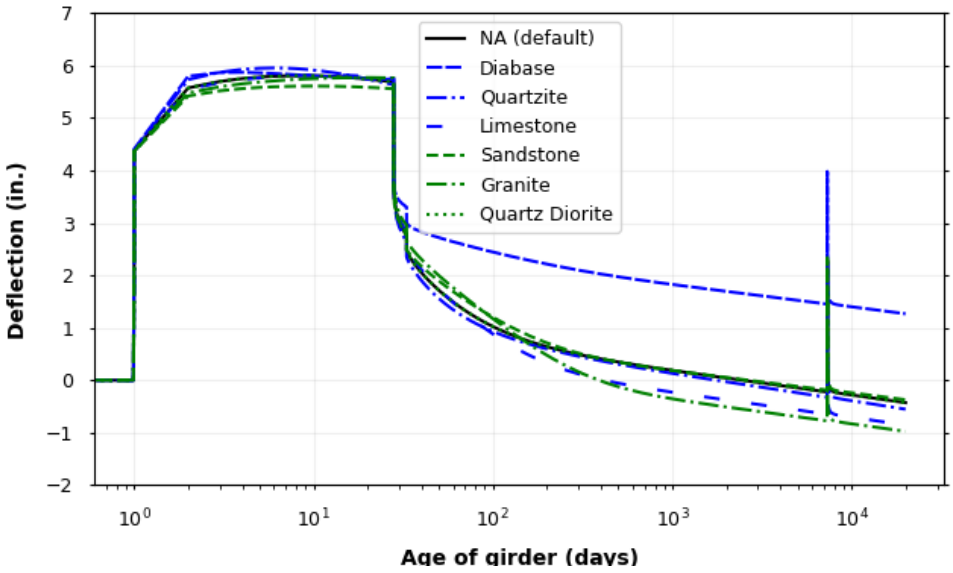

Figure 4.29: Midspan Deflection Over Time by Aggregate Type

4.7.6 Aggregate-Cement Ratio

The aggregate-cement ratio was varied between 3 and 9 to study the impact of varying this input parameter on model output. Results of this analysis are presented in Table 4.16 and Table 4.17. Creep and shrinkage strain both increased as aggregate-cement ratio decreased, causing

higher prestress loss. Aggregate-cement ratio was shown to be a major contributing factor to the development of shrinkage strain. Use of the smallest aggregate-cement ratio resulted in the highest deflection and prestress loss of the girder. Figure 4.30 shows total deflection throughout the girder lifespan with varying aggregate-cement ratio. The influence of the aggregate-cement ratio on girder deflection was evident when changing the value from 9 to 3 resulted in a change in deflection at 20,000 days from 0.274 in. to -5.41 in. Additionally, prestress loss increased by 258 kips when the aggregate-cement ratio was changed from 9 to 3, as shown in Table 4.16.

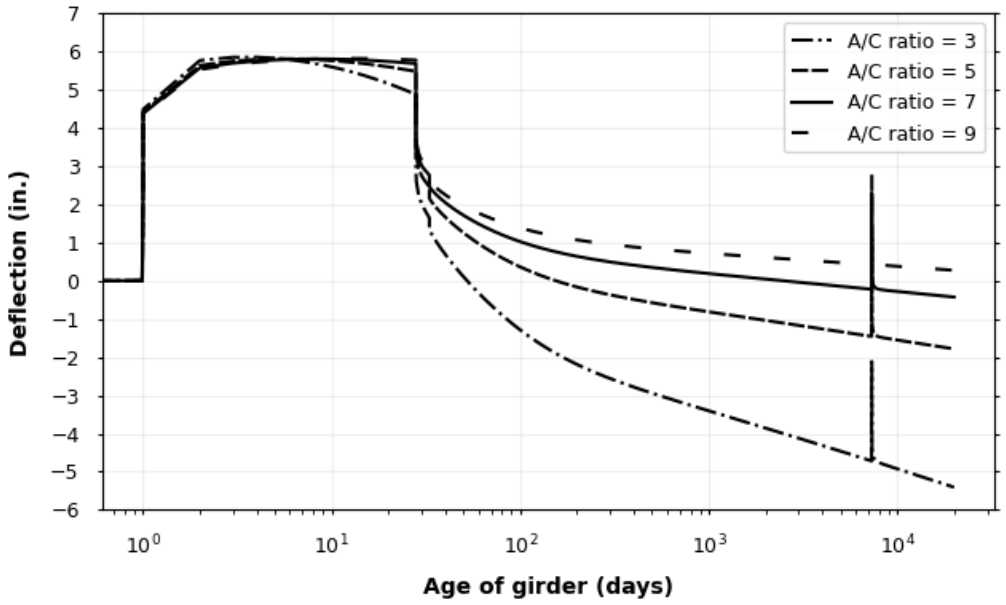

Figure 4.30: Midspan Deflection Over Time for Various Aggregate-Cement Ratios

4.7.7 Volume-to-Surface Area Ratio

To change the volume-to-surface area ratio (V/S-ratio) of a girder, the girder geometry must be modified, which is unrealistic. However, to study the effect of the V/S-ratio alone on girder behavior, this study varied only the V/S-ratio while everything else was kept constant. The V/S-ratio results ranged from 0.06 ft to 0.20 ft, as shown in Tables 4.16 and 4.17. Figure 4.31 shows prestressing force in the girder versus time for various V/S-ratios. The V/S-ratio was shown to affect the rate at which the prestress loss occurred, resulting in nearly similar values of

prestressing force at later ages. Analysis results showed that the V/S-ratio affected the initial prestress force of the girder more than the long-term prestress force; initial prestress losses were higher for girders with small V/S-ratios, but the losses converged as the girder aged. In contrast, the V/S-ratio had a greater impact on long-term deflection than on initial deflections of the girder, as shown in Figure 4.32, potentially due to the cumulative effect of the concrete deformation in the girder over time. Girder rebound was essentially the same for any value of the parameter.

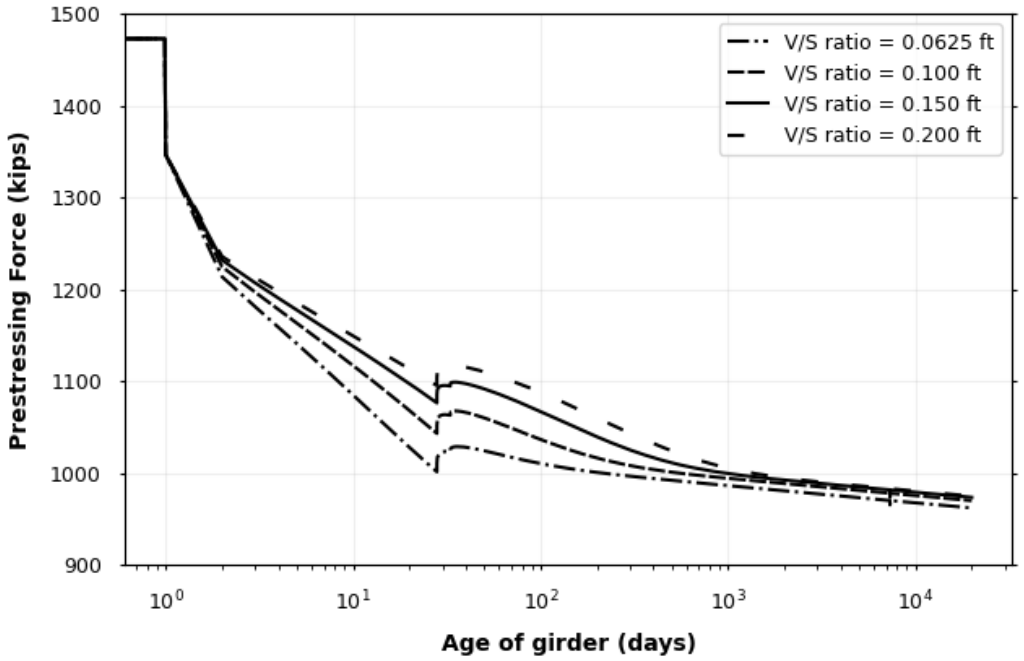

Figure 4.31: Effective Prestress Over Time for Various V/S-Ratios

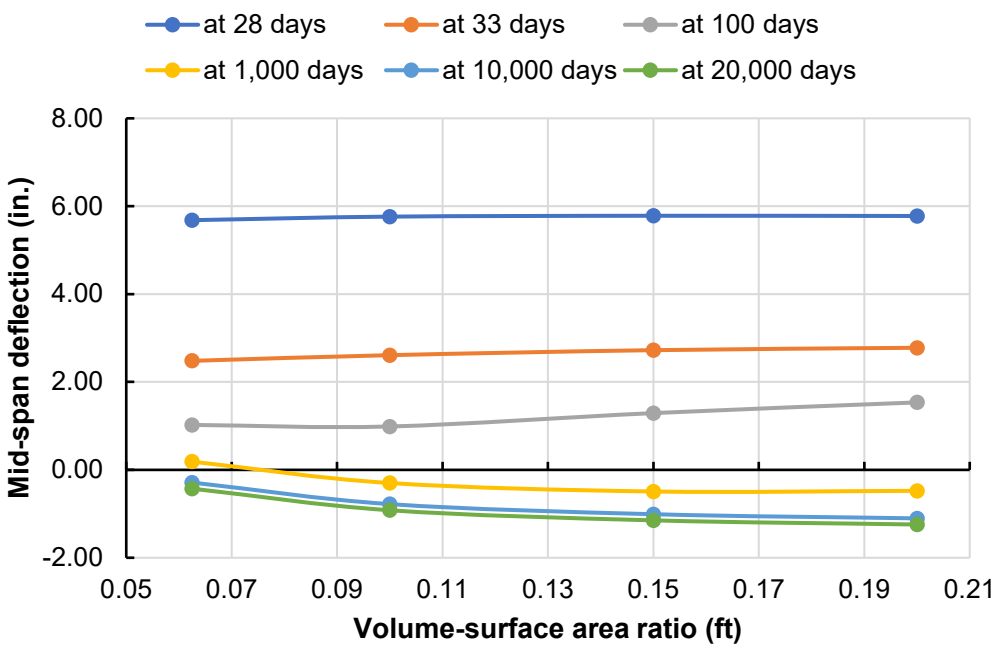

Figure 4.32: Midspan Deflection at Various Ages by V/S-Ratios

4.7.8 Prestress Transfer Age

The age at which the prestress force is transferred to the concrete is important for determining the initial behavior of the girder. Prestress transfer ages ranging from 0.75 days to 5 days were considered to study how the change in the prestress transfer age impacts the model output. The percentage changes were calculated based on the age of prestress transfer of 0.75 days. Results showed that changing the prestress transfer age from 0.75 days to 5 days caused a fluctuation of up to 15% in the camber of the girder at 28 days (Table 4.18). A reduction of 0.9 in. was observed in deflection at 33 days when prestress transfer age was changed from 0.75 days to 5 days. No other parameters were sensitive to the age of prestress transfer, including those related to deck replacement. Rebound of the girder and difference in deflection due to deck replacement did not change due to variation in prestress transfer age. Although a higher prestress transfer age somewhat improved short-term girder performance, 0.75 to 1 days is more practical in the casting yard.

Table 4.18: Comparison of Results for Various Ages of Prestress Transfer

Parameters	Age of prestress transfer								
	0.75 days	1 day		1.5 days		2 days		5 days	
	Value	Value	% change	Value	% change	Value	% change	Value	% change
Camber at 28 days (in.)[1]	5.8	5.7	-2%	5.5	-6%	5.4	-8%	5.0	-15%
Deflection after 33 days (in.)[1]	2.6	2.5	-6%	2.3	-13%	2.1	-18%	1.7	-34%
Rebound due to deck removal (in.)	2.7	2.7	0%	2.7	0%	2.7	0%	2.7	0%
Δdeflection due to deck replacement (in.)	0.6	0.6	0%	0.6	0%	0.6	0%	0.6	0%
Total deflection at 20,000 days (in.)	-0.4	-0.4	-0%	-0.4	-0%	-0.4	-0%	-0.4	-0%
Final bottom creep strain at 20,000 days	-0.002	-0.002	0%	-0.002	0%	-0.002	0%	-0.002	0%
Total prestress loss (kips)	962	962	0.%	962	0%	962	-0%	962	-0%

[1] Until 28 days, the deflection/camber occurs due to girder self-weight and prestressing force only.
[2] Deck loads are applied at 28 days and superimposed loads are applied at 33 days, which caused the camber at 28 days to decrease. Hence, there is a significant difference in the deflection/camber at 28 days and at 33 days.

4.7.9 Age of Deck Placement

The age of the girder when the first deck is placed is an important parameter that impacts long-term girder behavior. Figure 4.33 shows the variation in results for creep strain at the bottom of the girder and corresponding prestress loss due to creep for various girder ages at deck placement. The figure shows that long-term creep strains and prestress losses increased as the age at deck placement increased. Final creep strain at 20,000 days was less when the deck was cast at 28 days and increased with the increase in age of deck placement. The deck and associated loads

reduced the upward camber and counteracted the stresses due to prestressing force, thereby reducing stresses in the girder that caused creep. Since creep is most significant in the initial days after construction, applying additional downward loads in the early days will reduce the stress that causes creep and the magnitude of subsequent creep strain. When the deck was cast at 365 days, approximately 80% of the long-term creep occurred, and the reduction of stress due to the counteracting load did not significantly change the behavior of the girder, as shown in Figure 4.33. Shrinkage strains are not shown in the figure, but they are independent of the age at deck placement.

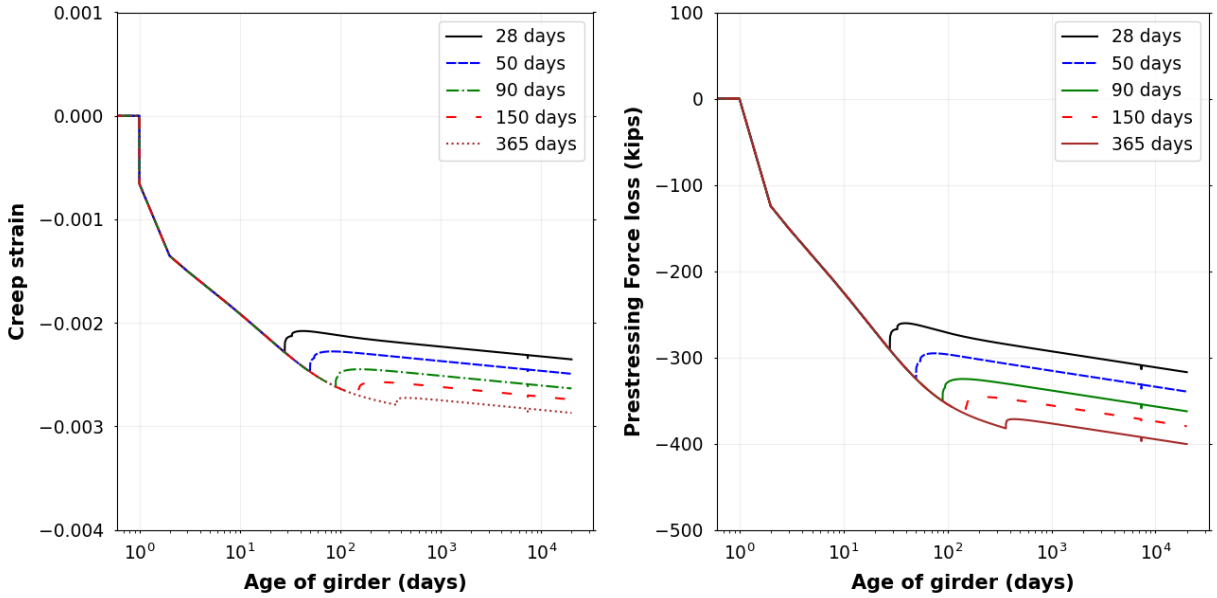

Figure 4.33: Various Ages at Deck Placement: a) Creep Strain at the Bottom Fiber of the Girder at Midspan; b) Prestress Loss Due to Creep at Girder Midspan

Figure 4.34 shows that girder deflection decreased substantially with increased age at deck placement. The midspan deflection of the girder at 20,000 days was -0.42 in. for a deck cast at 28 days and 1.43 in. for a deck cast at 365 days. Rebound due to deck removal changed by 7% when the age at deck placement increased from 28 to 365 days.

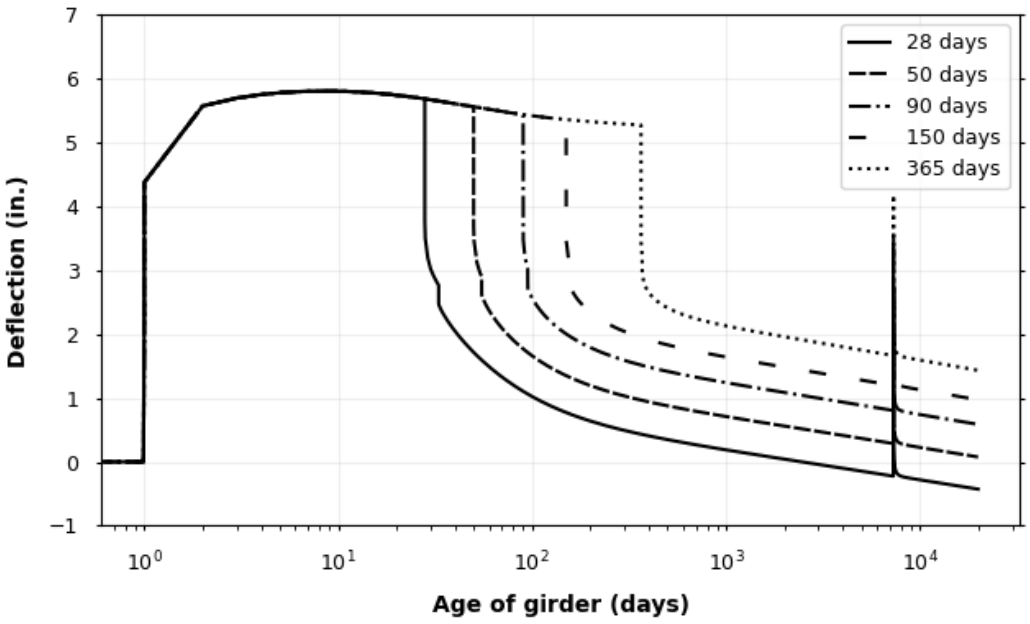

Figure 4.34: Midspan Girder Deflection by Age at Deck Placement

4.7.10 Deck Loads

Because a new bridge deck may have different properties than the old deck, this study considered three cases to determine how changes in deck loads affect girder behavior: 1) new deck loads were identical to old deck loads, 2) new deck loads increased by 20%, and 3) new deck loads decreased by 20%. The resulting plot for prestressing force in the girder between 6,000 days and 18,000 days after girder construction under these three cases is shown in Figure 4.35. When the deck load increased by 20%, the prestressing force increased by 2 kips at 12,000 days. A corresponding decrease in prestressing force resulted from decreasing the deck loads because the prestress gain caused by instantaneous creep strain developed due to the application of new downward loads on the prestressing strand. The stresses and deflections of the girder varied with the load, increasing at +20% deck load and decreasing when the load decreased by -20%.

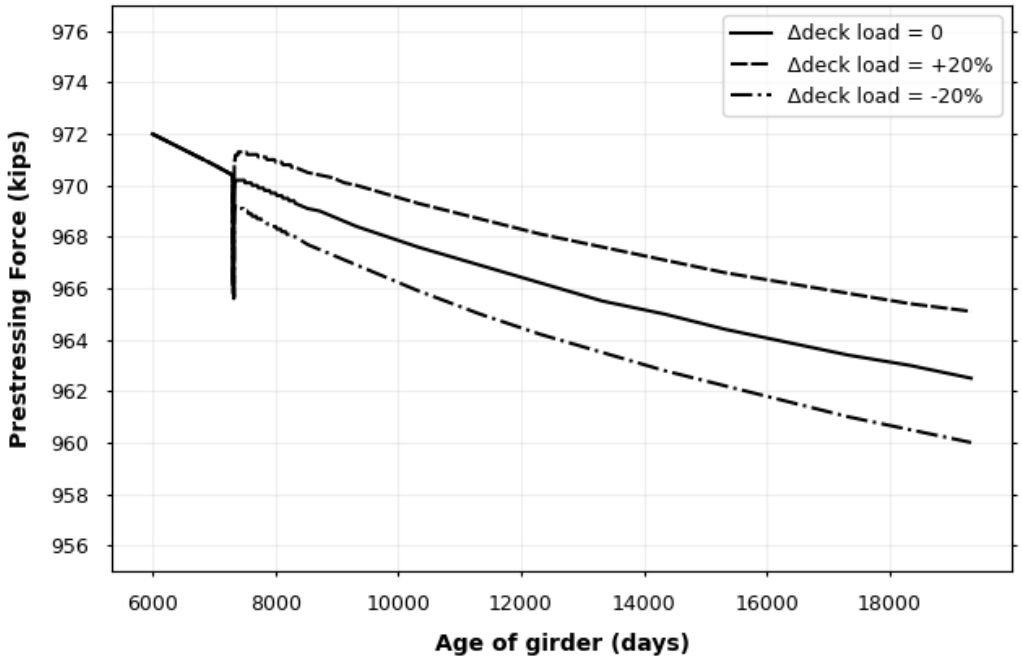

Figure 4.35: Effective Prestress Force Over Time for Various Deck Loads

4.7.11 Deck Removal Time

This study also considered the effects of the time of deck removal, with deck replacement dates of 10 to 40 years after girder construction. The influence of this parameter was evaluated based on girder rebound, deflection, creep strain, and total prestress loss (Table 4.19). Changing the age of deck removal had less than a 2% difference in the deflection and rebound of the girder, no important impact was observed on the total prestress loss, and no substantial difference in the girder behavior was shown if the deck was removed any time after 10 years of girder construction.

Table 4.19: Comparison of Results for Various Deck Removal Times

Parameters	Age of deck removal				
	10 years	20 years	25 years	30 years	40 years
Rebound due to deck removal (in.)	2.51	2.50	2.50	2.50	2.50
Total deflection at 20,000 days (in.)	-0.43	-0.43	-0.43	-0.43	-0.43
Final creep strain at bottom at 20,000 days	-2.4E-03	-2.4E-03	-2.4E-03	-2.4E-03	-2.4E-03
Total prestress loss (kips)	962	962	962	962	962

4.7.12 Time Between Deck Removal and Deck Replacement

This study examined whether the time interval between old deck removal and new deck placement affects girder performance using time intervals of 1 to 30 days. Analysis results are presented in Table 4.20. Although deflection of the girder after the new load application showed a small percentage change depending on the time interval, no substantial difference was observed over the long term. These results suggest that the time interval between old deck removal and new deck placement has minimal impact on girder performance.

Table 4.20: Results for Various Time Intervals Between Deck Removal and Deck Replacement

Output Parameters	Units	Time between deck removal and new deck placement				
		1 day	5 days	10 days	20 days	30 days
Deflection at 7360 days	in.	-3.5E-03	5.3E-03	1.7E-02	4.5E-02	7.9E-02
Change in deflection due to deck replacement	in.	0.22	0.23	0.24	0.27	0.30
Total deflection at 20,000 days	in.	-0.43	-0.43	-0.43	-0.43	-0.43
Creep strain at 7,360 days	με	-2,310	-2,310	-2,310	-2,310	-2,310
Final creep strain at 20,000 days	με	-2,350	-2,350	-2,350	-2,350	-2,350
Effective prestress at 7,360 days	kips	970	970	970	970	970
Total effective prestress at 20,000 days	kips	962	962	962	962	962

Note: Old deck is removed at 7305 days for all cases

4.7.13 Girder Properties

This study also investigated the impact of various girder properties, including concrete compressive strength, girder length, and girder spacing, on the long-term behavior of the prestressed concrete girder. The compressive strength of the girder (f_{cg}) was set at 6.5 ksi based on the PCI Design Example. Any alteration in compressive strength required corresponding adjustments to the concrete mixture proportions. However, to isolate the impact of compressive strength on the long-term behavior of the girder, only the compressive strength of the concrete was varied while all other parameters were held constant. Varying the compressive strength by ±15% resulted in a ±1% change in the initial girder camber and the girder rebound variation between -8% and 6%. The final deflection at 20,000 days shifted from -0.43 in. to -0.58 in. for a 15% increase in compressive strength and to -0.31 in. for a 15% decrease. Relatively small changes were also observed in the preliminary losses and creep strain.

Girder length was shown to have a notable impact on the deflections, stresses, creep strain, and prestress force of the girder, as shown in Figure 4.36, where substantial differences in deflection and prestress force are evident. A 20-ft increase in length led to a midspan deflection increase of 5.60 in., while a 20-ft reduction caused the midspan deflection to decrease by 2.41 in. Reducing the length increased the preliminary loss and loss due to creep strain, resulting in a 9% decrease in total effective prestress at 20,000 days. Increasing the length, on the other hand, resulted in a 10% increase in the total effective prestress force at 20,000 days. Girder rebound increased from 2.69 in. for the 120-ft girder to 4.65 in. for the 140-ft girder. Although increasing the length decreased the prestress loss, long girders had very high deflection values. As expected, girder length was shown to substantially impact long-term behavior and deck replacement.

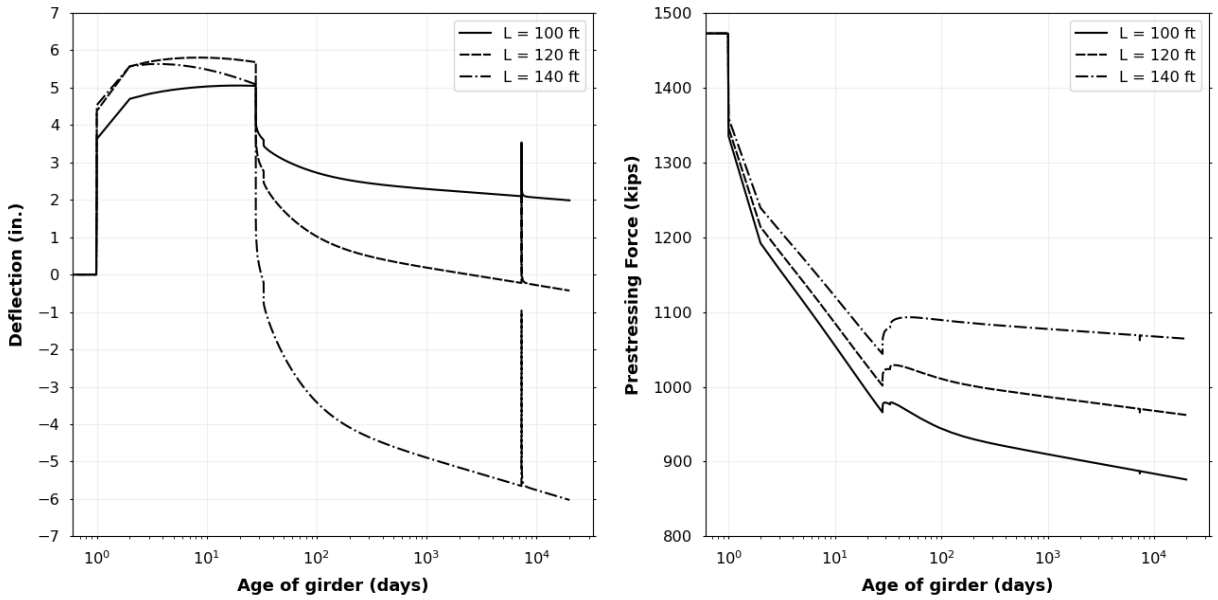

Figure 4.36: a) Total Midspan Girder Deflection and b) Effective Prestress Force at Girder Midspan for Various Girder Lengths

The effective width of the deck used to calculate deck loads on the girder is typically determined by the distance between girders, meaning changes in girder spacing alter loads on the girder, causing variations in the stresses, strains, and deflections. Table 4.21 lists the impacts of girder spacing on deflection, creep strain, preliminary losses, and total effective prestress force. As shown, an increase in girder spacing caused an increase in downward deflection, an increase in girder rebound after deck removal, a reduction in total creep strain, and an increase in effective prestress force. A ±10% change in girder spacing resulted in a change in girder rebound by ±9%. Similarly, the midspan deflection of the girder varied from 0.05 in. for a girder spacing of 8 ft to -0.43 in. for a spacing of 9 ft and to -0.91 in. for a spacing of 10 ft. The reduction in creep strain was because the added deck load from increased girder spacing decreased the total stresses in the girder caused by prestressing, thereby reducing the resulting creep strain.

Table 4.21: Comparison of Results for Various Girder Spacings

Output Parameters	Girder spacing		
	8 ft	9 ft	10 ft
Camber after 28 days (in.)	5.68	5.68	5.68
Deflection after all loads applied (33 days) (in.)	2.76	2.48	2.20
Rebound due to deck removal (in.)	2.27	2.50	2.73
Δdeflection due to deck replacement (in.)	0.39	0.43	0.46
Total deflection at 20,000 days (in.)	0.05	-0.43	-0.91
Final creep strain at 20,000 days	-2.42E-03	-2.35E-03	-2.28E-03
Preliminary prestress losses (kips)	141	141	141
Total effective prestress at 20,000 days (kips)	951	962	973

Chapter 5: Conclusions and Recommendations for Future Work

This study developed a model in Python to calculate the effective prestress force and prestress losses, creep and shrinkage strains, concrete stresses, and deflections of a prestressed concrete I-girder at any point in time during the life of the girder. The model was structured using a time-step analysis approach to perform calculations at various time steps to explicitly account for changes in load throughout the girder life and highlight the effects of deck removal and replacement. The B4 model (Wendner et al., 2013) was used to calculate concrete creep and shrinkage.

The model was applied to an example bridge with prestressed concrete I-girders for validation and to illustrate the effects of deck replacement performed at 20 years on the selected structure. Results included long-term prestress loss, deflections, stresses, and the impact of deck replacement on the prestressed concrete girders. A parametric study was also conducted to show the influence of each input variable on model outputs for the structure.

5.1 Conclusions

Preliminary conclusions and observations were made based on application of the model described in this report to the bridge example described in Chapter 4. It should be noted that future modifications to the model and evaluation of other structures, as proposed in Section 5.2, may result in different conclusions. Conclusions of the current study include:

1. Deck replacement in the example bridge only minimally affected long-term bridge behavior. Although several input parameters had an important effect on the long-term behavior of the girder, the effects of deck replacement were small and insensitive to most model inputs.
2. Creep and shrinkage significantly affected the long-term performance of the girder. Concrete creep in the example bridge caused approximately 60% of the prestress loss, and shrinkage caused 15% of the loss. Girder deflection was also affected by concrete creep, particularly during the initial days when creep rate was highest.

3. Removing the deck caused the girder to rebound and camber upward, but the camber after deck removal was less than the camber before the deck was initially applied for the cases considered due to concrete deformation during deck placement and deck removal. Girder rebound remained within acceptable limits for the cases considered.
4. Deck replacement after 10 years of construction had minimal impact on the remaining service life of the girder for the bridge considered. The time elapsed between deck removal and placement of the new deck also was shown to have minimal effect on girder behavior.
5. Continuity diaphragms restrain girder-end rotations and alter stress distribution. Nevertheless, the restraint moments, which are limited by the moment strength at the girder end, had minimal effect on the long-term behavior of prestressed concrete girders.

Results from the parametric study showed that, for the bridge and model considered:

1. Environmental relative humidity significantly affected the effective prestress, shrinkage strain, and girder deflection.
2. Cement content had a minor effect on long-term girder behavior.
3. The type of cement used affected the magnitude of creep strain and rate of shrinkage deformation differently depending on the stage of deformation.
4. The volume-to-surface area ratio changed the rate of deformation but produced almost the same value of creep and shrinkage in the long run.
5. The age of prestress transfer influenced the initial camber and deflection of the girder but had little effect on long-term behavior.
6. The age of the girder when the deck concrete is placed had an important effect on the effective prestress force; an earlier age led to less prestress loss and more deflection.
7. Girder length strongly affected prestress loss and deflections.

8. Concrete compressive strength and girder spacing had little effect on the model output.
9. Girder shrinkage and deflection were most affected by the aggregate type selected.
10. The importance of the deck replacement was dependent on girder length, environmental relative humidity, and the diaphragm removal, which caused variations in girder rebound. Other variables did not influence girder behavior during deck replacement.

5.2 Recommendations for Future Research

Future work should address the following issues:

1. Modeling the interaction of deck creep and girder creep: deck creep was calculated in this study, but the interaction of deck creep and girder creep was not modeled and should be accounted for in future research. Furthermore, strain compatibility at the girder and deck interface should be enforced at each time step, and the stresses should be redistributed accordingly.
2. Suitability for deck replacement: The model output relies on multiple input parameters. Large variations were observed when varying a single parameter, which suggests that a different result could be obtained for different combinations of input parameters. Hence, additional research is required to determine conditions for viable deck replacement.
3. Monte-Carlo simulation: The reported parametric study showed how changing each variable individually affected long-term behavior of the example bridge, with some parameters demonstrating greater impact than others. To generalize conclusions, a Monte Carlo simulation should be performed to simulate the importance of input parameters on a wider range of bridge configurations and to examine interactions between input parameters. A Monte-Carlo simulation would identify which input

combinations result in acceptable behavior and identify cases that result in unusual behavior after the replacement process.

4. Field verification: Although verification of individual steps was performed using comparisons with published examples, overall model outputs could not be verified due to a lack of field data. Field verification of the results from the entire model would increase confidence in the results. To validate the creep and shrinkage strains and the girder deflection provided by the model, strains and deflection data from the bridge monitored over a long period of time (>10 years) could be useful. Data from the continuously monitored bridge, including information on all load changes, could help verify the entire long-term behavior estimated by the model. Data collected at discrete points in time could also help fulfill this objective if the information is collected at every change in loading conditions.

References

AASHTO. (2012). *AASHTO LRFD bridge design specifications*. American Association of State Highway Transportation Officials.

ACI Committee 209. (1997). *ACI 209R-92: Prediction of creep, shrinkage and temperature effects in concrete structures.* American Concrete Institute.

ACI Committee 209. (2008). *ACI 209.2R-08: Guide for modeling and calculating shrinkage and creep in hardened concrete*. American Concrete Institute.

Alberta Technical Services Branch. (2018). *NU girder bridge design and detailing manual*. Alberta Transportation.

Atrushi, D. S. (2003). *Tensile and compressive creep of young concrete: Testing and modelling* [Doctoral dissertation, Norwegian University of Science and Technology].

Assad, S. A., & Morcous, G. (2016). Evaluating the impact of bridge-deck removal on the performance of precast/prestressed concrete I-girders. *Journal of Performance of Constructed Facilities*, *30*(3).

Bažant, Z. P. (1972). Prediction of concrete creep effects using age-adjusted effective modulus method. *Journal of the American Concrete Institute*, *69*(4), 212-217.

Bažant, Z. P. (Ed.). (1988). *Mathematical modeling of creep and shrinkage of concrete*, John Wiley and Sons.

Bažant, Z. P. (2001). Prediction of concrete creep and shrinkage: Past, present and future. *Nuclear Engineering and Design*, *203*(1), 27-38.

Bažant, Z. P., Hubler, M. H., & Yu, Q. (2015). Damage in prestressed concrete structures due to creep and shrinkage of concrete. In *Handbook of damage mechanics: Nano to macro scale for materials and structures* (pp. 515-564). Springer Link.

Bažant, Z. P., Jirásek, M., Hubler, M. H., & Carol, I. (2015). RILEM draft recommendation: TC-242-MDC multi-decade creep and shrinkage of concrete: Material model and structural analysis model B4 for creep, drying shrinkage and autogenous shrinkage of normal and high-strength concretes with multi-decade applicability. *Materials and Structures*, *48*(4), 753-770.

Bažant, Z. P., & Jirásek, M. (2018). *Creep and hygrothermal effects in concrete structures*. Springer.

Bažant, Z. P., & Li, G.-H. (2008). *Comprehensive database on concrete creep and shrinkage*. Infrastructure Technology Institute.

Bažant, Z. P., & Murphy, W. P. (1995). Creep and shrinkage prediction model for analysis and design of concrete structures - Model B-3. *Materiaux et Constructions*, *28*(180), 357-365.

Bažant, Z. P., & San, D. (1994). Creep and shrinkage revisited. Paper by N. J. Gardner and J. W. Zhao. *ACI Materials Journal*, *91*(2), 204-211.

Bažant, Z. P., Yu, Q., Hubler, M. H., Kristek, V., & Bittnar, Z. (2011). Wake-up call for creep, myth about size effect and black holes in safety: What to improve in fib model code draft. In *fib Symposium PRAGUE 2011: Concrete Engineering for Excellence and Efficiency*. Czech Concrete Society.

Bažant, Z. P., Yu, Q., & Li, G.-H. (2012a). Excessive long-time deflections of prestressed box girders. I: Record-span bridge in Palau and other paradigms. *ASCE Journal of Structural Engineering*, *138*(6), 676-686.

Bažant, Z. P., Yu, Q., & Li, G.-H. (2012b). Excessive long-time deflections of prestressed box girders. II: Numerical analysis and lessons learned. *ASCE Journal of Structural Engineering*, *138*(6), 687-696.

Birhane, F. N., Kim, S.-I., & Jang, S.Y. (2020). Long-term deflection of prestressed concrete bridge considering nonuniform shrinkage and crack propagation by equivalent load approach. *Applied Sciences*, *10*(21).

Birkeland, H. W. (1960). Differential shrinkage in composite beams. *ACI Journal Proceedings*, *56*(5), 1123-1136.

Boatman, B. (2010). *Prestressed vs. steel beams: Expected service life.* Michigan Department of Transportation.

Buckler, J. D., & Scribner, C. (1985). *Relaxation characteristics of prestressing strand* (Report SRS-520). University of Illinois Civil Engineering.

CEB-fip. (1993). *CEB-FIP model code 1990*. Thomas Telford Publishing.

Freyermuth, C. L. (1969). Design of continuous highway bridges with precast, prestressed girders. *PCI Journal*, 14-39.

Garber, D. B., Gallardo, J. M., Deschenes, D. J., & Bayrak, O. (2015). Experimental investigation of prestress losses in full-scale bridge girders. *ACI Structural Journal*, *112*(5), 553-564.

Garber, D. B., Gallardo, J. M., Deschenes, D. J., & Bayrak, O. (2016). Prestress loss database for pretensioned concrete members. *ACI Structural Journal*, *113*(2), 313-324.

Garber, D., Gallardo, J., Deschenes, D., Dunkman, D., & Bayrak, O. (2012). *Effect of new prestress loss estimates on pretensioned concrete bridge girder design*. Texas Department of Transportation.

Gardner, N., & Lockman, M. (2001). Design provisions for drying shrinkage and creep of normal-strength concrete. *ACI Materials Journal*, *98*(2), 159-167.

Gardner, N. J., & Zhao, J. W. (1994). Creep and shrinkage revisited. *ACI Materials Journal*, *91*(2), 204-216.

Gedam, B. A. (2019). Time-dependent behaviour prediction of the prestressed HPC I-girder. *Engineering Structures*, 201.

Ghali, A., Favre, R., & Elbadry, M. (2018). *Concrete structures: Stresses and deformations: Analysis and design for serviceability*. CRC Press.

Ghimire, S. (2014). *Restraint moments due to thermal gradients in continuous prestressed concrete girder bridges* [Doctoral dissertation, Louisiana State University].

Gilbert, R. I. (1988). *Time Effects in Concrete Structures*.

Granata, M. F., Margiotta, P., & Arici, M. (2013). Simplified procedure for evaluating the effects of creep and shrinkage on prestressed concrete girder bridges and the application of European and North American prediction models. *ASCE Journal of Bridge Engineering*, *18*(12), 1281-1297.

Hastak, M., Mirmiran, A., Miller, R., Shah, R., & Castrodale, R. (2003). State of practice for positive moment connections in prestressed concrete girders made continuous. *ASCE Journal of Bridge Engineering*, *8*(5), 267-272.

Hearn, G., & Xi, Y. (2007). *Service life and cost comparisons for four types of CDOT bridge decks*. Colorado Department of Transportation.

Hossain, T., Okeil, A. M., & Cai, C. (2014). Calibrated finite element modeling of creep behavior of prestressed concrete bridge girders. *ACI Structural Journal*, *111*(6).

Hubler, M. H., Wendner, R., & Bažant, Z. P. (2015). Statistical justification of model B4 for drying and autogenous shrinkage of concrete and comparisons to other models. *Materials and Structures*, *48*(4), 797-814.

Kamel, M. R. (1996). *Innovative precast concrete composite bridge systems* [Doctoral dissertation, University of Nebraska-Lincoln].

Kamatchi, P., Rao, K. B., Dhayalini, B., Saibabu, S., Parivallal, S., Ravisankar, K., & Iyer, N. R. (2014). Long-term prestress loss and camber of box-girder bridge. *ACI Structural Journal*, *111*(6).

Kasera, S. C. (2014). *Simulation of the effect of deck cracking due to creep and shrinkage in single span precast/prestressed concrete bridges* [Doctoral dissertation, University of Cincinnati].

KDOT. (2021). *Bridge design manual*. Kansas Department of Transportation.

Khazanovich, L. (1990). Age-adjusted effective modulus method for time-dependent loads. *Journal of Engineering Mechanics*, *116*(12), 2784-2789.

Kovach, J. D. (2008). *Horizontal shear capacity of composite concrete beams without interface ties* [Doctoral dissertation, Lehigh University].

Kytölä, U., & Laaksonen, A. (2018). Prediction of restraint moments in precast, prestressed structures made continuous. *Nordic Concrete Research*, *59*(1), 73-93.

Lockman, M. J. (2002). *Compliance, relaxation and creep recovery of normal strength concrete*. National Library of Canada/Bibliothèque Nationale du Canada, Ottawa.

Li, C., Lequesne, R. D., & Matamoros, A. (2019). Girder–deck interface: Partial debonding, deck replacement, and composite action. *ASCE Journal of Bridge Engineering*, *24*(1).

Ma, Z., Huo, X., Tadros, M. K., & Baishya, M. (1998). Restraint moments in precast/prestressed concrete continuous bridges. *PCI Journal*, *43*(6), 40-57.

Manning, D. G. (1991). *Removing concrete from bridges*. Transportation Research Board.

Menkulasi, F., Patel, A., & Baghi, H. (2018). An investigation of AASHTO's requirements for providing continuity in simple span bridges made continuous. *Engineering Structures*, 158**,** 175-198.

Miller, R. A., Castrodale, R., Mirmiran, A., & Hastak, M. (2004). *Connection of simple-span precast concrete girders for continuity* (NCHRP Report). Transportation Research Board.

Mirmiran, A., Kukarni, S., Castrodale, R., Miller, R., & Hastak, M. (2001). Nonlinear continuity analysis of precast prestressed girders with cast-in-place decks and diaphragms. *PCI Journal*, *46*(5), 60-80.

Naaman, A. E. (1982). *Prestressed concrete analysis and design: Fundamentals*. McGraw-Hill.

Nilson, A. H. (1978). *Design of prestressed concrete.* John Wiley & Sons.

PCI. (1997). *Precast prestressed concrete bridge design manual* (1st ed, MNL-133). Precast/Prestressed Concrete Institute.

PCI. (2020). *Bridge geometry manual (CB-02-20H)*. Precast/Prestressed Concrete Institute.

Peterman, R. J., & Ramirez, J. (1998). Restraint moments in bridges with full-span prestressed concrete form panels. *PCI Journal*, *43*(1).

Phares, B., & Shane, J. (2014). *Methods for removing concrete decks from bridge girders.* Iowa State University.

Reybrouck, N., Van Mullem, T., Taerwe, L., & Caspeele, R. (2020). Influence of long-term creep on prestressed concrete beams in relation to deformations and structural resistance: Experiments and modeling. *Structural Concrete*, *21*(4), 1458-1474.

Robertson, I. N. (2005). Prediction of vertical deflections for a long-span prestressed concrete bridge structure. *Engineering Structures*, *27*(12), 1820-1827.

Rodriguez-Gutierrez, J., & Aristizabal-Ochoa, J. D. (2007). Short- and long-term deflections in reinforced, prestressed, and composite concrete beams. *ASCE Journal of Structural Engineering*, *133*(4), 495-506.

Rossi, P., Tailhan, J.-L., & Le Maou, F. (2013). Comparison of concrete creep in tension and in compression: Influence of concrete age at loading and drying conditions. *Cement and Concrete Research*, 51, 78-84.

Saha, G. (1984). Differential shrinkage stresses in composite construction of reinforced and prestressed concrete structures. *Indian Concrete Journal*, *58*(2), 47-52.

Swartz, B. D. (2010). *Time-dependent analysis of pretensioned concrete bridge girders* [Doctoral dissertation, Pennsylvania State University].

Tadros, M. K., & Baishya, M. C. (1998). *Rapid replacement of bridge decks*. Transportation Research Board.

Trost, H., & Marsh, J. (1967). Effects of the principle of superposition on creep and relaxation problems in concrete and prestressed concrete. *Beton und Stahlbetonbau*, *62*(11).

Wang, W., & Gong, J. (2019). New relaxation function and age-adjusted effective modulus expressions for creep analysis of concrete structures. *Engineering Structures*, *188*, 1-10.

Wendner, R., Hubler, M., & Bažant, Z. (2013). The B4 model for multi-decade creep and shrinkage prediction. *Mechanics and Physics of Creep, Shrinkage, and Durability of Concrete: A Tribute to Zdeňk P. Bažant*.

Wendner, R., Hubler, M. H., & Bažant, Z. P. (2015). Optimization method, choice of form and uncertainty quantification of model B4 using laboratory and multi-decade bridge databases. *Materials and Structures*, *48*(4), 771-796.

Wendner, R., Hubler, M. H., & Bažant, Z. P. (2015). Statistical justification of model B4 for multi-decade concrete creep using laboratory and bridge databases and comparisons to other models. *Materials and Structures*, *48*(4), 815-833.

Zhang, Y. (2020). *The nteraction between shrinkage, creep and cracking of cement material* [Doctoral dissertation, University of Colorado at Boulder].

APPENDIX A – Survey of DOT Engineers

Full-Depth Deck Replacements on Prestressed Concrete Girder Bridges
Survey for Departments of Transportation

Thank you for your participation in this survey designed to gather information on full-depth deck replacements on prestressed concrete girder bridges. This information may be included in a final report to the Kansas Department of Transportation and related publications. However, other than documenting participation, no identifying information will be associated in published documents with your responses.

This survey has three parts. The first gathers contact information for our internal purposes (this information will not be shared outside the research team). The second section is aimed at gathering information about how your state/locality deals with the issue of full-depth deck replacements on prestressed concrete girder bridges. The last section asks about plans for dealing with this issue in the near future.

1: Contact Information

1.1
State/Locality: _____

1.2 Contact Information:

Name: _____

Address: _____

_____

Telephone: _____

Email: _____

2: Experience with Full-Depth Deck Replacements on Prestressed Concrete Bridges:

2.1 Has your state done a full-depth deck replacement on a prestressed-concrete-girder bridge?

Yes _____ No _____

2.2 If yes to 2.1, did your engineers have concerns about how the deck replacement would affect long-term:

Creep and/or shrinkage strains? Yes _____ No _____

Bridge deflections / camber? Yes _____ No _____

Other? Yes _____ No _____

Briefly summarize the concerns: _____

_____

_____

_____

_____

_____

2.3 If yes to 2.1, how were long-term effects of the deck replacement assessed/modeled? If possible, please attach supporting documentation.

_____

_____

_____

_____

_____

_____

_____

2.4 If yes to 2.1, what would you change or improve about the modeling approach? In your view was the result satisfactory?

_____

_____

_____

_____

_____

_____

_____

2.5 If yes to 2.1, have any of the following in-situ problems been observed following the deck replacement:

Cracking in deck or girders?	Yes _____	No _____
Evidence of horizontal joint slip?	Yes _____	No _____
Excessive deflections?	Yes _____	No _____
Other?	Yes _____	No _____

Briefly summarize the observations:_____

_____

_____

_____

_____

2.6 If yes to 2.1, was any long-term monitoring done to document deformations?

Yes _____ No _____

If data are available, please describe:_____

_____

_____

_____

3: Future Full-Depth Deck Replacements on Prestressed Concrete Bridges:

3.1 Does your state have prestressed concrete bridges that may require full-depth deck replacements within the next 10 years?

Yes _____ No _____

3.2 If yes to 3.1, do you have plans for how you will analyze the system for long-term effects of the deck replacement?

Yes _____ No _____

Briefly summarize the approach. In particular, please indicate how you plan to assess long-term strain demands and bridge deflections: _____

_____

_____

_____

_____

_____